FH Aachen University of Applied Sciences
Aerospace Engineering

Master Thesis

Development of a finite element model to describe the dynamic behavior of the maneuverable ice exploration probe IceMole

Kai Schüller
Matriculation-no. 356885

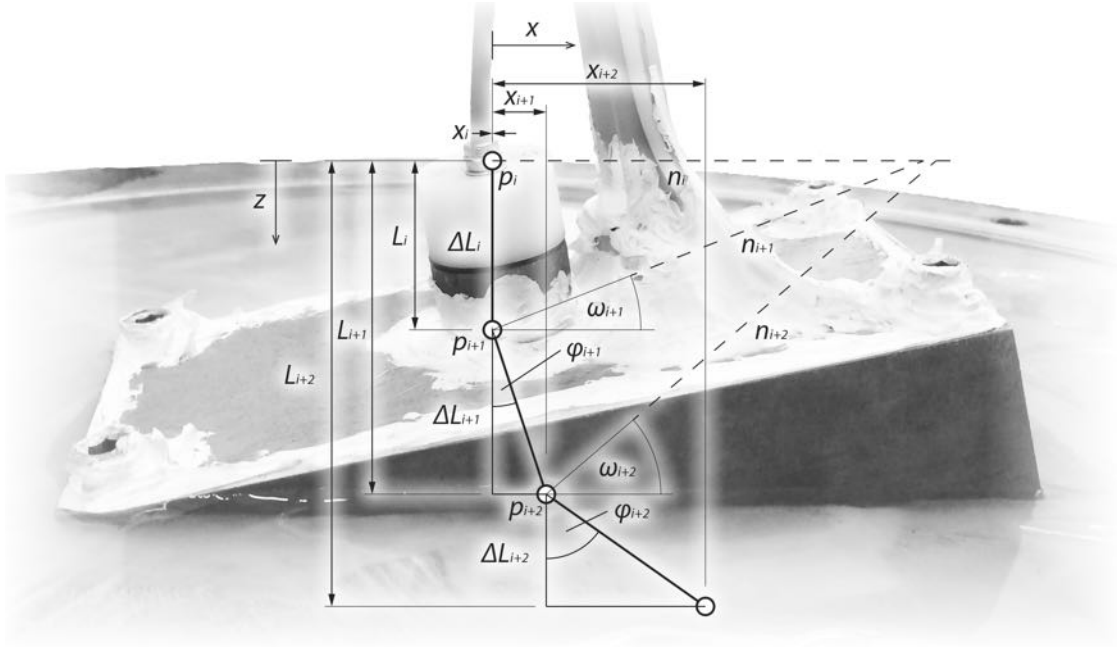

1st Supervisor: Prof. Dr.-Ing. Bernd Dachwald
2nd Supervisor: Dr. Julia Kowalski

Aachen, February 2015

Statutory declaration

I declare that I have authored this thesis independently, that I have not used other than the declared sources / resources and that I have explicitly marked all material which has been quoted either literally or by content from the used sources.

Aachen, February 2015

Kai Schüller

Abstract

It is believed, that there is liquid water on some planets, moons or other satellites of our solar system, which is covered by a layer of ice. To investigate these water resources for the existence of life, a technology is needed that can melt through the ice. One possibility is the maneuverable melting probe IceMole that is developed at FH Aachen University of Applied Sciences since 2008. The maneuverability is possible due to the melting head design, that uses a combination of an ice screw and controllable differential heating cartridges to melt along a curved trajectory. This also makes it possible to avoid obstacles or even reach a specific position in the ice. This, however, requires a navigation solution, in which the position can be determined and the melting trajectory can be predicted over a certain distance.

In this study, a finite element model is developed that is capable to predict such a melting trajectory. A simplified version of the IceMole is used, in which the effects of the probe length and the geometry of the ice screw on the curve radius are neglected. In addition, a Dirichlet boundary condition (temperature) along the melting head surface is used. The model is based on a theory to describe the melting curve, which was derived for the first time in this work. Starting from the assumption that there is a linear velocity profile along the melting head, which is a function of the curve radius, an equation for the pressure distribution within the melt film is derived by using the fundamental equations of close-contact melting. Using an appropriate solution procedure, the curve radius can be determined, when it is required that the torque must be zero at the center of the melting head.

For validation, a melting device was designed and manufactured that was used to perform a series of experiments. These were then compared with the results of the theory and the FEM model and showed good agreement.

Kurzfassung

Es wird vermutet, dass einige Planeten, Monde oder andere Satelliten unseres Sonnensystems flüssiges Wasser beherbergen, welches durch eine Eisschicht bedeckt ist. Um diese Wasservorkommen auf mögliches Leben zu untersuchen, wird eine Technologie benötigt, welche die Eisschicht durchqueren kann. Eine Möglichkeit bietet die manövrierfähige Schmelzsonde IceMole, die an der Fachhochschule Aachen seit 2008 entwickelt wird. Die Manövrierfähigkeit ist durch das gewählte Schmelzkopfdesign möglich, das eine Kombination aus Eisschraube und differentiell schaltbaren Heizpatronen nutzt, um entlang einer gekrümmte Bahn zu schmelzen. Dadurch ist es auch möglich Hindernissen auszuweichen oder sogar eine bestimmte Position im Eis zu erreichen. Hierzu wird jedoch eine Navigationslösung benötigt, die sowohl aus einer Positionsbestimmung, als auch aus einer Vorhersage der Schmelzkurve über eine bestimmte Distanz besteht.

In dieser Arbeit wird ein Finite-Elemente-Modell entwickelt, mit dem es möglich ist eine solche Schmelzkurve vorherzusagen. Dabei wird das Design des IceMoles vereinfacht, indem der Einfluss der Sondenlänge und der Eisschraubengeometrie auf den Kurvenradius vernachlässigt wird. Zusätzlich wird eine Dirichlet-Randbedingung (Temperatur) entlang der Schmelzkopfoberfläche vorgeschrieben. Das Modell basiert auf einer Theorie zur Beschreibung des Kurvenschmelzens, die in dieser Arbeit erstmals aufgestellt wird. Ausgehend von der Annahme, dass sich ein lineares Geschwindigkeitsprofil entlang des Schmelzkopfes einstellt, das eine Funktion des Kurvenradius ist, wird mit den Grundgleichungen des Kontaktschmelzens eine Gleichung für die Druckverteilung innerhalb des Schmelzfilms hergeleitet. Durch einen geeigneten Lösungsweg kann daraus der Kurvenradius ermittelt werden, wenn gefordert wird, dass das Drehmoment um den Mittelpunkt des Schmelzkopfes gegen Null gehen muss.

Zur Validierung wurde ein Schmelzgerät entwickelt und gefertigt, das verwendet wurde um eine Reihe von Experimenten durchzuführen. Diese wurden anschließend mit den Ergebnissen der Theorie und des FEM Modells verglichen und es zeigte sich eine gute Übereinstimmung.

Contents

List of figures i

List of tables v

List of symbols, constants and acronyms vii

1 Introduction 1
1.1 Motivation for the description of the IceMole dynamics 1
1.2 Objectives and outline 2

2 Literature review 3
2.1 Mathematical description of the Stefan problem 3
2.2 Melting probes 4
2.3 Close-contact melting 6
2.3.1 ΔT-driven close-contact melting of a spherical heat source 8
2.3.2 ΔT-driven close-contact melting of a cylindrical heat source 9
2.3.3 ΔT-driven close-contact melting of a flat heat source 12
2.3.4 Generalization of ΔT-driven close-contact melting 12
2.3.5 Heat flux driven close-contact melting of a cylindrical heat source 14
2.3.6 Asymmetric Load 16

3 Theory of curvilinear melting 19
3.1 Physical model 19
3.2 Approximation 20
3.3 Theoretical analysis of the close-contact melting process 22
3.3.1 Calculation of the melt film thickness 26
3.3.2 Solution Procedure 27
3.3.3 Alternative solution 29
3.4 Example results and comparison of the solution methods 30

4 FEM Analysis 35
4.1 Static Analysis 35
4.2 Kinetic Analysis 36
4.3 Dynamic Analysis 36
4.3.1 Computation of the melt film thickness 39
4.3.2 Descriptive example of the algorithm 40
4.3.3 Implementation in Elmer 44

5 Experimental investigation 49
5.1 General design overview 49
5.2 Experimental setup 51
5.3 Measurement hardware and data acquisition 51
5.4 Determination of the curve radius from experimental data 52

5.5 First experimental results and determination of the final configuration 53
5.6 Overview of all conducted experiments 56
5.7 Example results and post-processing 56

6 Results and discussion 61
6.1 Rectilinear melting 61
6.1.1 Comparison with analytical solutions 61
6.1.2 Comparison with experimental results 63
6.2 Curvilinear melting 65
6.2.1 Comparison of the FEM model with the theoretical results 65
6.2.2 Comparison with experimental results 67

7 Summary and conclusions 71

References 73

Appendix 78

A Thermophysical properties of water-ice 79

B Conducted experiments 81

C Curvilinear melting of a cylindrical heat source 83

D User defined function to calculate the melt film thickness and heat transfer coefficient 87

E Solver input files 91
E.1 Description 91
E.2 Solver input file to find the melting velocity 91
E.3 Solver input file to find the curve radius 96

F Matlab files 103
F.1 Shreve 103
F.2 Zhao 107
F.3 Curvilinear melting 109

G Drawings 115

List of figures

1.1 Photography of the EnEx-IceMole at Blood Falls, Antarctica 2014. 1

2.1 Schematic of the Stefan problem. 3

2.2 Shape factors for some representative profiles of the frontal surface. 5

2.3 Schematic of the cose-contact melting situation of an arbitrary shaped heat source. 7

2.4 Schematic of the ΔT-driven close-contact melting over a spherical surface. 8

2.5 Schematic of the ΔT-driven close-contact melting over a cylindrical surface. . . . 10

2.6 Schematic of the ΔT-driven close-contact melting over a flat surface. 12

2.7 Schematic of the definition of the contact melting area A and the perimeter $L_{\text{perimeter}}$. 13

2.8 Physical model of the close-contact melting problem with an asymmetric load. . 16

3.1 Physical model and coordinates for a migrating heat source with a rectangular shape. 20

3.2 Schematic of the curvilinear melting approximation. 20

3.3 Sketch of the curved melting path and velocity profile for two different curve radii. 25

3.4 Schematic of the pressure distribution of the melt film below a rectangular heat source for a linear decreasing temperature profile, when the curve radius is forced to be infinitely large. 28

3.5 Plot of function (3.39) over r_c. 30

3.6 Visualization of the tested temperature profiles. 31

3.7 Curve radii for a rectangular heat source for ΔT-driven close-contact melting. . . 32

3.8 Comparison of the curve radii of a rectangular heat source and a cylindrical heat source for ΔT-driven close-contact melting, using the same temperature gradient $\Delta T = 10\,°\text{C}$. 33

4.1 Difference between the dynamic thermal model domains using the variable grid and the fixed grid. 37

4.2 Determination of the normal velocity. 38

4.3 Temperature and heat flux distribution of the 1-dimensional two-phase Stefan problem at an arbitrary time. 39

4.4 Variables and coordinates of the 1-dimensional ΔT-driven close-contact melting example. 41

4.5 Temperature over melt film thickness for a 1-dimensional ΔT-driven close-contact melting example. 42

4.6 Convergence for different relaxation factors for a 1-dimensional ΔT-driven close-contact melting example. 43

4.7 Required boundaries for solving 2 and 3-dimensional close-contact melting problems in Elmer. 44

4.8 Flow sheet of the overall simulation to obtain the melting velocity and curve radius. 46

5.1 Isometric and section view of the assembled CME. 50

5.2 Photography of the interior of the assembled CME and the numbering of the heaters. 50

5.3 Overview of the experimental setup. 51

5.4 Determination of the curve radius from the distance and the inclination angle. . 53

5.5 Configuration with an ice-screw inserted into the CME. 54

5.6 Pictures of the ice core that builds up for the CME configuration without an ice-screw or a bolt in its center hole. 55

5.7 Configuration with a bolt inserted into the CME. 55

5.8 Plot of the measured ice temperature distribution over time. 57

5.9 Plot of the measured temperatures over time. 58

5.10 Comparison of the measured temperature profile with the target temperature profile. 59

5.11 Measured inclination angle and distance over time. 59

5.12 Calculated melting trajectory and determination of the curve radius from the measured inclunation angle and distance. 60

6.1 Comparison of the simulation results with analytical solutions for rectilinear melting. 63

6.2 Comparison of the simulation with the experimental data in terms of the melting velocity for rectilinear melting. 64

6.3 Simulation results compared to the theoretical solution for different ice temperatures and temperature profiles. 66

6.4 Comparison of theoretical results with the experimental data in terms of the curve radius over the temperature at the center using the predefined temperature values. 68

6.5 Comparison of theoretical results with the experimental data in terms of the curve radius over the temperature at the center using the measured temperature values. 69

6.6 Comparison of theoretical results with the experimental data in terms of the curve radius over the total temperature difference using the measured temperature values. 69

C.1 Physical model and coordinates for a migrating heat source with a cylindrical shape. 83

List of tables

3.1 Parameters, which are used for the example results. 30

4.1 Iteration steps to obtain the melt film thickness for a 1-dimensional ΔT-driven close-contact melting example. 43

5.1 Amount of experiments for different temperature gradients and minimum temperatures (a) with bolt (b) without bolt (c) with ice screw in the central hole of the melting head. 56

6.1 Parameters which were used for comparison of the results of the simulation with analytical solutions. 62

6.2 Error between the theoretical results and the simulation for the experimental data points in terms of the curve radius. 67

A.1 Thermophysical properties of water-ice. 79

B.1 Chronological overview of all conducted experiments. 81

E.1 Description of the entries in the Elmer solver input file. 91

List of symbols, constants and acronyms

Symbols

$\alpha = k/(\rho c_p)$	thermal diffusivity	$\mathrm{m^2/s}$
δ	melt film thickness	m
$\Delta P = F/A_{\mathrm{proj}}$	excess pressure experienced by the melt film	$\mathrm{N/m^2}$
ϵ_{abs}	absolute error	$^\circ C$
ϵ_{rel}	relative error	%
$\hat{F}$	exerted force per unit length	N/m
κ	heat transfer coefficient	$\mathrm{W/(m^2\,K)}$
Λ	performance number	-
λ	relaxation factor	-
$\mu = \nu\,\rho$	dynamic viscosity	$\mathrm{N\,s/m^2}$
ν	kinematic viscosity	$\mathrm{m^2/s}$
Ω	domain	-
ϕ	angular position	rad
ρ	density	$\mathrm{kg/m^3}$
$\mathrm{Ste} = c_{p,L}(T_w - T_m)/h_m$	Stefan number	-
θ	normal angle on the phase interface	rad
$\vec{v} = (v_x, v_y, v_z)^T$	velocity vector of the melt film	m/s
ξ	coordinate normal to the heat source surface	m
A	area	$\mathrm{m^2}$
c_p	specific heat capacity	$\mathrm{J/(kg\,K)}$
D	diameter	m
F	exerted force	N
H	volume-specific enthalpy	$\mathrm{J/m^3}$
h	mass-specific enthalpy	J/kg
$h_m^* = h_m + c_{p,S}(T_m - T_S)$	reduced latent heat of fusion	J/kg
h_m	latent heat of fusion	J/kg
J	compression coefficient	-
J_0, Y_0	Bessel functions	-
k	thermal conductivity	W/(mK)
l	longitudinal length scale	m
M	mass	kg
M^{screw}	torque at the center or ice screw	N m

N	performance number	-
P	power	W
q	heat rate	W
q''	heat flux	$\mathrm{W/m^2}$
q_{Cond}	lateral heat rate requirement	W
q_{M}	heat rate required for melting	W
R	radius	m
r_c	curve radius	m
S	shape factor	-
T	temperature	K
t	time	s
U_0	melting rate	m/s
V	volume	$\mathrm{m^3}$
V_{sp}	specific volume	$\mathrm{m^3/kg}$
X	Position of the phase interface	m
x_R	position of the resulting force	m
x_s	position of the center of mass	m

Indices

$\square_L$	at liquid phase
$\square_m$	at melt point
$\square_S$	at solid phase
$\square_w$	heat source surface
$\square_{\mathrm{eff}}$	effective
$\square_{sp}$	specific quantity

Constants

$g_0 = 9.80665\,\mathrm{m/s^2}$	earth standard gravitational acceleration

Acronyms

CME	curvilinear melting experiment
FEM	finite elements method
FE	finite elements
GUI	graphical user interface
IMU	inertial measurement unit
PDE	partial differential equation
SIF	solver input file
UDF	user defined function

1 Introduction

It is believed that there is liquid water within or under glacier ice on planets, moons and other satellites of our solar system, which brings the potential to find extraterrestrial life. Such icy environments are the polar caps of the Mars, the Jovian moon Europa and the Saturnian moon Enceladus. Direct exploration and in-situ analysis of those regions requires advanced accessing and sampling technologies. One possible approach is to use a melting probe, such as the IceMole (figure 1.1).

The IceMole is a maneuverable melting probe, which equips a conventional melting head with a differential heating system and an ice screw. It is developed at FH Aachen University of Applied Sciences since 2008. During this time, the probe has been further developed for sample taking and clean access capabilities.

The current version of the IceMole has a cross section of $0.15 \times 0.15\,\mathrm{m}$, a length of $1.995\,\mathrm{m}$ and a mass of $60\,\mathrm{kg}$. It is equipped with 2×8 heating cartridges of $200\,\mathrm{W}$ and $160\,\mathrm{W}$ respectively, which add to a maximum heating power of $2.88\,\mathrm{kW}$. The internal structure is protected by an aluminum hull. The inner sides of this hull are equipped with foil heaters, which provide a linear power profile. This enhances the maneuverability due to a smaller possible curve radius for the same probe-length.

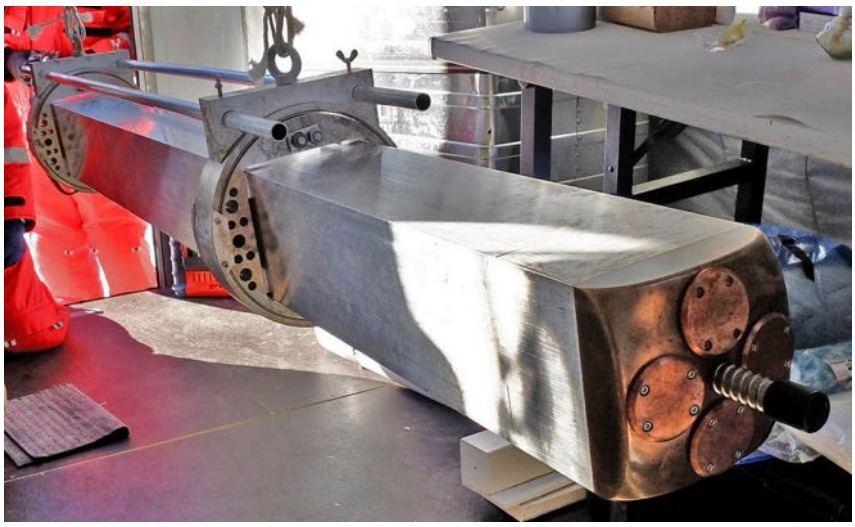

Figure 1.1: Photography of the EnEx-IceMole at Blood Falls, Antarctica 2014.
Source: Marco Feldmann / FH Aachen

1.1 Motivation for the description of the IceMole dynamics

One of the key technologies of the IceMole is the hybrid melting-screwing approach to assure close-contact, as well the melting of curved trajectories. This enables the IceMole to avoid obstacles and to reach a certain position. An accurate navigation requires the prediction of the dynamic melting characteristics of the system, i.e. in addition to a determination of the position, there is a need of a method to predict the motion through the ice over a certain distance.

Unfortunately, the motion of the IceMole results from a combination of heat transfer including phase change and fluid dynamics, which translates into a difficult multi-physical problem.

A possible approach to solve such multi-physical problems is to use the finite element method (FEM). It has been used for this thesis, because it can be easily adapted to solve the necessary partial differential equations even for complicates geometries, such as the IceMole melting head.

1.2 Objectives and outline

The objective of this thesis is to develop a FEM model, which is able to describe the dynamic melting characteristics (i.e. the melting velocity and the melting trajectory) of the IceMole, instead of just predicting the temperature distribution of its surrounding. Compared to other melting probes, the IceMole is special. It uses differential heating of its melting head in combination with an ice screw to move not only in a straight direction, but also on a curved trajectory through the ice. So the developed FEM model must be able to predict the curve radius, which results from this specific type of configuration. This thesis concentrates on the physical phenomena of rectilinear and curvilinear melting, rather than on a full description of the melting characteristics of the current design, because this would go beyond the scope of this thesis. Therefore, a simplified version of the IceMole is considered, in which all secondary effects on the curve radius are neglected. These are the length of the IceMole and the effect of the ice screw geometry on the curve radius. Moreover, no internal heat transfer of the IceMole is considered, which translates into the necessity of a boundary condition on the melting head surface. This boundary condition will be of the Dirichlet-type (prescribed temperature) within this thesis.

Within section 2, the most relevant literature regarding melting probes and close-contact melting are reviewed. Since close-contact melting is the fundamental framework for the developed FEM model, this section contains a detailed overview of the already existing analytical solutions for different configurations and geometries.

Within section 3, the theory of curvilinear melting is given. First, an approximate solution is derived, which can be used for rough estimates of the curve radius. Then, a more accurate solution is given, which is based on close-contact melting theory. It was derived exactly for the specific configuration of the IceMole head, i.e. an asymmetrically distributed temperature (differential heating) along the surface in combination with a continuously acting force normal to the surface in the direction of the ice (ice screw).

Within section 4, the developed FEM model and its implementation into the open source FEM software Elmer is explained in detail. The model includes the basic idea of curvilinear melting theory. So it is capable to describe both rectilinear and curvilinear melting.

Within section 5, the melting device is described, which has been used for experimental validation of the theoretical and FEM model. Moreover, the post-processing is explained, i.e. how the curve radius is determined from the experimental data.

Within section 6, experimental data and analytical solutions are compared with the numerical results using the FEM model, both for rectilinear and curvilinear melting.

2 Literature review

In this section, the most relevant work found in the literature regarding the theory of melting probes will be presented. Beginning from the general mathematical description of melting in subsection 2.1, subsection 2.2 summarizes available theories of melting probes. During the work on this thesis, it turned out, that these theories are good tools for preliminary design or consistency checks, but they are not sufficient for the formulation of a finite element model to simulate the melting characteristics of a complex melting probe like the IceMole. A better starting point for such a model can be found in the theory of close-contact melting, since it is more general. In subsection 2.3, the concept of close-contact melting will be explained and then available publications on this field will be summarized.

2.1 Mathematical description of the Stefan problem

The melting of an initially solid phase change material (PCM) is a time-dependent process. It takes place when a PCM acquires a certain amount of thermal energy (heat) to overcome the binding forces which maintain its solid structure. The name for this amount of energy is latent heat of melting h_m, which is a material-dependent property. There exists a certain temperature where the phase change from solid to liquid occurs, namely the melting temperature T_m, which depends on pressure and on the PCM properties. The solid and liquid regions in the PCM are separated by either a sharp or a mushy phase-transition region (phase interface). The thickness of a mushy phase interface, which typically results from supercooling, can be up to a few centimeters, whereas a sharp interface, which is typical for most pure materials, the thickness can be very thin (a few angstroms[1]). [Alexiades & Solomon, 1993]

A common phase change problem is the so-called Stefan problem [Stefan, 1889], in which heat is supplied through a surface of a PCM (see figure 2.1). During the melting, the position of the heat supply does not change, whereas the phase interface moves with time. This causes a continuous deceleration of the phase interface velocity with increasing time, because the distance between the phase interface and the position of the heat input increases. The formulation of the Stefan problem requires a special condition, which relates the phase interface velocity to a jump in heat flux over this interface.

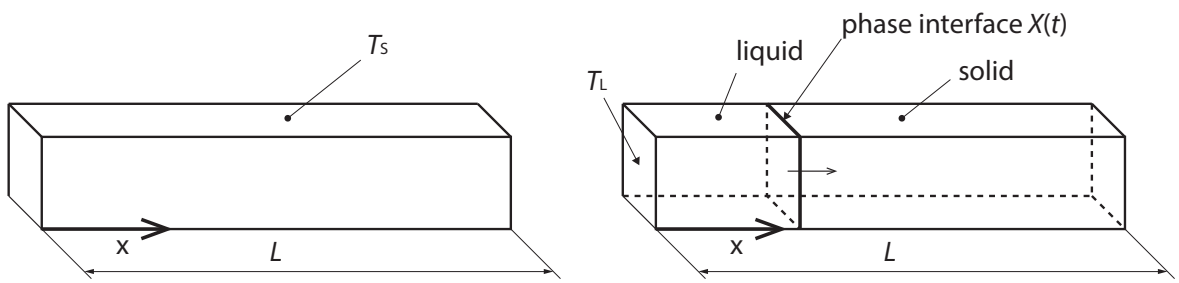

(a) $t = 0$ (b) $t > 0$

Figure 2.1: Schematic of the Stefan problem.

[1] 1 Angstrom = 10^{-10} meters

This condition is denoted as the Stefan condition. In one dimensional formulation it can be written as [Alexiades & Solomon, 1993]

$$\rho h_m \frac{\partial}{\partial t} X(t) = -k_L \frac{\partial T(X(t)^-, t)}{\partial x} + k_S \frac{\partial T(X(t)^+, t)}{\partial x} \tag{2.1}$$

where $X(t)$ is the time-dependent position of the phase interface, $\partial T(X(t)^-, t)/\partial x$ is the heat flux at the phase interface on the liquid side, $\partial T(X(t)^+, t)/\partial x$ is the heat flux at the phase interface on the solid side, ρ is the density, k_L is the thermal conductivity of the liquid phase and k_S is the thermal conductivity of the solid phase.

If the densities of the solid and liquid phase of a PCM differ considerably, the density in the Stefan condition (2.1) must be chosen carefully. Since the velocity of the phase interface depends only on the rate at which new ice melts $v_{n,S}$, it is necessary to insert the the density of the solid phase ρ_S. If one would insert the density of the liquid phase ρ_L in the Stefan condition (2.1), the term $\partial/\partial t X(t)$ must be interpreted as the rate at which new melt is produced, which is due to mass conservation ($\rho_L v_{n,L} = \rho_S v_{n,S}$) the same mass but a different volume and gives therefore a wrong velocity of the phase interface.

2.2 Melting probes

The development and usage of the first thermal melting probes was followed by several studies and publications concerning the theoretical description of the corresponding melting characteristics (e.g. melting velocity).

Shreve [1962] was the first who analyzed the melting characteristics of thermal melting probes theoretically. He focused on the melting head and analyzed the influence of its shape on the melting velocity in temperate ice, by introducing the melting head efficiency. It is defined as the ratio of the cross-sectional area of the melting head to the cross-sectional area of the hole it makes. He also defined the performance number

$$N = \frac{\Lambda\, q\, S}{R F^{1/4}} \tag{2.2}$$

in which S is the melting head's shape factor (figure 2.2), the coefficient $\Lambda = (\mu c_L^3/(4\, k_L\, h_m^4\, \rho_L))^{1/4}$ is a constant that contains the latent heat of melting and the thermo-physical properties of the liquid phase, q is the heat rate, R is the radius of the melting probe and F is the exerted force.

To calculate the melting head efficiency, it is necessary to determine the melting characteristics (melting velocity, pressure distribution ...). Based on close-contact melting theory, which will be described more detailed in subsection 2.3, he derived a set of partial differential equations (PDEs), which can only be solved numerically. It is assumed that the input heat rate leads to an isothermal melting head. However, the restriction of a isothermal melting head is only valid, if it consists of material with infinite thermal conductivity or if it has a special shape [Shreve, 1962].

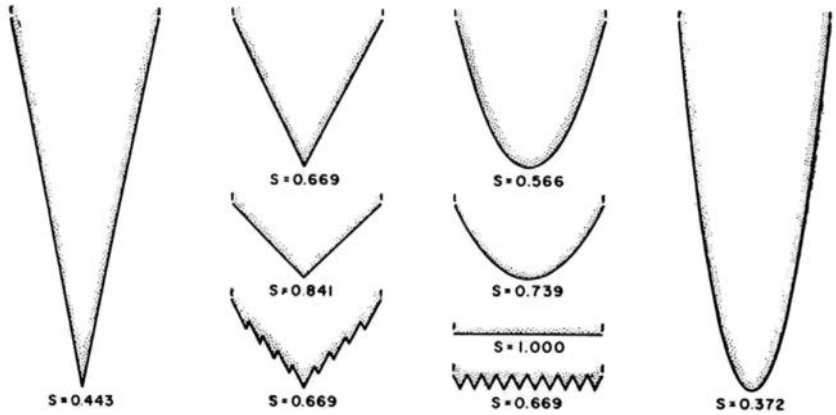

Figure 2.2: Shape factors for some representative profiles of the frontal surface.
Source: [Shreve, 1962]

He confirmed the intuitive observation, that the melting velocity always increases with increasing power and that it varies with respect to variations in design and operation. Another interesting result is, that the efficiency decreases with increasing performance number, whereas the surface temperature increases. Therefore a low shape factor (e.g. paraboloidal shape) leads to a better efficiency than a high shape factor.

[Aamot, 1967] provided a more practical approach. Neglecting the influence of the head shape on the melting velocity, he focused on the determination of the required minimum power for a target velocity of a melting probe with a given length L. He stated that the total power requirement can be calculated by

$$P = q_{\mathrm{M}} + q_{\mathrm{Cond}} \tag{2.3}$$

where q_{M} is the minimum heat rate required for melting, based upon a straight-forward estimation of heat required to melt the channel in the vicinity of the probe. q_{Cond} is the lateral heat rate requirement to ensure that the melt water stays liquid all around the probe's hull.

The minimum heat rate required for melt penetration is given by

$$q_M = U_0 \, A \, \rho_S \, [h_m + c_{p,S}(T_m - T_S)] \tag{2.4}$$

where A is the probe's cross-sectional area, U_0 is the melting velocity, h_m is the latent heat of fusion, ρ_S is the density, $c_{p,S}$ is the specific heat capacity and T_S is the temperature of the solid phase.

Equation (2.4) would also result from the Stefan condition (2.1) by assuming a constant velocity of the phase interface $\partial X(t)/\partial t$ and that the heat flux jump over the phase interface equals the heat flux at heat source surface.

For a cylindrical probe, the lateral heat flux requirement to ensure that the melt water stays

liquid all around the probe's hull is

$$q''_{\text{Cond}} = \frac{4k_S T_S}{R\pi^2} \int_0^\infty \frac{e^{-\alpha_S u^2 t}}{u\left[J_0^2(R\,u) + Y_0^2(R\,u)\right]} du \tag{2.5}$$

where u is the integration argument for Bessel functions J_0 and Y_0, R is the probe's radius and $t = s/U_0$ is the time that corresponds to a certain lateral position of the moving melting probe. The total lateral heat rate can be found by integrating (2.5) over the probe's length

$$q_{\text{Cond}} = \frac{4k_S T_S}{R\pi^2} \int_0^L \int_0^\infty \frac{e^{-\alpha_S u^2 s/U_0}}{u\left[J_0^2(R\,u) + Y_0^2(R\,u)\right]} du ds \tag{2.6}$$

Even though, this approach to estimate the required power for a target velocity is still used for several feasibility studies (e.g. [Ulamec et al., 2007]), it is not sufficient for calculations regarding a real melting probe with an ice screw, because of the missing treatment of the internal heat transfer and the acting forces.

2.3 Close-contact melting

When a heat source moves with time relative to a PCM, the position of the phase interface also depends on the position of the heat source. This is denoted as a moving heat source problem with phase change. Close-contact melting is a special case of a moving heat source problem with phase change in which the spacing between the phase interface and the heat source surface is narrow [Alboudwarej, 1998].

Close-contact melting can be subdivided into internal close-contact melting (the PCM moves relative to the heat source) and external close-contact melting (the heat source moves relative to the PCM). Internal close-contact melting can be found mainly in the field of thermal energy storage systems [Yaojiang et al., 1999], whereas external close-contact melting can be found in a variety of fields, e.g. geology [Marsh, 1978], nuclear technology [Jansen & Stepnewski, 1973], welding [Jackson, 1965], manufacturing technologies [Mayer & Moaveni, 2008] and thermal drilling of rocks [Fisher, 1976] and glaciers Shreve [1962]. Because this thesis focuses on the analysis of melting probes in ice, which is an external close-contact melting problem, the term close-contact melting will correspond to this case in the ongoing of this thesis.

The governing equations for solving close-contact melting problems are the incompressible balance laws for mass, momentum and energy. With respect to the coordinate system defined in figure 2.3 these are given for the melt by

$$\nabla \vec{v} = 0 \tag{2.7}$$

$$\rho_L \left(\frac{\partial \vec{v}}{\partial t} + \vec{v}\,\nabla \vec{v} \right) = -\nabla p + \mu_L \nabla^2 \vec{v} \tag{2.8}$$

$$\frac{\partial T}{\partial t} + \vec{v}\,\nabla T = \alpha_L \nabla^2 T \tag{2.9}$$

where p is the pressure, $\vec{v}$ is the velocity, ρ_L is the density, μ_L is the dynamic viscosity and α_L is the thermal diffusivity of the melt.

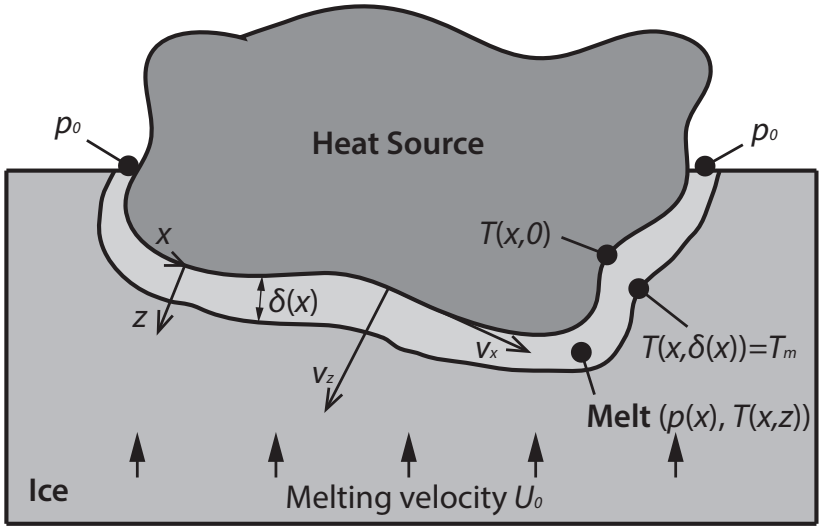

Figure 2.3: Schematic of the cose-contact melting situation of an arbitrary shaped heat source.

The main characteristic of close-contact melting problems with a constant heat source temperature is, that the melting velocity of the migrating heat source will be constant as soon as the heat source and the solid PCM in front of it have reached a quasi-steady state. Moreover, the melt film thickness is assumed to be very thin (i.e. $\delta/L << 1$, where L is the characteristic length in the direction of the flow). This assumption, which is well justified by experimental observations [Moallemi & Viskanta, 1985], permits using the so-called lubrication approximation [Schlichting, 1979], i.e. as long as $\delta/L << 1$ and $(\delta/L)\mathrm{Re} = (\delta/L)\rho_L U_0 L/\mu_L << 1$ (U_0 is the melting velocity), the inertia terms can be neglected and also $\partial^2/\partial x^2 << \partial^2/\partial z^2$. This simplifies the Navier-Stokes equations for incompressible flow (2.7) and (2.8) and the energy equation (2.9) to (a more detailed derivation is given in section 3.3)

$$\rho_L \underbrace{\left(\frac{\partial \vec{v}}{\partial t} + \vec{v}\,\nabla\vec{v}\right)}_{\substack{\approx 0 \\ \text{(negligable due to} \\ \text{lubrication assumption)}}} = -\nabla p + \mu_L \nabla^2 \vec{v} \quad \Rightarrow \quad \frac{dp}{dx} = \mu_L \frac{\partial^2 v_x}{\partial z^2}, \quad \frac{dp}{dz} = 0 \tag{2.10}$$

$$v_x \frac{\partial T}{\partial x} + v_z \frac{\partial T}{\partial z} = \alpha_L \frac{\partial^2 T}{\partial z^2} \tag{2.11}$$

Equations (2.7), (2.10) and (2.11) can be used to calculate the pressure and film thickness distribution for a given melting velocity. However, in most cases the melting velocity is not known a priori. Therefore an additional equation must be introduced, which relates the pressure distribution inside the melt film to the exerted force of the heat source on the PCM. This force balance is given by

$$F = \int_0^L p(x)dx \tag{2.12}$$

where F denotes the sum of forces acting on the melt film (e.g. weight of the heat source superposed by the force due to an ice screw).

Almost all publications on close-contact melting use the presented system of equations (conservation of mass (2.7), conservation of momentum (2.10), conservation of energy (2.11) and force balance (2.12), i.e. 4 Equations for the 4 unknowns p, v_x, T, δ) to solve close-contact melting problems for different conditions at the surface of the heat source (Dirichlet boundary condition, so-called ΔT-driven close-contact melting or Neumann boundary condition, so-called heat flux driven close-contact melting), as well as various geometries. In most cases, the system of equations can only be solved numerically. But under certain circumstances (e.g. simple geometries), there exists also an analytical solution. In the following subsections, some of those solutions will be presented.

First, the existing solutions for the ΔT-driven close-contact melting of a spherical heat source (subsection 2.3.1), cylindrical heat source (subsection 2.3.2) and flat heat source (subsection 2.3.3) will be presented. A generalization of ΔT-driven close-contact melting will be given in subsection 2.3.4. Although a boundary condition of the Neumann-type (i.e. heat flux) will not be part of this thesis, the heat flux driven close-contact melting of a cylindrical heat source will be presented in subsection 2.3.5 to give the idea of what the differences are compared to the ΔT-driven cases. Finally in 2.3.6, close-contact melting with an asymmetric exerted force is shown, which is the most relevant work so far for the description of curvilinear melting.

2.3.1 ΔT-driven close-contact melting of a spherical heat source

Emerman & Turcotte [1983] studied the ΔT-driven close-contact melting of a hot rigid sphere, which melts its way through a solid PCM. The situation is shown in figure 2.4.

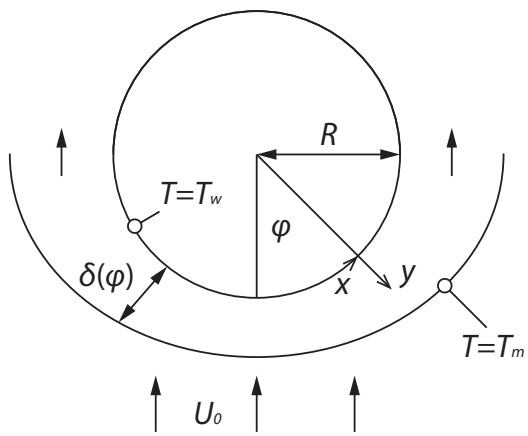

Figure 2.4: Schematic of the ΔT-driven close-contact melting of a spherical surface.

In this case the Stefan condition simplifies to

$$\left.\frac{\partial T}{\partial y}\right|_{y=\delta(x)} = -\frac{\rho_L\, U_0\, h_m^*}{k_L} \tag{2.13}$$

in which $h_m^* = h_m + c_{p,S}(T_m - T_S)$ is the reduced latent heat of melting to take into account the ice temperature T_S.

The variation of the melt film thickness δ as a function of angular position has been derived from the governing equations and the Stefan condition (2.13) for the considered problem. It is

$$\delta(\phi) = \frac{\alpha_L\, f(\mathrm{Ste})}{U_0\, \cos\phi}, \quad \text{with} \quad f(\mathrm{Ste}) = \frac{1}{2}\left[-\frac{3}{2}\mathrm{Ste} - 10 + \left(\frac{9}{4}\mathrm{Ste}^2 + 70\mathrm{Ste} + 100\right)^{1/2}\right] \tag{2.14}$$

in which $\alpha_L = k_L/(\rho_L\, c_{p,L})$ is the thermal diffusivity of the melt, U_0 is the melting velocity, ϕ is the angular position and $\mathrm{Ste} = c_{p,L}(T_w - T_m)/h_m^*$ is the Stefan number. For small Ste, $f(\mathrm{Ste}) \approx \mathrm{Ste}$.

The exerted force of the heat source on the PCM is

$$F = 2\pi R^2 \int_0^{\pi/2} (p - p_0)\cos\phi \sin\phi\, d\phi \tag{2.15}$$

where p_0 is the pressure at $\phi = \pi/2$ and R is the radius of the sphere. Buoyancy and sheer stress forces can be neglected since they are small compared to the pressure force.

Integration of (2.15) yields

$$F = \frac{\pi\, \mu_L\, R^4\, U_0^4}{2\alpha_L^3\, f^3(\mathrm{Ste})} \quad \Leftrightarrow \quad \boxed{U_0 = \left(\frac{2\alpha_L^3\, f^3(\mathrm{Ste})}{\pi\, \mu_L\, R^4} F\right)^{1/4}} \tag{2.16}$$

Hu & Shi [1997] recognized that in the model presented by Emerman & Turcotte [1983] $\delta(\pm\pi/2) \rightarrow \infty$. This problem arises when assuming, that the normal on the phase interface points always in the direction of the sphere's center ($d\delta/(R\, d\phi) << 1$). But this is paradoxical, as the melt film thickness is not constant in general. To overcome this problem, Hu & Shi [1997] introduced an additional angle θ, which defines the normal on the phase interface at every angular position ϕ. This enables the use of the right interface energy equation (Stefan condition), which differs from (2.13)

$$\frac{\partial T}{\partial y}\frac{1}{\cos(\phi - \theta)} = -\frac{\rho_L\, U_0\, h_m^*}{k_L} cos(\theta) \tag{2.17}$$

Unfortunately the resulting system of differential equations can only be solved numerically. Chen et al. [2008b] used a similar approach and compared their results with the analytical solution of Emerman & Turcotte [1983]. They found out that the corrected interface energy equation has no obvious effect on the pressure distribution inside the melt film. Therefore, the analytical results (2.16) can be employed approximately to analyze the contact melting process except for the film thickness close to $\phi = \pm\pi/2$.

2.3.2 ΔT-driven close-contact melting of a cylindrical heat source

Moallemi & Viskanta [1985] studied the ΔT-driven close-contact melting of a cylindrical heat

source, which melts through the PCM n-octadecane ($T_m = 27.5\,°\mathrm{C}$) under its own weight. They considered experiments and compared them to theoretical results. N-octadecane has been chosen because it permits flow visualization, since its liquid phase is transparent. The situation is shown in figure 2.5.

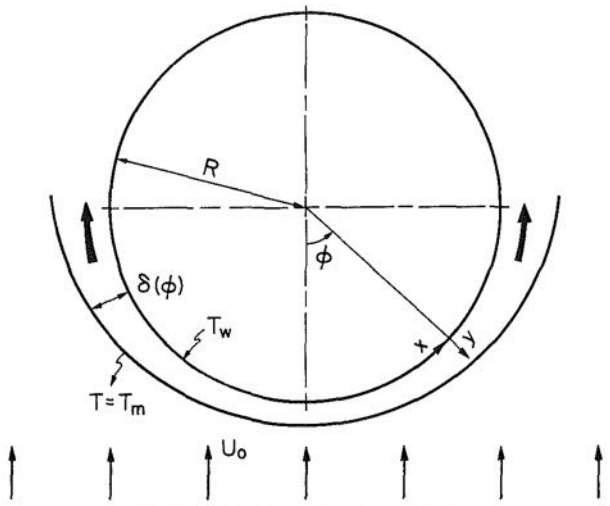

Figure 2.5: Schematic of the ΔT-driven close-contact melting of a cylindrical surface. Source: [Moallemi & Viskanta, 1985]

The experiments showed that the melt film thickness is very thin in the vicinity of the heat source's lower stagnation point ($\phi = 0$) and that it increases with ϕ. This suggests that the motion of the heat source is essentially defined by the motion of the phase interface at $\phi = 0$. At this region, conduction is the dominant mode of heat transfer. With increasing ϕ, the mass flux and the bulk temperature of the melt increases, which suggests that a transition from conduction melting to convection melting occurs along the melt film channel. They also mentioned that in the region behind the heat source (i.e. $\phi > \pi/2$), convection between the liquid and the solid PCM is the dominant mechanism that dictates the motion and the shape of the phase interface.

Another important observation was, that the melting velocity of the heat source reaches a constant value shortly after the experiments started ($t \geq 3.5\,\mathrm{min.}$). This observation can be made for both starting configurations, i.e. for initially positioned at the top and initially embedded in the PCM. Consequently, the terminal melting velocity must be independent of the initial position and also of the initial surface temperature of the heat source, if all other parameters are the same. The only difference is seen in the acceleration. For example, an embedded and initially cold heat source accelerates until the final melting velocity is reached, whereas an initially hot heat source positioned at the top of the PCM decelerates until its final melting velocity is reached. Since this was the case even before the source has been fully covered by the melt, this also suggests that the melting velocity is defined by the heat transfer characteristics below the heat source.

The above observations indicate that in a heat-source-fixed reference frame, the distance to the phase interface at the front of the heat source ($\phi < \pi/2$) will be constant after the final constant melting velocity has been reached, so it can be treated as a quasi-steady state problem. This

however is not the case for $\phi > \pi/2$, since the phase interface is continuously moving with respect to the heat source, e.g. due to refreezing behind the heat source.

Similar to [Emerman & Turcotte, 1983], Moallemi & Viskanta [1985] also derived an approximate analytical solution for the ΔT-driven close-contact melting over a cylindrical surface.

The melt film thickness as a function of angular position is

$$\delta(\phi) = \frac{\alpha_L\, f(\mathrm{Ste})}{U_0\, \cos\phi}, \quad \text{with} \quad f(\mathrm{Ste}) = \frac{1}{4}\left[\left(400 + 280\mathrm{Ste} + 9\mathrm{Ste}^2\right)^{\frac{1}{2}} - 20 - 3\mathrm{Ste}\right] \tag{2.18}$$

in which for small Ste, $f(\mathrm{Ste}) \approx \mathrm{Ste}$, as it was also mentioned for the spherical case in section 2.3.1.

The following equations differ from the results presented in [Moallemi & Viskanta, 1985], since they used the weight (Mg_0) of the heat source and not a summarized exerted force ($Mg_0 + F_{\mathrm{screw}}$), as it is the case for melting probes with an ice screw. To derive an equation for the melting velocity for a summarized exerted force, the equation for the pressure gradient along the melt film must be used, which is

$$\frac{dp}{dx} = -\frac{12\mu_L R U_0 \sin\phi}{\delta^3} \tag{2.19}$$

The exerted force of the heat source on the PCM without buoyancy and shear stress forces is found to be

$$\hat{F} = 2\int_0^{\pi/2} (p - p_0)\cos\phi R d\phi \tag{2.20}$$

where $\hat{F}$ is the force per unit length, which must have the dimension N/m, because the considered geometry is 2-dimensional.

Substituting the melt film thickness (2.18) into (2.19) and integrating yields

$$p - p_0 = \frac{3\mu_L R^2 U_0^4}{\alpha_L^3 f^3(\mathrm{Ste})}\cos^4\phi \tag{2.21}$$

The melting velocity can be found by substituting (2.21) into (2.20) and integrating

$$\boxed{U_0 = \left(\frac{5\alpha_L^3 f^3(\mathrm{Ste})}{16R^3\mu_L}\hat{F}\right)^{1/4}} \tag{2.22}$$

Moallemi & Viskanta [1985] compared their analytical model with the experimental results and found out that the measured dimensionless velocities ($U_0^* = U_0 R/\alpha_L$) are between 64 percent to 47 percent lower than those predicted by the analysis. They mentioned that the main reasons for this discrepancy are

1. nonuniform melting along the axis of the source in the vicinity of its lower stagnation point due to non-considered heat losses
2. nonuniform surface temperature due to inhomogeneous heat extraction from the source

Chen et al. [2008a] again considered the difference of the normal angle between the cylinder surface and the phase interface, because the melt film thickness (2.18) will be infinite for $\phi \to \pm\pi/2$ as in the spherical case. They found out that their results are in accordance to the model of Moallemi & Viskanta [1985] within a certain range of ϕ and differ only in the vicinity of $\pm\phi/2$. Since the melting velocity is essentially defined by the motion of the phase interface at $\phi = 0$, both models predict nearly the same melting velocitys.

2.3.3 ΔT-driven close-contact melting of a flat heat source

Moallemi et al. [1986] investigated ΔT-driven close-contact melting over a flat surface by performing a series of experiments in which blocks of solid n-octadecane were melted by an isothermal planar heat source. They continuously measured the height of the solid with a cathetometer with 0.05 mm resolution. The situtation is shown in figure 2.6.

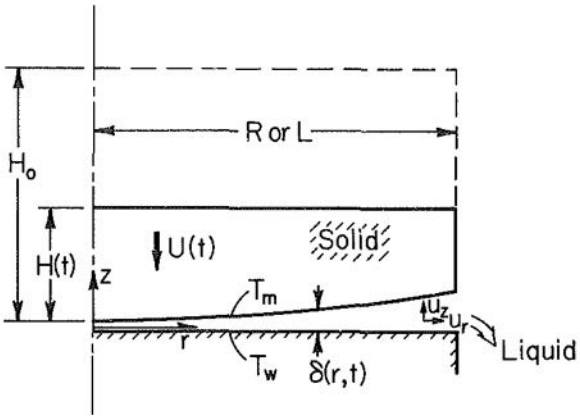

Figure 2.6: Schematic of the ΔT-driven close-contact melting of a flat surface.
Source: [Moallemi et al., 1986]

Using lubrication approximation similar to subsections 2.3.1 and 2.3.2, they derived an approximate analytical solution for this case. It also contains the time-dependent height of the solid PCM, which drives the exerted force on the heated plate. For the present work, this is not necessary, since it focuses on cases, were the heat source moves through the PCM. Therefore a simplified equation, which contains a summarized force will be presented here, which is

$$\boxed{U_0 = \left(\frac{\alpha_L^3 f^3(\mathrm{Ste})}{8L^3\mu_L}\hat{F}\right)^{1/4}} \quad \text{with} \quad f(\mathrm{Ste}) = \frac{1}{2}\left[\sqrt{400 + 200\mathrm{Ste} + 9\mathrm{Ste}^2} - 3\mathrm{Ste} - 20\right] \tag{2.23}$$

2.3.4 Generalization of ΔT-driven close-contact melting

All of the previous explicit results can be generalized in the following framework. Bejan [1992] tried to generalize the findings in close-contact melting, which were derived based on lubrication approximation in several different internal and external configurations.

Using l for the longitudinal length scale of the liquid flow through the melt film, and further assuming that the contact surface is not necessarily a plane, the governing equations (conservation of mass, momentum and energy) require that

$$v_x \delta \sim U_0 l \tag{2.24}$$

$$\frac{\Delta P}{l} \sim \mu \frac{v_x}{\delta^2} \tag{2.25}$$

$$k \frac{\Delta T}{\delta} \sim \rho_S h_m U_0 \tag{2.26}$$

where v_x is the velocity of the melt in tangential direction and ΔP is the excess pressure experienced by the melt film, which is defined as the net weight of the object surrounded by liquid divided by the horizontal projected area of the object (e.g. $\Delta P = g(\rho_L - \rho_w)(\pi D/4)$ for a horizontal cylinder embedded in a PCM, in which ρ_w is the density of the heat source). In the case of a melting probe with an ice screw, the excess pressure would also include the force exerted by the ice screw.

Scaling laws (2.24)-(2.26) can be used in combination with the definition of the Stefan number ($\mathrm{Ste} = c_p \left(T_w - T_m\right)/h_m$) to find a scaling law for the melting velocity that can be nondimensionalized in the form of the Peclet number based on l

$$\frac{U_0 l}{\alpha_L} \sim \left(\frac{\rho_L}{\rho_S}\mathrm{Ste}\right)^{\frac{3}{4}} \left(\frac{\Delta P l^2}{\mu_L \alpha_L}\right)^{\frac{1}{4}} \tag{2.27}$$

The length scale l has to be defined in a way that (2.27) is suitable for all the configurations. One possibility is to define it as the actual dimension of the projected area of contact (e.g. the diameter D for the cylindrical or spherical heat source and the minimum value of length or width of a planar heat source). For the planar heat source, this would reproduce exactly the analytical result for $\rho_L \approx \rho_S$. But unfortunately, not all geometries are reproduced well with this definition of l.

The correlation (2.27) would work better if l is chosen on a rule, which accounts for the shape and curvature of the heat source surface. This can be achieved by defining l as the ratio of the contact melting area A divided by the perimeter of that area projected on the plane perpendicular to the normal force $L_{\mathrm{perimeter}}$, e.g. for the semi-infinite ($L \to \infty$) cylindrical heat source the length scale is then $l = l_0 = \pi D/4$ as it is shown in figure 2.7.

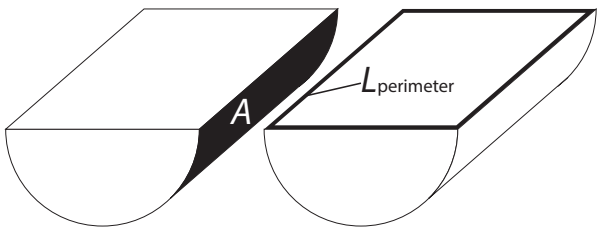

Figure 2.7: Schematic of the definition of the contact melting area A and the perimeter $L_{\mathrm{perimeter}}$.

Using the length scale l_0, the considered theoretical results can be rewritten as:

Plane rectangular heater

$$\frac{U_0 l_0}{\alpha_L} = 0.71\mathrm{Ste}^{3/4}\left(\frac{\Delta P l_0^2}{\mu_L \alpha_L}\right)^{1/4}, \quad (\rho_S \approx \rho_L) \tag{2.28}$$

Cylindrical capsule

$$\frac{U_0 l_0}{\alpha_L} = 0.90\frac{\rho_L}{\rho_S}\mathrm{Ste}^{3/4}\left(\frac{\Delta P l_0^2}{\mu_L \alpha_L}\right)^{1/4} \tag{2.29}$$

Spherical capsule

$$\frac{U_0 l_0}{\alpha_L} = 0.92\frac{\rho_L}{\rho_S}\mathrm{Ste}^{3/4}\left(\frac{\Delta P l_0^2}{\mu_L \alpha_L}\right)^{1/4} \tag{2.30}$$

Embedded cylinder

$$\frac{U_0 l_0}{\alpha_L} = 1.11\mathrm{Ste}^{3/4}\left(\frac{\Delta P l_0^2}{\mu_L \alpha_L}\right)^{1/4} \tag{2.31}$$

Embedded sphere

$$\frac{U_0 l_0}{\alpha_L} = 1.19\mathrm{Ste}^{3/4}\left(\frac{\Delta P l_0^2}{\mu_L \alpha_L}\right)^{1/4} \tag{2.32}$$

The numerical factor on the right-hand side of equations (2.28)-(2.32) is a measure for the similarity to the scaling law (2.27). A numerical factor of 1 would exactly reproduce (2.27), if $(\rho_L/\rho_S)^{3/4} \approx 1$, which is the case for the PCM water-ice (≈ 1.07).

Fomin et al. [1995] used another method for generalization. They developed a general mathematical model of close-contact melting of a PCM with temperature-dependent physical properties by a heating surface of an arbitrary and non-isothermal shape. A curvilinear coordinate system was used to express the governing equations. The resulting set of differential equations was solved numerically by an iterative procedure based on boundary elements method. They had good agreements between their computed results and analytical solutions of previous studies (elliptical and parabolic shape [Fomin & Cheng, 1991]). Another result of their study was, that there are two ways to control the thickness of the melt film. One is to change the length of the heater, the other is to maintain an appropriate temperature distribution along the working surface.

2.3.5 Heat flux driven close-contact melting of a cylindrical heat source

Zhao et al. [2008] studied the close-contact melting of a cylindrical heat source with a constant surface heat flux on its surface. Using the same coordinate system as for the ΔT-driven case (figure 2.5), the boundary condition at the surface of the heat source ($y = 0$) is given by the heat flux instead of the surface temperature

$$\frac{\partial T}{\partial y} = -\frac{q_w''}{k_L} \tag{2.33}$$

The equation for the force equilibrium and the pressure gradient are the same as for the ΔT-driven case from subsection 2.3.2, because the difference of the boundary conditions has no effect on the equations of momentum and mass conservation. The force equilibrium (2.20) and the pressure gradient (2.19) were

$$\hat{F} = 2\int_0^{\pi/2} (p - p_0)\cos\phi R d\phi \tag{2.34}$$

$$\frac{dp}{dx} = -\frac{12\mu_L R U_0 \sin\phi}{\delta^3} \tag{2.35}$$

In order to fulfill the Stefan condition at the phase interface, $T(\delta) = T_m$ and the boundary condition at the heat source surface (2.33), the temperature distribution in the melt film has been approximated by the following quadratic polynomial[2]

$$T(y) = \frac{1}{2\delta k_L}\left(q_w'' - \rho_L U_0 h_m \cos\phi\right) y^2 - \frac{q_w''}{k_L} y + \frac{\delta}{2k_L}\left(q_w'' + \rho_L U_0 h_m \cos\phi\right) + T_m \tag{2.36}$$

(2.33) and (2.36) together with the governing equations for contact melting yields

$$3q_w''\frac{d}{d\phi}\left(\delta(\phi)\sin\phi\right) + 3.5\rho_L U_0 h_m \frac{d}{d\phi}\left(\delta(\phi)\sin 2\phi\right) = 20\alpha_L\left(\frac{q_w''}{U_0} - \rho_L h_m \cos\phi\right) \tag{2.37}$$

Equation (2.37) is a first-order ordinary differential equation for δ, which can be solved numerically, if an initial condition is given. Applying product rule on (2.37) yields

$$\frac{d\delta(\phi)}{d\phi} = \frac{20\alpha_L\left(\frac{q_w''}{U_0} - \rho_L h_m \cos\phi\right) - \delta(\phi)\left(3q_w''\cos\phi + 7\rho_L U_0 h_m \cos 2\phi\right)}{3q_w''\sin\phi + 3.5\rho_L U_0 h_m \sin 2\phi} \tag{2.38}$$

The melt film thickness is assumed to have a minimum at the heat source's lower stagnation point ($\phi = 0$). Substituting $d\delta/d\phi = 0$ in (2.38) yields

$$\delta(0) = 20\alpha_L \frac{q_w'' - \rho_L U_0 h_m}{3U_0 q_w'' + 7\rho_L U_0^2 h_m} \tag{2.39}$$

The force balance (2.34), the pressure gradient (2.35), the derivative of the melt film thickness (2.38) and melt film thickness at $\phi = 0$ (2.39) are the 4 equations to calculate the heat flux driven close-contact melting of a cylindrical heat source. One possible iteration procedure to solve this set of equations has been developed within the scope of this thesis. It is (see appendix F.2 for the corresponding Matlab-script):

1. Set an initial guess for the melting velocity U_0.
2. Solve (2.38) with the initial condition (2.39) for $0 < \phi \leq \pi/2$ to obtain $\delta(\phi)$.
3. Solve (2.35) to obtain the pressure distribution in the melt film $p(\phi)$.
4. Insert $p(\phi)$ into (2.34) and integrate to obtain $\hat{F}$.

[2] There is a typo in Zhao et al. [2008]. The linear term $-(q_w''/k_L)y$ in (2.36) is missing. However, it was used in the further analysis of the publication and the final results of Zhao et al. [2008] coincide.

5. If $\hat{F}$ is equal to the real exerted force $\hat{F}_{\text{screw}}$, the melting velocity U_0 is the melting velocity, which corresponds to the exerted force. Else if $\hat{F}$ is not equal to the exerted force, then change the melting velocity (increase U_0 if $\hat{F} < \hat{F}_{\text{screw}}$, decrease U_0 if $\hat{F} > \hat{F}_{\text{screw}}$) and go to step 2.

The results, which were presented in [Zhao et al., 2008] show that the melt film thickness in the vicinity of $\phi = \pm\pi/2$ is equal to a finite value, which is different from the theoretical results for the ΔT-driven cases, in which it was assumed that the normal on the phase interface points always in the direction of the heat source's center. Furthermore, the melt film thickness and pressure distribution becomes smoother when the heat flux is increased. The most important conclusion is that a quasi-steady melting velocity is determined by the heat flux of the heat source, and the density of the heat source and therefore the exerted force has less effect on the velocity.

2.3.6 Asymmetric Load

Kumano et al. [2005] studied internal close-contact melting with an asymmetric exerted force acting on the PCM. They considered both experimental and theoretical results. The considered situation is shown in figure 2.8. Compared to a melting probe, the situation is reversed, i.e. the heating plate is fixed and the PCM moves. But the solution is also valid for cases in which the heat source moves instead of the PCM, when assuming a constant mass of the PCM.

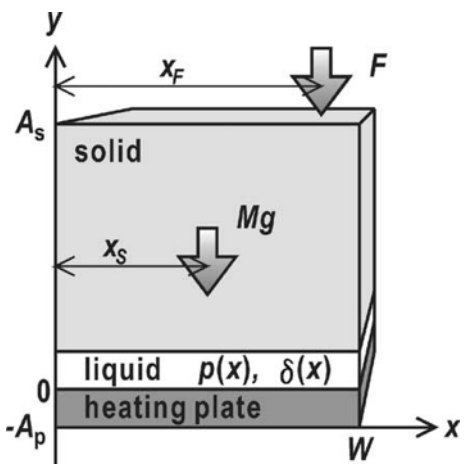

Figure 2.8: Physical model of the close-contact melting problem with an asymmetric load. Source: [Kumano et al., 2005]

In analogy to Moallemi & Viskanta [1985], it was assumed that the melting process progresses in a quasi-steady state. Therefore, the change in the mass of the PCM and the displacement of the center of gravity with time were neglected in the governing equations, but were later considered in an external iterative time-stepping procedure to obtain a quasi-transient melting process.

Additionally to the force balance considered in the so far mentioned theories, Kumano et al. [2005] require that the torque due to the melt film pressure around the position, where the

resulting force is acting, must be zero. For the considered 2-dimensional model this balance equation can be written as

$$\int_0^W p(x)(x - x_R)dx = 0 \tag{2.40}$$

where W is the width of the solid PCM and x_R is the position of the resulting force, which can be calculated by

$$x_R = \frac{Fx_F + Mg_0x_s}{F + Mg_0} \tag{2.41}$$

in which x_F is the position of the force F, M is the mass of the PCM (or transferred to the case of a melting probe, the mass of the melting probe), x_s is the position of the center of mass and $g_0 = 9.80665\,\mathrm{m/s^2}$ is the earth standard gravitational acceleration.

It was shown that their analytical results for the time dependency of the amount of melting and the inclination angle of the PCM agreed with the experimental results. The most important result is that the mass of the PCM over its inclination angle is constant for different values of Ste. Transferred to the application of melting probes, which would use an asymmetric located force for steering, this implies that the curve radius is constant even if the melting head temperature varies for the same resulting force acting at the same position.

3 Theory of curvilinear melting

In subsection 2.3, existing studies regarding several different close-contact melting situations were reviewed. Except for the case with an asymmetric load (subsection 2.3.6), only cases were treated, in which the heat source does not change its orientation. However, the IceMole is able to change its orientation. This is done by differential heating of its melting head in combination with the rotating ice screw, which results in a continuously acting force normal to the melting head.

In this section, the theory of close-contact melting will be extended to cover quasi-stationary curvilinear melting. Starting from a description of the underlying physical model in subsection 3.1, an approximate solution of the curve radius is derived in subsection 3.2. In subsection 3.3, a theoretical analysis and a solution procedure to obtain the curve radius from the resulting equations is given. For simplicity, the considered geometry is a 2-dimensional rectangular plate. However, the translation to other geometries is straight forward, as it is shown in appendix C for the case with a cylindrical geometry. Finally, subsection 3.4 shows some example results of the numerical and approximate solutions for curvilinear melting.

3.1 Physical model

The front view of the physical problem is illustrated in figure 3.1. A rectangular heat source with cross section of $2L \times W$ with $L << W$, height H and a constant force F, which is acting normal to the cross sectional area, is placed on a block of a phase change material (PCM) and induces a motion of the heat source into the PCM. Having the IceMole in mind, the heat source will be given by a copper melting head and the PCM will be given by water ice. It is assumed that a force F is continuously acting normal to the heat source's surface in the direction to the PCM. As a result, a portion of the produced melt will be squeezed out at the ends of the heat source, where the pressure is equal to the surrounding pressure p_{atm}, so that only a thin melt channel with the clearly defined thickness $\delta(x)$ remains between the heat source and the solid part of the PCM. Furthermore a time-independent temperature profile $T_w(x)$ along the surface of the heat source is assumed. Therefore the melting process will soon become quasi-stationary ($U(x) = \text{const.}$) as melting proceeds [Moallemi & Viskanta, 1985].

The migrating heat source will follow a specific path, depending on how the temperature distribution is chosen at the heat source surface. If the temperature $T_w(x)$ and therefore the pressure $p(x)$ inside the melt film is asymmetrically distributed the path will be curved ($U(x) \neq \text{const.}$).

This analysis focuses on the close-contact melting process at the melting head. Therefore the forces due to geometrical constrictions along the melting channel will be neglected, which translates into assuming that the height of the heat source H is small.

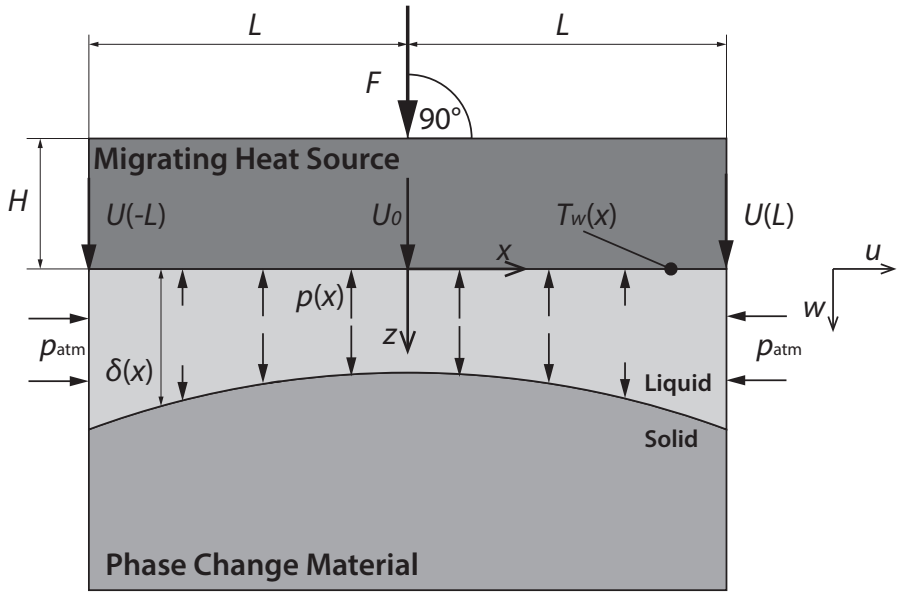

Figure 3.1: Physical model and coordinates for a migrating heat source with a rectangular shape.

3.2 Approximation

Before the full problem will be solved in section 3.3 to calculate the curve radius for a rectangular heat source numerically, an approximate solution will be derived in this section, because sometimes a rough estimate is more useful if it is not necessary to find the exact curve radius. Furthermore, such an approximation might be used to validate the numerical solution. In this subsection, an approximation will be derived, which is based on the replacement of a real geometry of a heat source by two point heat sources, as it is shown in figure 3.2.

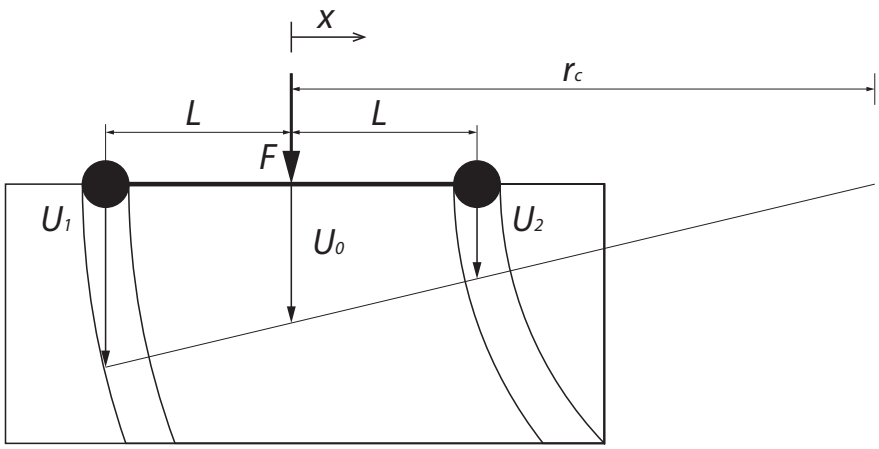

Figure 3.2: Schematic of the curvilinear melting approximation. Two point heat sources with a constant distance to each other (e.g. connected by a rigid rod) and different surface heat fluxes melt through an initially solid PCM. Due to the heat flux difference, one heat source melts faster through the PCM than the other. This results in a curved trajectory, because a force is continuously acting normal to the heat source's connection.

The constant distance of the heat sources is the same as the total length of the real heat source, which is approximated. A continuously acting force at the center of and normal to the connection line causes both heat sources to melt through a PCM. If the surface heat flux of the two heat sources is not equal, the melting velocities of the heat sources are also different. This results in a curved trajectory.

Following the Stefan condition, the surface heat fluxes of the two heat sources must be equal to the velocity of the phase interface in front of them

$$q''_{w,1} = U_1 \rho_S h_m \tag{3.1}$$

$$q''_{w,2} = U_2 \rho_S h_m \tag{3.2}$$

The velocities U_1 and U_2 can be substituted by using a linear velocity profile (3.22), which will be explained later in subsection 3.3. Substituting the linear velocity profile (3.22) in equations (3.1) and (3.2) yields

$$q''_{w,1} = U_0 \left(1 + \frac{L}{r_c}\right) \rho_S h_m \tag{3.3}$$

$$q''_{w,2} = U_0 \left(1 - \frac{L}{r_c}\right) \rho_S h_m \tag{3.4}$$

The curve radius as a function of the heat flux of the left and right point heat sources can be found by substituting (3.3) into (3.4)

$$r_c = L \frac{q''_{w,1} + q''_{w,2}}{q''_{w,1} - q''_{w,2}} \tag{3.5}$$

For the ΔT-driven case, the heat fluxes in equation (3.5) can be substituted by $q''_{w,i} = -k_L \left(T_{w,i} - T_m\right)/\delta_i$

$$r_c = L \frac{\frac{T_{w,1}-T_m}{\delta_1} + \frac{T_{w,2}-T_m}{\delta_2}}{\frac{T_{w,1}-T_m}{\delta_1} - \frac{T_{w,2}-T_m}{\delta_2}} \tag{3.6}$$

When assuming $\delta_1 \approx \delta_2$, equation (3.6) simplifies to

$$r_c = L \frac{T_{w,1} + T_{w,2} - 2T_m}{T_{w,1} - T_{w,2}} \tag{3.7}$$

Equation (3.7) can be used to calculate an approximated curve radius for the ΔT-driven case directly from the temperatures and half of the distance of the heat sources. Additionally, the melting temperature of the PCM must be given. This means that the curve radius can be calculated from 3 parameters, namely the temperature profile along the heat source surface $T_{w,1}$ and $T_{w,1}$, the melting temperature T_m and the half-length of the heat source L.

3.3 Theoretical analysis of the close-contact melting process

In the realistic case of a copper melting head, which melts into water ice, the thickness of the melt channel, that separates the heat source and the PCM in front of it is going to be very thin, i.e. $\delta/L << 1$ and therefore $(\delta/L)\mathrm{Re} << 1$. In this case one can apply the so-called lubrication approximation in which the inertia terms are negligible[3] compared to the pressure gradient term in the momentum equation and also $\partial^2/\partial x^2 << \partial^2/\partial z^2$ [Moallemi & Viskanta, 1985].

By using the above assumptions, the governing balance equations for mass, momentum and energy simplify to

Continuity (incompressible flow $\rho = const.$):

$$\nabla \vec{v} = 0$$

$$\boxed{\frac{\partial u}{\partial x} + \frac{\partial w}{\partial z} = 0} \tag{3.8}$$

Momentum (incompressible fluid without body forces):

$$\rho_L \frac{D\vec{v}}{Dt} = -\nabla p + \mu_L \nabla^2 \vec{v}$$

$$\rho_L \underbrace{\left(\frac{\partial \vec{v}}{\partial t} + \vec{v}\,\nabla \vec{v}\right)}_{\substack{\approx 0 \\ \text{(negligable due to} \\ \text{lubrication assumption)}}} = -\nabla p + \mu_L \nabla^2 \vec{v}$$

$$\nabla p = \mu_L \nabla^2 \vec{v}$$

Lubrication approximation leads to

$$\boxed{\frac{dp}{dx} = \mu_L \frac{\partial^2 u}{\partial z^2}} \tag{3.9}$$

$$\boxed{\frac{\partial^2 u}{\partial x^2} = 0 \Rightarrow \frac{dp}{dz} = 0} \tag{3.10}$$

Energy:

$$\frac{\partial T}{\partial t} + \vec{v}\,\nabla T - \alpha_L \nabla^2 T = 0$$

$$\underbrace{\frac{\partial T}{\partial t}}_{<<1} + u\frac{\partial T}{\partial x} + w\frac{\partial T}{\partial z} = \alpha_L \left(\underbrace{\frac{\partial^2 T}{\partial x^2}}_{<<1} + \frac{\partial^2 T}{\partial z^2}\right)$$

Because the dominant effects are convection as well as vertical conduction:

$$\boxed{u\frac{\partial T}{\partial x} + w\frac{\partial T}{\partial z} = \alpha_L \frac{\partial^2 T}{\partial z^2}} \tag{3.11}$$

[3] In Stokes's problem the inertial effects are negligible if $\mathrm{Re} << 1$. However, if the flow is confined to a thin layer, then the inertial terms can be neglected if $(\delta/L)\mathrm{Re} << 1$. [Emerman & Turcotte, 1983]

where	u	velocity in x-direction
	w	velocity in z-direction
	$\vec{v} = (u, w)^{\mathrm{T}}$	velocity vector
	T	temperature
	p	pressure in the melt film
	μ_L	dynamic viscosity of the melt
	α_L	thermal diffusivity of the melt
	ρ_L	density of the melt

No-slip condition, no velocity of the melt in normal direction and a given wall temperature $T_w(x)$ lead to the following boundary conditions at the heat source ($z = 0$)

$$u(x, 0) = w(x, 0) = 0, \qquad T(x, 0) = T_w(x) \tag{3.12}$$

At the phase interface ($z = \delta(x)$), no-slip condition for the velocity and melting temperature T_m are present. Additionally, the velocity of the melt in normal direction must be equal to the inverted velocity of the heat source times the density ratio, due to mass conservation over the phase interface ($\rho_L w_L = \rho_S w_S$)

$$u(x, \delta(x)) = 0, \qquad w(x, \delta(x)) = -\frac{\rho_S}{\rho_L} U(x), \qquad T(x, \delta(x)) = T_m \tag{3.13}$$

To take into account the phase change at the phase interface, the Stefan condition must be introduced, which depends on the velocity of the heat source $U(x)$, the latent heat of melting h_m, the temperature of the solid phase of the PCM T_S and some thermo-physical properties. In this case the Stefan condition reads as

$$\left.\frac{\partial T}{\partial z}\right|_{z=\delta(x)} = -\frac{\rho_S U(x)}{k_L} \left[h_m + c_{p,S}(T_m - T_S)\right] \tag{3.14}$$

The pressure at the right- and left-hand side of the melt film is

$$p(-L) = p(L) = p_{\mathrm{atm}} \tag{3.15}$$

where p_{atm} must not be necessarily the real atmospheric pressure. It is also possible to use the pressure due to a hydrostatic head instead.

Integration of the momentum equation (3.9) yields

$$\begin{aligned}
\mu_L \frac{\partial^2 u}{\partial z^2} &= \frac{dp}{dx} \\
\frac{\partial^2 u}{\partial z^2} &= \frac{1}{\mu_L} \frac{dp}{dx} \\
\frac{\partial u}{\partial z} &= \frac{1}{\mu_L} \frac{dp}{dx} \int dz \\
u(x, z) &= \frac{1}{\mu_L} \frac{dp}{dx} \int \int dz dz = \frac{1}{\mu_L} \frac{dp}{dx} \int (z + C_1)\, dz = \frac{1}{\mu_L} \frac{dp}{dx} \left(\frac{1}{2} z^2 + C_1 z + C_2\right)
\end{aligned} \tag{3.16}$$

The integration constants C_1 and C_2 can be found by inserting the boundary conditions (3.12)

and (3.13) into (3.16)

$$u(x,0) = 0 \quad \Rightarrow \quad C_2 = 0, \qquad u(x,\delta(x)) = 0 \quad \Rightarrow \quad C_1 = -\frac{1}{2}\delta(x)$$

$$\boxed{u(x,z) = \frac{1}{2\mu_L}\frac{dp}{dx} z\left(z - \delta(x)\right)} \tag{3.17}$$

The pressure gradient can be found by substituting (3.17) into continuity equation (3.8) and integrating over the melt film thickness

$$\begin{aligned}
\frac{\partial u}{\partial x} + \frac{\partial w}{\partial z} &= 0 \\
\frac{\partial w}{\partial z} &= -\frac{\partial u}{\partial x} \\
\int_0^{\delta(x)} \frac{\partial w(x,z)}{\partial z} dz &= -\int_0^{\delta(x)} \frac{\partial u(x,z)}{\partial x} dz \\
w(x,\delta(x)) - w(x,0) &= -\int_0^{\delta(x)} \frac{\partial u(x,z)}{\partial x} dz
\end{aligned} \tag{3.18}$$

Inserting the boundary conditions (3.12) and (3.13) on the left side of equation (3.18) and applying Leibniz integral rule on the right side yields

$$\begin{aligned}
-\frac{\rho_S}{\rho_L} U(x) &= -\frac{d}{dx}\int_0^{\delta(x)} u(x,z)dz + \underbrace{u(x,\delta(x))\frac{d\delta(x)}{dx}}_{=0 \text{ (no slip (3.13))}} \\
\frac{\rho_S}{\rho_L}\int_0^x U(\tilde{x})d\tilde{x} + C_4 &= \int_0^{\delta(x)} u(x,z)dz
\end{aligned} \tag{3.19}$$

Substituting (3.17) in (3.19) and integrating yields

$$\begin{aligned}
\frac{\rho_S}{\rho_L}\int_0^x U(\tilde{x})d\tilde{x} + C_4 &= \frac{1}{2\mu_L}\frac{dp}{dx}\left(\frac{1}{3}z^3 - \frac{1}{2}z^2\delta(x)\right) \\
&\boxed{\frac{dp}{dx} = -\frac{12\mu_L\left(\frac{\rho_S}{\rho_L}\int_0^x U(\tilde{x})d\tilde{x} + C_4\right)}{\delta^3(x)}}
\end{aligned} \tag{3.20}$$

Combining equations (3.17) and (3.20) yields

$$u(x,z) = -6z\left(z - \delta(x)\right)\frac{\frac{\rho_S}{\rho_L}\int_0^x U(\tilde{x})d\tilde{x} + C_4}{\delta^3(x)} \tag{3.21}$$

In the case of a circular melting curve, the angular velocity $\omega(x)$ must be constant for each position on the migrating heat source (figure 3.3). This results in a linear velocity profile

$$U(x) = U_0\left(1 - \frac{x}{r_c}\right) \tag{3.22}$$

where r_c is the curve radius. If $r_c > 0$ the melting path will be anti-clockwise, else if $r_c < 0$ the melting path will be clockwise.

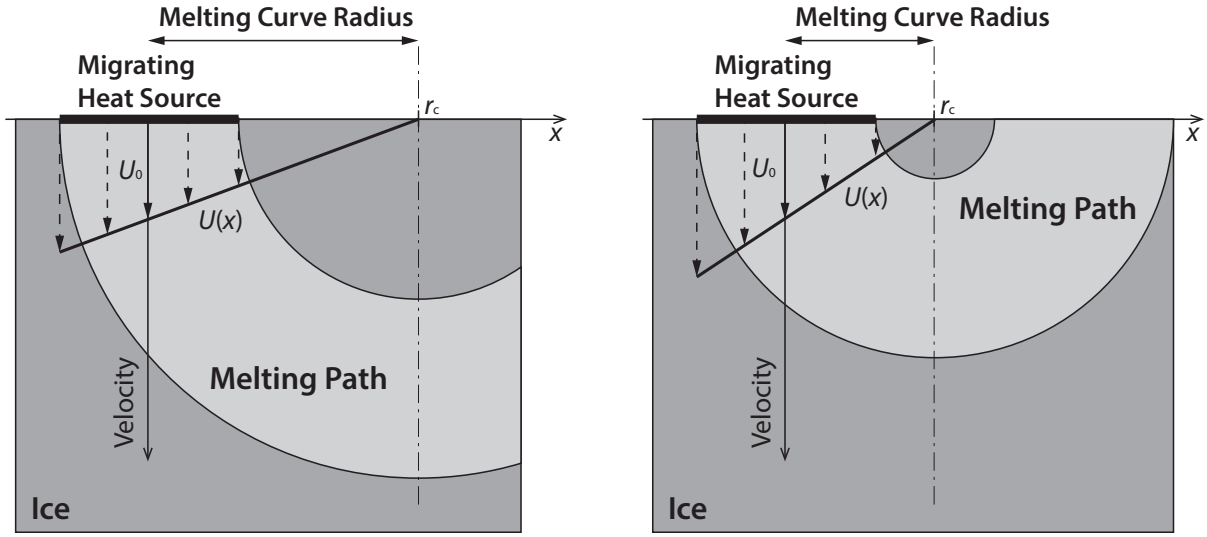

Figure 3.3: Sketch of the curved melting path and velocity profile for two different curve radii. The melting path for a large curve radius is shown on the left and the melting path for a smaller curve radius is shown on the right.

Inserting the linear velocity profile (3.22) into the pressure gradient (3.20) yields

$$\frac{dp}{dx} = -\frac{12\mu_L \left[\frac{\rho_S}{\rho_L} U_0 x \left(1 - \frac{x}{2r_c}\right) + C_4\right]}{\delta^3(x)} \tag{3.23}$$

Integrating (3.23) yields

$$\begin{aligned} p(x) - p(0) &= -12\mu_L \int_0^x \frac{1}{\delta(\tilde{x})^3} \left[\frac{\rho_S}{\rho_L} U_0 \tilde{x} \left(1 - \frac{\tilde{x}}{2r_c}\right) + C_4\right] d\tilde{x} \\ p(x) &= -12\mu_L \left[\frac{\rho_S}{\rho_L} U_0 \int_0^x \frac{\tilde{x}}{\delta(\tilde{x})^3} \left(1 - \frac{\tilde{x}}{2r_c}\right) d\tilde{x} + C_4 \int_0^x \frac{1}{\delta(\tilde{x})^3} d\tilde{x}\right] + p(0) \end{aligned} \tag{3.24}$$

The integration constants C_4 and $p(0)$, which is the pressure at $x = 0$ can be found by inserting the pressure at the right- and left-hand side of the melt film (3.15) into (3.24)

$$p(L) = p_{\text{atm}} = -12\mu_L \left[\frac{\rho_S}{\rho_L} U_0 \int_0^L \frac{x}{\delta(x)^3} \left(1 - \frac{x}{2r_c}\right) dx + C_4 \int_0^L \frac{1}{\delta(x)^3} dx\right] + p(0) \tag{3.25}$$

$$p(-L) = p_{\text{atm}} = -12\mu_L \left[\frac{\rho_S}{\rho_L} U_0 \int_0^{-L} \frac{x}{\delta(x)^3} \left(1 - \frac{x}{2r_c}\right) dx + C_4 \int_0^{-L} \frac{1}{\delta(x)^3} dx\right] + p(0) \tag{3.26}$$

Subtracting (3.26) from (3.25) yields

$$\begin{aligned} p(L) - p(-L) = 0 &= \frac{\rho_S}{\rho_L} U_0 \int_{-L}^L \frac{x}{\delta(x)^3} \left(1 - \frac{x}{2r_c}\right) dx + C_4 \int_{-L}^L \frac{1}{\delta(x)^3} dx \\ C_4 &= -\frac{\frac{\rho_S}{\rho_L} U_0 \int_{-L}^L \frac{x}{\delta(x)^3} \left(1 - \frac{x}{2r_c}\right) dx}{\int_{-L}^L \frac{1}{\delta(x)^3} dx} \end{aligned} \tag{3.27}$$

The pressure at $x = 0$ can be found by substituting (3.27) in (3.25)

$$\begin{aligned} p(0) =& 12\mu_L \left[\frac{\rho_S}{\rho_L} U_0 \int_0^L \frac{x}{\delta(x)^3} \left(1 - \frac{x}{2r_c}\right) dx \right. \\ & \left. - \frac{\frac{\rho_S}{\rho_L} U_0 \int_{-L}^L \frac{x}{\delta(x)^3} \left(1 - \frac{x}{2r_c}\right) dx}{\int_{-L}^L \frac{1}{\delta(x)^3} dx} \int_0^L \frac{1}{\delta(x)^3} dx \right] + p_{\text{atm}} \end{aligned} \tag{3.28}$$

Using (3.24) together with (3.27) and (3.28), the pressure distribution in the melt film can be calculated by

$$\begin{aligned} p(x) =& -12\mu_L \left[\frac{\rho_S}{\rho_L} U_0 \int_0^x \frac{\tilde{x}}{\delta(\tilde{x})^3} \left(1 - \frac{\tilde{x}}{2r_c}\right) d\tilde{x} - \frac{\frac{\rho_S}{\rho_L} U_0 \int_{-L}^L \frac{x}{\delta(x)^3} \left(1 - \frac{x}{2r_c}\right) dx}{\int_{-L}^L \frac{1}{\delta(x)^3} dx} \int_0^x \frac{1}{\delta(\tilde{x})^3} d\tilde{x} \right] \\ & + 12\mu \left[\frac{\rho_S}{\rho_L} U_0 \int_0^L \frac{x}{\delta(x)^3} \left(1 - \frac{x}{2r_c}\right) dx - \frac{\frac{\rho_S}{\rho_L} U_0 \int_{-L}^L \frac{x}{\delta(x)^3} \left(1 - \frac{x}{2r_c}\right) dx}{\int_{-L}^L \frac{1}{\delta(x)^3} dx} \int_0^L \frac{1}{\delta(\tilde{x})^3} d\tilde{x} \right] \\ & + p_{\text{atm}} \end{aligned}$$

$$\boxed{p(x) = 12\mu_L \frac{\rho_S}{\rho_L} U_0 \left[\int_x^L \frac{\tilde{x}}{\delta(\tilde{x})^3} \left(1 - \frac{\tilde{x}}{2r_c}\right) d\tilde{x} - \frac{\int_{-L}^L \frac{x}{\delta(x)^3} \left(1 - \frac{x}{2r_c}\right) dx}{\int_{-L}^L \frac{1}{\delta(\tilde{x})^3} d\tilde{x}} \int_x^L \frac{1}{\delta(\tilde{x})^3} d\tilde{x} \right] + p_{\text{atm}}} \tag{3.29}$$

Equation (3.29) gives the pressure profile along the heat source surface as a function of $\delta(x)$. To calculate the pressure distribution in the melt film (3.29) for a given melting velocity U_0, the melt film thickness $\delta(x)$ for a given temperature profile at the heat source surface must be known.

3.3.1 Calculation of the melt film thickness

To derive an expression for the melt film thickness, a temperature profile through the melt film must be assumed. Two boundary conditions can be fulfilled by assuming a first order polynomial, whereas three boundary conditions can be fulfilled by assuming a second order polynomial.

The linear polynomial approximation of the temperature distribution can be found by using the boundary conditions 3.12 and 3.13

$$\begin{aligned} & T = Az + B \\ & T(0) = T_w(x) \quad \Rightarrow \quad B = T_w(x) \\ & T(\delta) = T_m \quad \Rightarrow \quad A = \frac{T_m - T_w(x)}{\delta(x)} \\ & \boxed{T(x,z) = \frac{T_m - T_w(x)}{\delta(x)} z + T_w(x)} \end{aligned} \tag{3.30}$$

Whereas the quadratic polynomial approximation, which is found by using the boundary conditions 3.12, 3.13 and the energy balance at the interface (3.14), would be (without derivation)

$$T(x,z) = T_w(x) + \left(\frac{\rho_S h_m^* U(x)}{k_L} - \frac{2\left(T_w(x) - T_m\right)}{\delta(x)} \right) z + \left(\frac{T_w(x) - T_m}{\delta(x)^2} - \frac{\rho_S h_m^* U(x)}{\delta(x) k_l} \right) z^2 \quad (3.31)$$

To solve the quadratic polynomial approximation (3.31) for the melt film thickness, it would be necessary to combine the energy equation (3.11) with the continuity equation (3.8), integrate the resulting equation over the melt film thickness, insert the boundary conditions and then substitute 3.31 in the resulting equation.

For small and non-zero Ste, the differences between the linear and quadratic polynomial approximations are small [Moallemi & Viskanta, 1986]. Because this is the case for the concrete example of a melting probe, which penetrates into water ice, a linear polynomial will be assumed in this study.

Substituting the temperature (3.30) into the Stefan condition (3.14) yields

$$\begin{aligned} \frac{T_m - T_w(x)}{\delta(x)} &= -\frac{\rho_S h_m^* U(x)}{k_L} \\ \delta(x) &= \frac{k_L\left(T_w(x) - T_m\right)}{\rho_S h_m^* U(x)} = \frac{k_L\left(T_w(x) - T_m\right)}{\rho_S h_m^* U_0 \left(1 - \frac{x}{r_c}\right)} \end{aligned} \quad (3.32)$$

3.3.2 Solution Procedure

There are two unknowns in the pressure profile along the heat source surface (3.29), namely the curve radius r_c and the melting velocity U_0. To find these unknowns, two additional relations are needed. The pressure integrated over the entire heat source must be equal to the force by which the heat source is pressed via the ice screw on the ice (force equilibrium), hence

$$F_{\text{screw}} = \int_{-L}^{L} p(x) dx \quad (3.33)$$

Typically, this force is known a priori. There are also some other forces acting, e.g. buoyancy force, but compared to the force exerted by the ice screw, these terms are small and can be therefore neglected. A typical plot of the pressure distribution in the melt film below the heat source $p(x)$ (3.29) for an infinite curve radius $r_c \to \infty$ and a linear temperature distribution is shown in figure 3.4(b).

In figure 3.4(b), the pressure is asymmetrically distributed. Therefore the center of pressure and the center of the heat source will not coincide, which will lead to a torque around the ice screw. By varying the curve radius, the center of pressure will also change. This leads to the second important relation to find the unknown quantities

$$\Sigma M^{\text{screw}} = 0 = \int_{-L}^{L} p(x) x dx \quad (3.34)$$

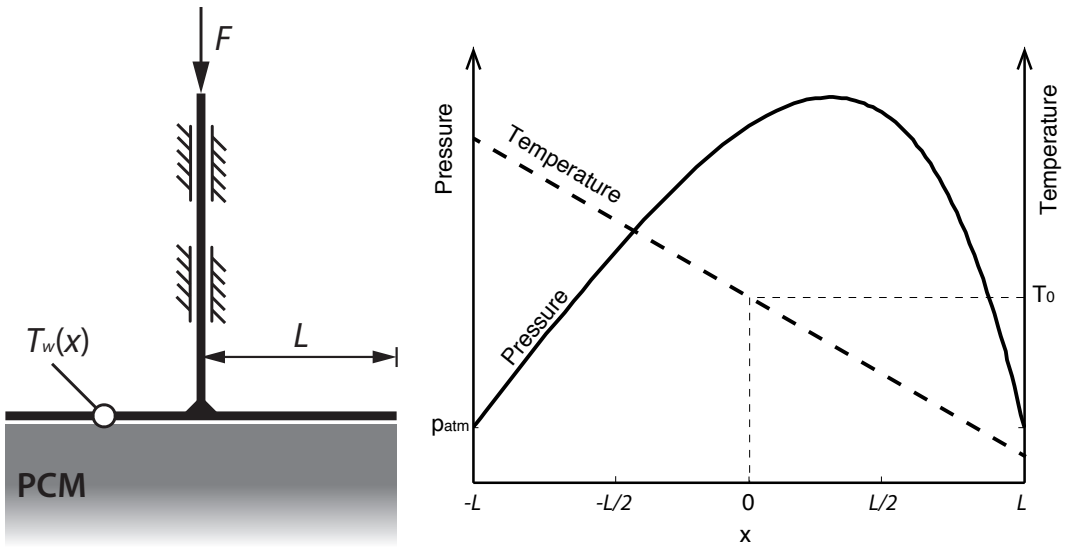

(a) (b)

Figure 3.4: Schematic of the pressure distribution of the melt film below a rectangular heat source for a linear decreasing temperature profile of the form $T(x) = T_0 - \Delta T\, x/(2L)$, when the curve radius is forced to be infinitely large ($r_c \to \infty$). (a) shows the situation in a mechanical sense, i.e. the infinite curve radius is equal to bearings, which only allow vertical motion. (b) shows the corresponding plot of the temperature and pressure distribution inside the melt film.

Substituting (3.29) and (3.32) into (3.34) yields

$$
\begin{aligned}
0 =& \int_{-L}^{L} \left(12\mu_L \frac{\rho_S}{\rho_L} U_0 \left[\int_x^L \frac{\tilde{x}}{\delta(\tilde{x})^3} \left(1 - \frac{\tilde{x}}{2r_c}\right) d\tilde{x} - \frac{\int_{-L}^{L} \frac{x}{\delta(x)^3}\left(1 - \frac{x}{2r_c}\right) dx}{\int_{-L}^{L} \frac{1}{\delta(x)^3} dx} \int_x^L \frac{1}{\delta(\tilde{x})^3} d\tilde{x} \right] \right) x dx \\
&+ \underbrace{\left[\frac{1}{2} p_{\text{atm}} x^2 \right]_{-L}^{L}}_{=0} \\
0 =& 12\mu_L \frac{\rho_S}{\rho_L} U_0 \int_{-L}^{L} \left(\int_x^L \tilde{x} \left(\frac{\rho_S h_m^* U_0 \left(1 - \frac{\tilde{x}}{r_c}\right)}{k_L \left(T_w(\tilde{x}) - T_m\right)} \right)^3 \left(1 - \frac{\tilde{x}}{2r_c}\right) d\tilde{x} \right. \\
&\left. - \frac{\int_{-L}^{L} x \left(\frac{\rho_S h_m^* U_0 \left(1 - \frac{x}{r_c}\right)}{k_L (T_w(x) - T_m)} \right)^3 \left(1 - \frac{x}{2r_c}\right) dx}{\int_{-L}^{L} \left(\frac{\rho_S h_m^* U_0 \left(1 - \frac{x}{r_c}\right)}{k_L (T_w(x) - T_m)} \right)^3 dx} \int_x^L \left(\frac{\rho_S h_m^* U_0 \left(1 - \frac{\tilde{x}}{r_c}\right)}{k_L \left(T_w(\tilde{x}) - T_m\right)} \right)^3 d\tilde{x} \right) x dx \\
0 =& 12\mu_L \frac{\rho_S^4 h_m^{*3}}{k_L^3 \rho_L} U_0^4 \int_{-L}^{L} \left(\int_x^L \tilde{x} \left(\frac{1 - \frac{\tilde{x}}{r_c}}{T_w(\tilde{x}) - T_m} \right)^3 \left(1 - \frac{\tilde{x}}{2r_c}\right) d\tilde{x} \right. \\
&\left. - \frac{\int_{-L}^{L} x \left(\frac{1 - \frac{x}{r_c}}{T_w(x) - T_m} \right)^3 \left(1 - \frac{x}{2r_c}\right) dx}{\int_{-L}^{L} \left(\frac{1 - \frac{x}{r_c}}{T_w(x) - T_m} \right)^3 dx} \int_x^L \left(\frac{1 - \frac{\tilde{x}}{r_c}}{T_w(\tilde{x}) - T_m} \right)^3 d\tilde{x} \right) x dx
\end{aligned}
\tag{3.35}
$$

$$0 = \int_{-L}^{L} \left(\int_{x}^{L} \tilde{x} \left(\frac{1 - \frac{x}{r_c}}{T_w(x) - T_m} \right)^3 \left(1 - \frac{\tilde{x}}{2r_c} \right) d\tilde{x} \right.$$
$$\left. - \frac{\int_{-L}^{L} x \left(\frac{1-\frac{x}{r_c}}{T_w(x)-T_m} \right)^3 \left(1 - \frac{x}{2r_c} \right) dx}{\int_{-L}^{L} \left(\frac{1-\frac{x}{r_c}}{T_w(x)-T_m} \right)^3 dx} \int_{x}^{L} \left(\frac{1 - \frac{\tilde{x}}{r_c}}{T_w(\tilde{x}) - T_m} \right)^3 d\tilde{x} \right) x dx \tag{3.36}$$

Since the curve radius does not depend on the melting velocity, as it was shown in equation (3.36), the suggested solution procedure to find both the melting velocity and curve radius for the ΔT-driven case is:

1. Initial guess of the velocity at the center of the heat source $U_0 > 0$ and the curve radius r_c.
2. Use (3.29) and (3.32) to find the root of (3.34), i.e. the curve radius for which the torque around the ice screw vanishes.
3. Solve (3.33) with (3.29), (3.32), the given ice screw force and the curve radius from step 2 to find the corresponding velocity at the center of the heat source U_0.

3.3.3 Alternative solution

There exists another way to obtain the curve radius. In equation (3.34) it was required that the torque around the ice screw must be zero. This can only be the case, if the pressure inside the melt film is distributed symmetrically. In this case the pressure gradient at the center of the heat source must be zero, i.e. $dp/dx|_{x=0} = 0$. Therefore, equation (3.23) can be rewritten

$$\left. \frac{dp}{dx} \right|_{x=0} = 0 = -\frac{12\mu_L \left[U_0 \cdot 0 \left(1 - \frac{0}{2r_c} \right) + C_4 \right]}{\delta^3(x)}$$
$$\Rightarrow C_4 \overset{!}{=} 0 \tag{3.37}$$

Substituting (3.37) in (3.27) yields

$$0 = \int_{-L}^{L} \frac{U_0 x}{\delta(x)^3} \left(1 - \frac{x}{2r_c} \right) dx$$
$$0 = \int_{-L}^{L} \frac{\tilde{x}}{\delta(x)^3} dx - \frac{1}{2r_c} \int_{-L}^{L} \frac{x^2}{\delta(x)^3} dx$$
$$0 = \frac{\int_{-L}^{L} \frac{x^2}{\delta(x)^3} dx}{2r_c \int_{-L}^{L} \frac{x}{\delta(x)^3} dx} - 1 \tag{3.38}$$

The melt film thickness distribution in (3.38) can be replaced by (3.32)

$$0 = \frac{\int_{-L}^{L} \frac{x^2 \left(1 - \frac{x}{r_c}\right)^3}{(T_w(x) - T_m)^3} dx}{2r_c \int_{-L}^{L} \frac{x \left(1 - \frac{x}{r_c}\right)^3}{(T_w(x) - T_m)^3} dx} - 1 \tag{3.39}$$

The curve radius can be obtained by finding the root of equation (3.39). It can be seen that the curve radius does only depend on 3 variables, namely the length of the heat source $2L$, the melting temperature of the PCM and the temperature distribution along the melting head, i.e. $r_c = f(L, T_m, T_w(x))$. Unfortunately, equation (3.39) has 4 roots in total (2 imaginary and 2 real values) as it can be seen in figure 3.5. However, the value of the real curve radius is always higher than the value of the other real root, which makes it possible to find the curve radius by numerical techniques from equation (3.39).

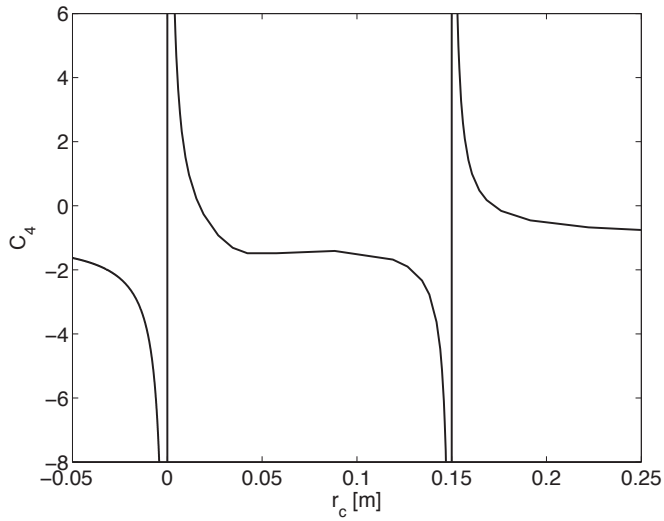

Figure 3.5: Plot of function (3.39) over r_c. The underlying temperature profile is $T_w(x) = 10\,°\mathrm{C} - 5\,°\mathrm{C} \cdot x/L$, where $L = 0.075\,\mathrm{m}$ and the melting temperature is $0\,°\mathrm{C}$.

3.4 Example results and comparison of the solution methods

In this subsection, some results of the numerical and approximate solution, which were derived in the previous subsections, will be shown and discussed. The equations were numerically solved with Matlab (see appendix F.3 for the source code). For describing the PCM, typical properties of water-ice were used, which are summarized in table 3.1. However, since the curve radius is independent of most of these properties, the results are also valid for other configurations, if the half-length L of the heat source, the melting temperature of the PCM T_m and the temperature profile along the heat source surface $T(x)$ are the same.

Symbol	Value	Unit	Comment
ρ_L	1000	$\mathrm{kg/m^3}$	density of the melt
k_L	0.57	$\mathrm{W/(m\,K)}$	thermal conductivity of the melt
$c_{p,L}$	4222.22	$\mathrm{J/(kg\ K)}$	specific heat of the melt
h_m	2.435×10^5	J/kg	latent heat of fusion
L	0.075	m	half the length of the rectangular heat source
T_S	-10	°C	ice temperature
T_m	0	°C	melting temperature
μ_L	0.001	$\mathrm{N\,s/m^2}$	dynamic viscosity of the melt

Table 3.1: Parameters, which are used for the example results. The thermo-physical properties correspond to the PCM water-ice.

Figure 3.7 shows the resulting curve radii for a rectangular heat source. The figure shows the results of the approximation (3.7) and close-contact melting theory using three different temperature profiles along the heat source surface. These are

linear temperature profile:

$$T(x) = T(0) - \frac{\Delta T}{2}\frac{x}{L} \tag{3.40}$$

cubic temperature profile:

$$T(x) = T(0) - \frac{\Delta T}{2}\left(\frac{x}{L}\right)^3 \tag{3.41}$$

step-function temperature profile:

$$T(x) = \begin{cases} T(0) - \frac{\Delta T}{2}, & \text{for} \quad x \geq 0 \\ T(0) + \frac{\Delta T}{2}, & \text{for} \quad x < 0 \end{cases} \tag{3.42}$$

in which x is the coordinate along the heat socrce surface starting at its center, $T(0)$ is the temperature at the center and ΔT is the difference between the maximum and minimum temperature. The temperature profiles are also visualized in figure 3.6.

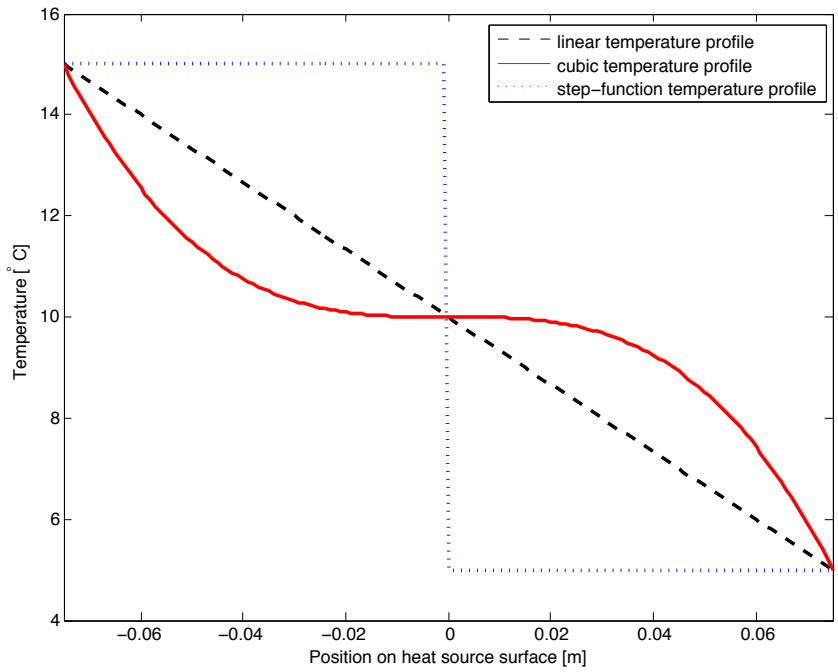

Figure 3.6: Visualization of the tested temperature profiles in figure 3.7. The curves were created using $T(0) = 10\,°\mathrm{C}$ and $\Delta T = 10\,°\mathrm{C}$.

Figure 3.7 shows that variations of the temperature difference along the heat source lead to higher or lower curve radii. The slope of the approximation and all temperature profiles is constant for all temperature gradients ΔT. A small curve radius is attained by a high temperature gradient and a small temperature at the center of the heat source wall. A large curve radius is the result, if the temperature gradient is small and the temperature at the center of the heat source surface is high. In the special case of $\Delta T \to 0$, $r_c \to \infty$, i.e. the path will be non-curved.

The resulting curve radius of the approximation is smaller than any curve radius using tem-

perature profiles. This is because the approximation does not include a temperature variation between the two point heat sources. In a real geometry, positions might exist, which slow down the rate of rotation due to the local temperature.

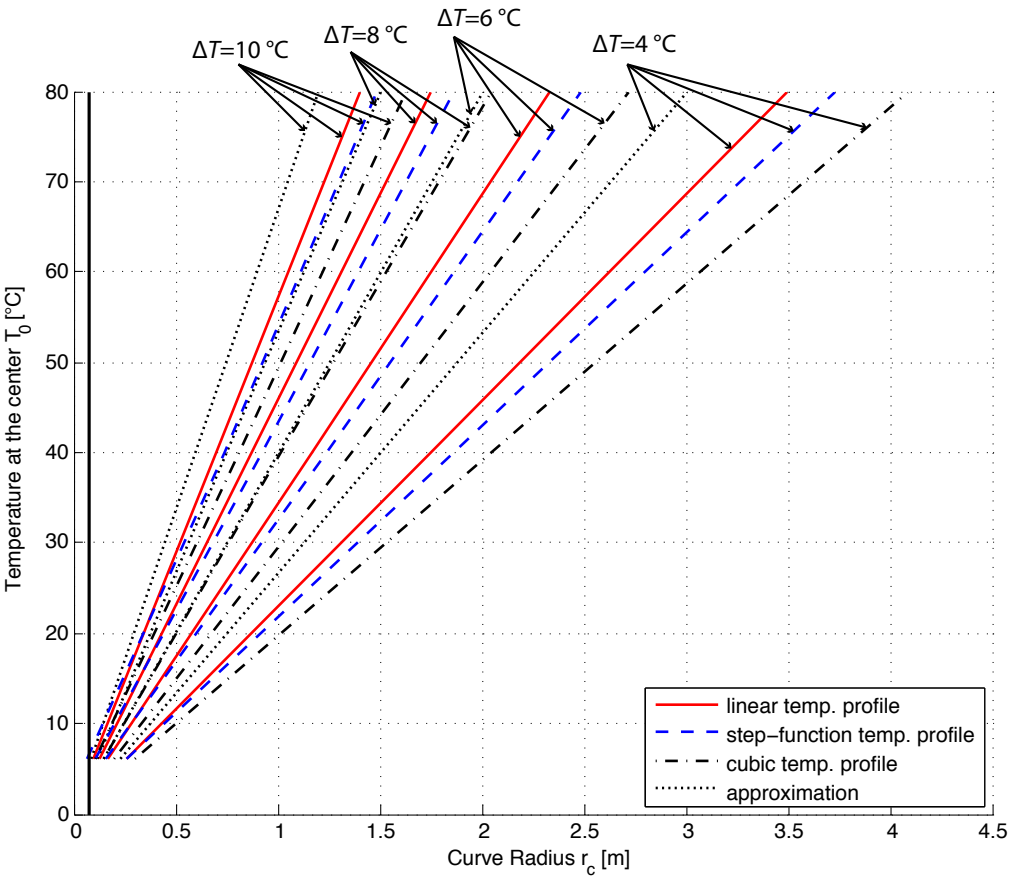

Figure 3.7: Curve radii for a rectangular heat source for ΔT-driven close-contact melting. The plot contains the results for three different temperature profiles: linear $T(x) = T_0 - (\Delta T/2)(x/L)$, step-function $T(x \geq 0) = T_0 - \Delta T/2$; $T(x < 0) = T_0 + \Delta T/2$ and cubic $T(x) = T_0 - (\Delta T/2)(x/L)^3$.

In figure 3.8, the corresponding curve radii for the rectangular and cylindrical (see appendix C) shaped heat source are shown. Two different temperature distributions were considered for the cylindrical heat source. A temperature profile, which changes linearly with the radian measure and a temperature profile, which would result by a parallel projection from a rectangular on a cylindrical surface.

It can be seen that the slope of the curve radius for cylindrical heat sources is constant, as it was also the case for the rectangular heat sources. This implies, that the slope is constant for any geometry.

The curve radii for the rectangular and cylindrical heat sources are nearly the same, if a projected temperature profile is used for the cylinder. They differ only a few millimeters, which might be the result of numerical errors. Since the torque is nearly the same for both geometries in the vicinity of the real curve radius, the pressure must be also distributed similarly, because the lever arms are the same along both geometries in Cartesian coordinates.

The curve radius for the cylindrical heat source with a temperature profile that changes linearly with the radian measure is the largest. The main reason for this is that the resulting torque is smaller for this temperature distribution.

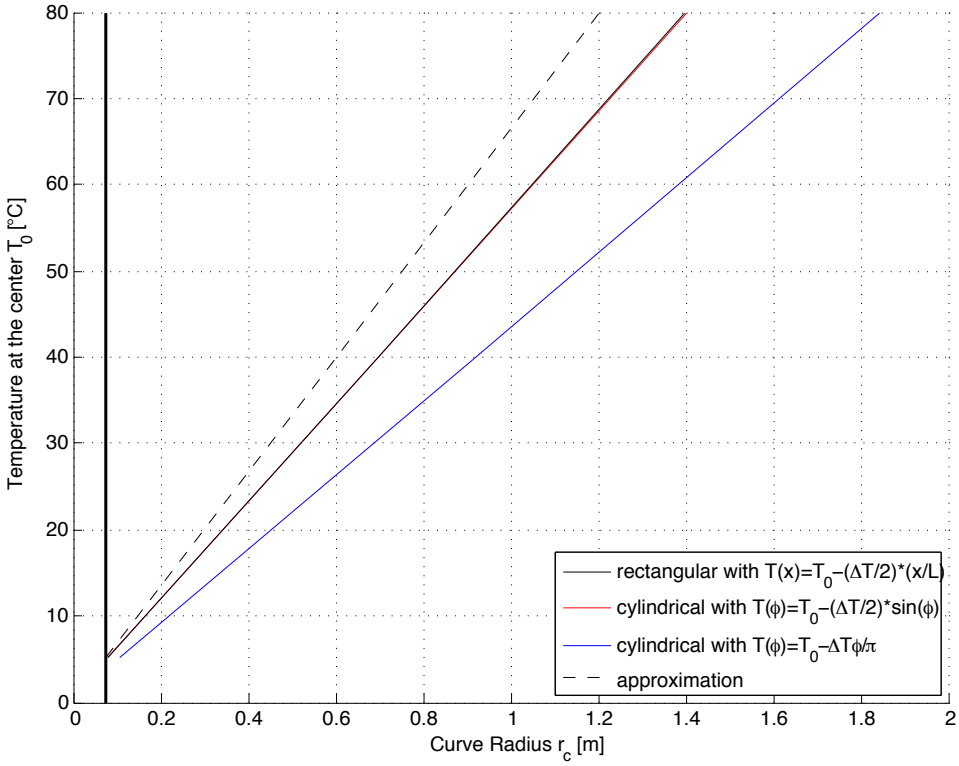

Figure 3.8: Comparison of the curve radii of a rectangular heat source and a cylindrical heat source for ΔT-driven close-contact melting, using the same temperature gradient $\Delta T = 10\,°\mathrm{C}$.

4 FEM Analysis

In section 2.3, various analytical solutions for close-contact melting problems have been derived. Unfortunately, the solutions are only applicable to very simple geometries with uniform boundary conditions. It is obvious, that the melting velocity can be extremely sensitive to changes in the heat transfer characteristics. For a real configuration, it is therefore necessary to model its geometry and heat transfer characteristics as good as possible to get reasonable results. One way to do this is to use FEM, because it allows to model complex geometries.

Close-contact melting is a multi-physical problem. Therefore, it is necessary to model all physical phenomena which are present, i.e. heat transfer with phase change and fluid dynamics to get reasonable results. Even advanced FEM tools which are developed to solve multi-physical problems, do not provide a ready-to-use solver for close-contact melting. Therefore, it is beneficial to use an open-source FEM software, because it allows full control over the implemented solvers. This was the main reason why Elmer has been chosen in this work.

In this section, the developed types of thermal analysis for melting probes using FEM will be presented. They can be categorized in static (subsection 4.1), kinematic (subsection 4.2) and dynamic (subsection 4.3) thermal analysis. After the fundamental model is described for the dynamic thermal analysis, the determination of the melt film thickness is explained in subsection 4.3.1, which is one of the key elements of the developed FEM model. To get an idea on how the model works, subsection 4.3.2 shows a descriptive example of the algorithm. Finally in subsection 4.3.3, it is shown how the developed model was implemented Elmer.

4.1 Static Analysis

The static thermal analysis of melting probes denotes an analysis including phase change but no motion. So it is basically an analysis, which is similar to the classical Stefan problem (see subsection 2.1), i.e. the velocity of the phase interface will continuously decrease.

There exist several ways to model phase change. Elmer also provides different methods to include phase change. In [Schüller, 2013] a method, which is based on a fixed-grid effective heat capacity method, has been chosen to include phase change, because it is one of the fastest methods available. The basic idea of the effective heat capacity method is to iteratively solve the heat equation, evaluate the resulting temperature field and assign a modified heat capacity to the nodes which are in a predefined temperature range in which the phase change occurs. So it is a nonlinear problem. For water-ice this temperature range should be chosen as small as possible. However, the smaller the temperature range, the larger the jump in the value of the heat capacity, which causes numerical difficulties. Therefore, the range should be chosen carefully. To calculate the effective heat capacity, it is necessary to know the enthalpy-temperature curve of the considered PCM. Elmer needs this quantity in a volume-specific declaration, i.e. $H = \rho h(T)$ in the units J/m^3. The modified value of the heat capacity is then calculated by [Raback et al.,

2014]

for steady-state simulations

$$c_{\text{eff}} = \frac{1}{\rho}\sqrt{\frac{\nabla H \cdot \nabla H}{\nabla T \cdot \nabla T}} \tag{4.1}$$

for transient simulations

$$c_{\text{eff}} = \frac{1}{\rho}\frac{\partial H/\partial t}{\partial T/\partial t} \tag{4.2}$$

What equations (4.1) and (4.2) basically do is spatial and time averaging[4] to ensure that no latent heat is lost if the node distances or time steps were chosen badly. The user must decide which equation should be used, because it depends on the mesh and the time step interval, which equation gives better results. Sometimes (4.1) gives even better results for transient simulations than (4.2), if the time steps were chosen small, but the mesh is too coarse.

4.2 Kinetic Analysis

The kinetic thermal analysis is based on the static analysis from section 4.1 with the extension, that the movement of the heat source is considered. In Elmer, this can be achieved by changing the sign of the expected heat source melting velocity and then use this value as the convection velocity for the PCM [Raback, 2013a]. This has the big advantage that a fixed-grid can still be used, which is beneficial for the computation time.

The convection velocity on the PCM will lead to a constant melt film thickness for $t \to \infty$. Therefore, it is also possible to do a steady-state analysis when using the kinetic model. And because the effective heat capacity method is used, the full geometry with the real boundary conditions (e.g. internal heat generation) can be solved. Furthermore, the refreezing behind the melting front is also considered in the simulation, which offers the opportunity to estimate[5] the melt film thickness along the wall of a melting probe for a given melting velocity.

4.3 Dynamic Analysis

The kinetic thermal model, which was presented in the previous subsection 4.2 has the disadvantage that it can be used only if the melting velocity is known a priori. But usually, this is not the case. One possibility to obtain the melting velocity using the kinematic model would be to iteratively change the melting velocity until the melt film[6] below the melting head becomes narrow. However, this method has two disadvantages. The mesh must be very fine in the vicinity of the melting head, where the melt film is assumed to be narrow, which drastically increases the time for computation. But more importantly, the melting velocity strongly depends on the melt

[4] Please note that the spatial averaging is only possible, if equation (4.1) is solved numerically.

[5] Please note that the convection inside the melt film is not considered. If the melt film thickness is not small, this could give wrong results.

[6] The melt film is represented by values above melting temperature in the results of the kinematic analysis, because the PCM is treated as one domain.

film thickness, which makes it impossible to estimate the melting velocity using this method, because it is unknown.

A better approach is to use a dynamic thermal model, i.e. to consider the quantity of the known force exerted on the ice as an additional parameter in the simulation, as it is already done in close-contact melting theory (subsection 2.3). Therefore it is necessary to not only consider heat transfer, but also fluid dynamics. This requires to split the PCM in two domains, namely the solid domain Ω_S, in which only heat transfer is present, and the liquid domain Ω_L, in which heat transfer in combination with fluid flow is occurs.

One possibility to do this could be to use a variable grid, which iteratively transforms during calculation to subdivide the two domains exactly at the phase interface. Then it would be possible to solve the Navier–Stokes equations or, if the inertial forces can be neglected, the Stokes equations for the liquid domain. But such an implementation would be extremely difficult and time consuming.

Because the melt film thickness is narrow in the vicinity of the hot point, which drives the melting velocity, it is also possible to use a fixed grid instead and treat the domain of the melt only at the boundary between the PCM and the heat source as it is shown in figure 4.1.

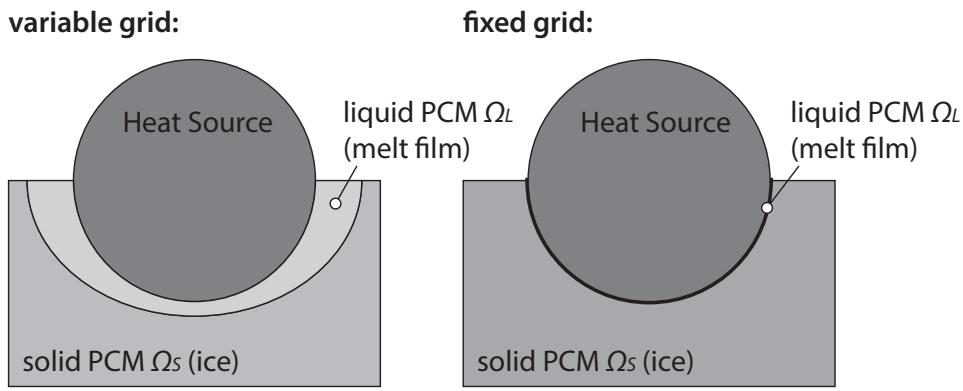

Figure 4.1: Difference between the dynamic thermal model domains using the variable grid and the fixed grid. In the case of using the variable grid, the melt film has to be adapted during the simulation, whereas using a fixed grid approach, the boundary between the PCM and the heat source is used to describe the melt film.

Using the fixed-grid approach, reduces the dimension of the fluid flow by one, i.e. the fluid flow dimension would be 1 (line) in a 2-dimensional geometry and 2 (surface) in a 3-dimensional geometry. Similar to close-contact melting theory (subsection 2.3), the full Navier-Stokes equations can then be simplified. The result is the so-called Reynolds equation, in which the pressure and viscous terms predominate. Following [Raback et al., 2014], the Reynolds Equation available in Elmer is given by[7]

$$\nabla \cdot \left(\frac{\rho_L \delta^3}{12\mu_L} \nabla p \right) = \frac{1}{2} \nabla \cdot (\rho_L \delta v_t) + \delta \frac{\partial \rho}{\partial t} + \rho_L v_n \tag{4.3}$$

[7]The derivation of the Reynolds equation both from the Navier-Stokes together with the continuity equations and from laws of viscous flow together with the principle of mass conservation can be found in [Hamrock et al., 2004].

where μ_L is the dynamic viscosity, δ is the melt film thickness or gap height, v_t is the tangential and v_n the normal velocity in the direction of the surface normal. The pressure p depends on two coordinates in a 3-dimensional geometry and on one coordinate in a 2-dimensional geometry.

The quasi-stationary Reynolds equation, which has to be solved by Elmer for close-contact melting problems can be found by removing the time-derivative of the density ($\partial\rho/\partial t = 0$ for stationary problems) and the tangential velocity v_t (no-slip condition) in (4.3)

$$\nabla \cdot \left(\frac{\rho_L \delta^3}{12\mu_L} \nabla p \right) = \rho_L v_n \tag{4.4}$$

The term on the left in equation (4.4) describes the net flow rates due to pressure gradients in the melt film. The term on the right describe the inflow due to melting.

For a better readability, the following equations will be given for a 2-dimensional geometry. Equation (4.4) then simplifies to

$$\frac{\partial}{\partial x} \left(\frac{\rho_L \delta^3}{12\mu_L} \frac{\partial p}{\partial x} \right) = \rho_L v_n \tag{4.5}$$

Equation (4.5) reproduces the pressure gradient along the melt film of the analytical solutions (e.g. (2.19)), if $\partial p(0)/\partial x = 0$ is assumed and the respective normal velocity v_n is used.

In order to solve (4.5) with Elmer, it is necessary to provide the normal velocity and melt film thickness. The normal velocity is the product of the local velocity and the local component of the heat source surface unit normal parallel to the melting direction, as it is shown in figure 4.2.

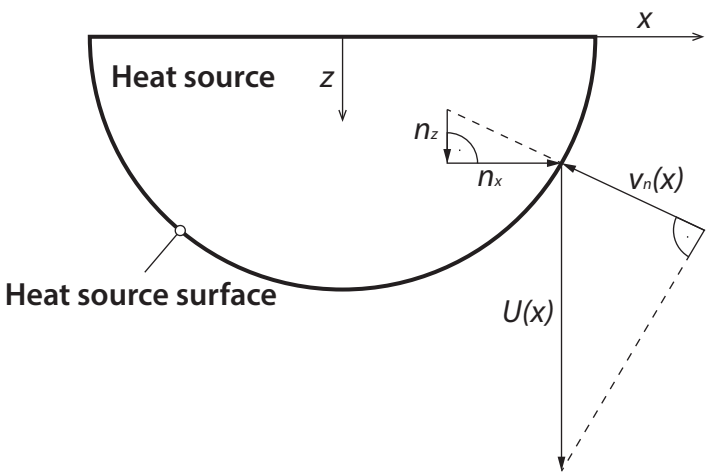

Figure 4.2: Determination of the normal velocity. The normal velocity is the product of the local velocity $v_n(x)$ and the local component of the heat source surface unit normal parallel to the melting direction $\hat{n}_z(x)$.

Using the linear velocity profile (3.22) and considering phase-dependent densities (i.e. the velocity of the melt and the rate at which the phase interface moves must differ due to conservation

of mass), the normal velocity is given by

$$v_n(x) = -\frac{\rho_S}{\rho_L} U(x)\hat{n}_z(x) = -\frac{\rho_S}{\rho_L} U_0 \left(1 - \frac{x}{r_c}\right) \hat{n}_z(x) \tag{4.6}$$

in which $\hat{n}_z(x)$ is the local component of the unit normal parallel to the melting direction.

In Elmer, the normal along the heat source surface can be computed by using an additional solver (`NormalSolver`).

4.3.1 Computation of the melt film thickness

The dimension of the melt film is reduced and therefore represented by the interface between the heat source wall and the PCM. The heat equation is solved in the PCM only. Nevertheless, by using the correct boundary condition at the phase interface, the liquid PCM is included implicitly. Figure 4.3 shows the temperature and heat flux distribution of the 1-dimensional two-phase Stefan problem at an arbitrary time, which is similar to the heat transfer of the considered close-contact melting problem, when ξ goes from an arbitrary position at the heat source wall through the liquid and solid phase of the PCM.

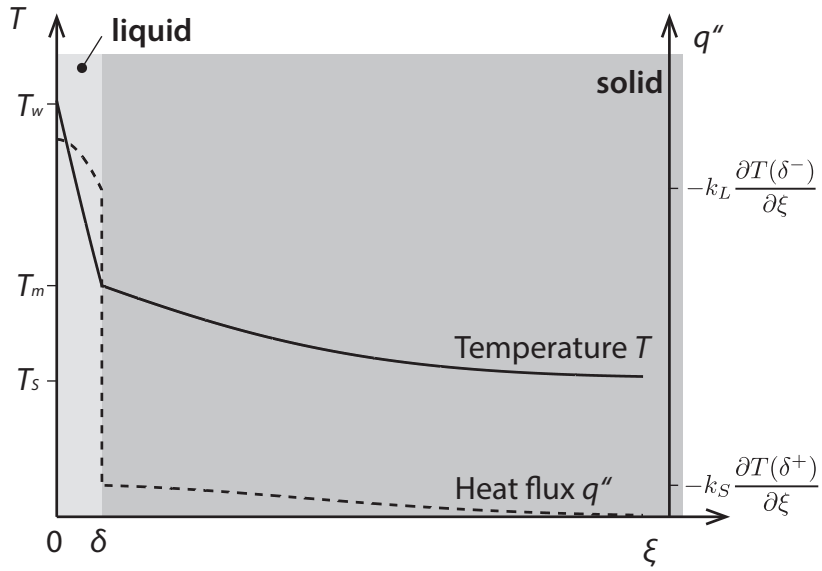

Figure 4.3: Temperature and heat flux distribution of the 1-dimensional two-phase Stefan problem at an arbitrary time. At the phase interface δ the phase change causes a jump in heat flux, which must be equal to the difference of the heat fluxes at the liquid side δ^- and the solid side δ^+ in the vicinity of the phase interface.

From figure 4.3 it follows, that the general 1-dimensional Stefan condition (2.1) for the considered situation is

$$\rho_S h_m U(x) = -k_L \frac{\partial T(\delta^-)}{\partial \xi} + k_S \frac{\partial T(\delta^+)}{\partial \xi} \tag{4.7}$$

in which ξ is the coordinate normal to the heat source surface through the melt film, $-k_L \partial T(\delta^-)/\partial\xi$ is the heat flux at the liquid side of the phase interface and $-k_S \partial T(\delta^+)/\partial\xi$ is the heat flux at the solid side of the phase interface.

Since the Stefan number is small for the considered PCM (water-ice), it is assumed that the temperature profile in the melt film can be approximated by a linear polynomial, as it was also done in [Moallemi & Viskanta, 1986]. Other than shown in figure 4.3, this would result in a constant heat flux through the melt film. Then, the heat flux at the liquid side is given by

$$-k_L \frac{\partial T(\delta^-)}{\partial \xi} = -k_L \frac{T_m - T_w}{\delta(x)} \tag{4.8}$$

Substituting (4.8) in the Stefan condition (4.7) yields

$$-k_S \frac{\partial T(\delta^+)}{\partial \xi} = -k_L \frac{T_m - T_w}{\delta(x)} - \rho_S h_m U(x) \tag{4.9}$$

Equation (4.9) is the required boundary condition (Neumann) at the phase interface to include the liquid domain implicitly, when the heat equation is only solved in the solid domain.

Starting with an initial guess for the melt film thickness $\delta_0(x)$, the melt film thickness can be found by solving the heat equation in the solid domain Ω_S, evaluating the resulting temperature at the interface between the heat source wall and the solid domain and iteratively change the boundary condition (4.9) at this interface until its temperature is equal to the melting temperature of the modeled PCM. The adjusted melt film thickness after each iteration can be found by [Raback, 2013b]

$$\delta_{i+1}(x) = \delta_i \left[1 + \lambda \left(C - 1\right)\right] \tag{4.10}$$

$$C = \frac{T_w(x) - T_m}{T_w(x) - T(x, \delta_i(x))} \tag{4.11}$$

in which λ is a user-defined relaxation factor to improve convergence.

4.3.2 Descriptive example of the algorithm

To get a better idea on how the iterative procedure to find the melt film thickness works, a simple 1-dimensional example will be considered in the following, in which a semi-infinite heat source melts through a semi-infinite PCM. The situation is shown in figure 4.4.

The 1-dimensional heat equation for the considered example is given by

$$-U_0 \frac{\partial T(\xi)}{\partial \xi} = \alpha_S \frac{\partial^2 T(\xi)}{\partial \xi^2} \qquad \text{for } \delta \leq \xi < \infty \tag{4.12}$$

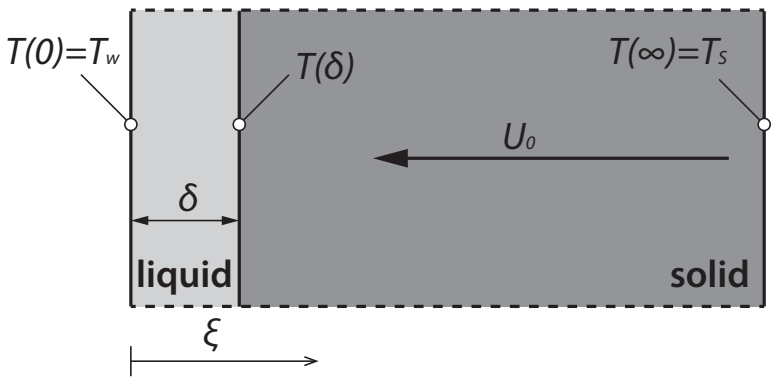

Figure 4.4: Variables and coordinates of the 1-dimensional ΔT-driven close-contact melting example.

The boundary conditions are

$$\text{at } \xi \to \infty: \qquad T(\infty) = T_S \tag{4.13}$$

$$-k_S \frac{\partial T(\xi)}{\partial \xi}\bigg|_{\xi\to\infty} = 0 \tag{4.14}$$

$$\text{at } \xi = \delta: \qquad -k_S \frac{\partial T(\xi)}{\partial \xi}\bigg|_{\xi=\delta} = -k_L \frac{T_m - T_w}{\delta} - \rho_S h_m U_0 \tag{4.15}$$

Integration of (4.12) yields

$$T(\xi) = -\frac{\alpha_S}{U_0}\frac{\partial T(\xi)}{\partial \xi} + C_1 \tag{4.16}$$

The integration constant C_1 is found by substituting the boundary conditions (4.13) and (4.14) into (4.16)

$$T_S = 0 + C_1 \qquad \Rightarrow C_1 = T_S \tag{4.17}$$

The temperature at $\xi = 0$ is found by substituting (4.15) into (4.16)

$$T(\delta) = \frac{\alpha_S}{U_0 k_S}\left(-k_L \frac{T_m - T_w}{\delta} - \rho_S h_m U_0\right) + T_S \tag{4.18}$$

Equation (4.18) has the big disadvantage that there is no limitation of the resulting temperature at the phase interface $T(\delta)$. This physically invalid property brings some numerical difficulties for the iterative procedure to calculate the melt film thickness, because $T(\delta) \to \infty$ for $\delta \to 0$.

A better approach is to define the heat flux due to the heat source wall temperature through the melt film as a convective boundary condition (Robin boundary condition), because then $T(\delta)$ will not exceed the wall temperature T_w, even if $\delta \to \infty$. The modified heat flux at the liquid

side of the phase interface is then

$$
\begin{aligned}
-k_L \frac{\partial T(\delta^-)}{\partial \xi} &= \kappa(T(\delta) - T_w) \\
&= -\frac{k_L}{\delta}(T(\delta) - T_w)
\end{aligned}
\tag{4.19}
$$

Substituting the term $-k_L(T_m - T_w)/\delta(x)$ in the temperature profile (4.18) by (4.19) yields

$$
T(\delta) = \frac{k_L T_w + \delta U_0 (\frac{k_S}{\alpha_S} T_S - \rho_S h_m)}{\delta U_0 \frac{k_S}{\alpha_S} + k_L} \tag{4.20}
$$

Figure 4.5 shows the temperature at the phase interface for different values of δ. It can be seen that the equation using a Neumann boundary condition (4.18) and the equation using a Robin boundary condition (4.20) intersect at 0 °C (melting temperature). So both equation can be used to obtain the melt film thickness. But it pointed out that the iteration procedure (4.10) does only work reliably when using the Robin boundary condition as it is shown in figure 4.6.

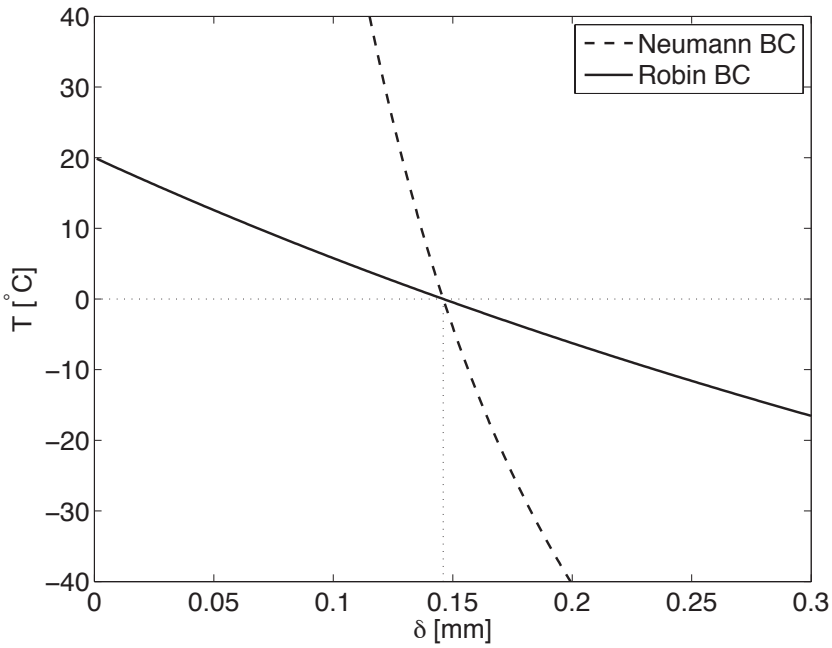

Figure 4.5: Temperature over melt film thickness for a 1-dimensional ΔT-driven close-contact melting example. The temperature using a Neumann boundary condition (4.18) and the temperature using a Robin boundary condition (4.20) intersect exactly at the melting temperature. The melt film thickness at this point is the solution for the considered parameters ($U_0 = 1\,\mathrm{m/h}$, $T_S = -20\,°\mathrm{C}$, $T_w = 20\,°\mathrm{C}$, $k_L = 0.57\,\mathrm{W/(m\,K)}$, $k_S = 2.18\,\mathrm{W/(m\,K)}$, $\rho_S = 1000\,\mathrm{kg/m^3}$, $c_{p,S} = 2049.41\,\mathrm{J/(kg\,K)}$).

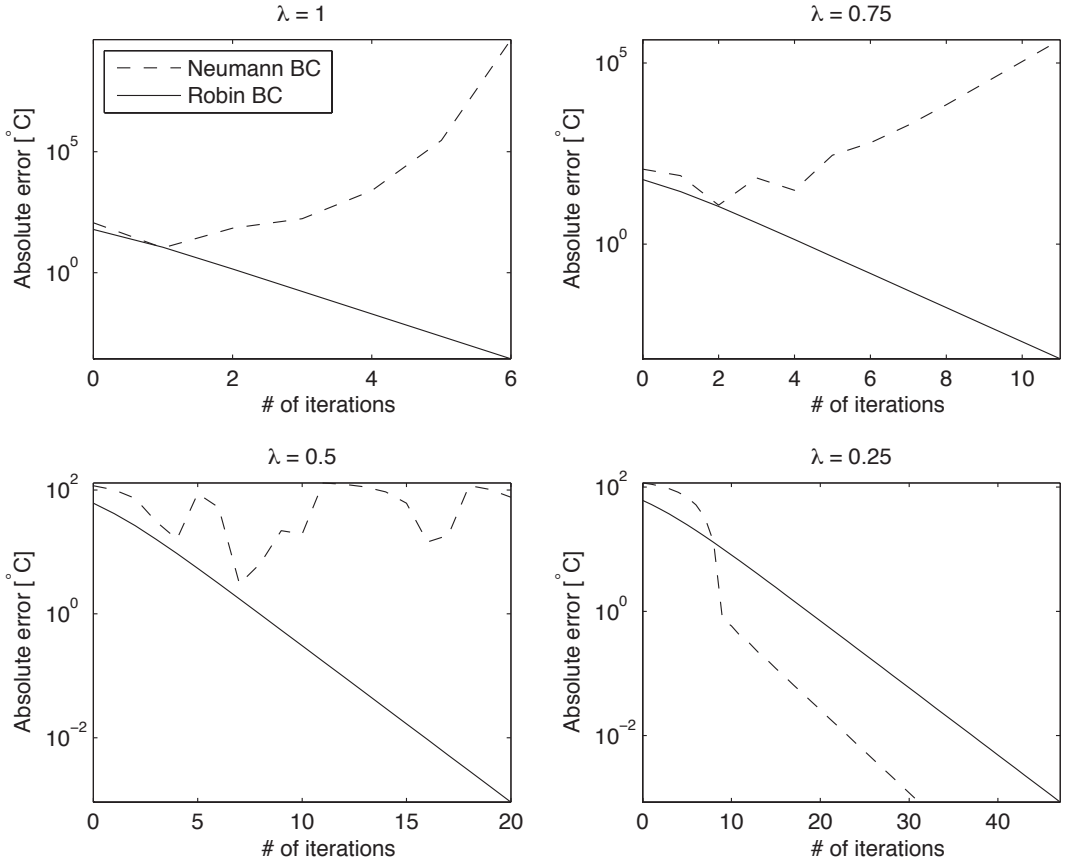

Figure 4.6: Convergence for different relaxation factors for a 1-dimensional ΔT-driven close-contact melting example. The temperature using a Robin boundary condition (4.20) converges for all relaxation factors, whereas for the temperature using a Neumann boundary condition (4.18) convergence is not guaranteed.
Parameters: $U_0 = 1\,\mathrm{m/h}$, $T_S = -20\,°\mathrm{C}$, $T_w = 20\,°\mathrm{C}$, $k_L = 0.57\,\mathrm{W/(m\,K)}$, $k_S = 2.18\,\mathrm{W/(m\,K)}$, $\rho_S = 1000\,\mathrm{kg/m^3}$, $c_{p,S} = 2049.41\,\mathrm{J/(kg\,K)}$

Table 4.1 shows the iteration steps for a 1-dimensional ΔT-driven close-contact melting example, in which the PCM consists of water-ice. The heat source wall temperature is $T_w = 20\,°\mathrm{C}$ and the ice temperature is $T_S = -20\,°\mathrm{C}$. For a melting velocity of $U_0 = 1\,\mathrm{m/h}$ and some standard [Myers et al., 2008] thermophysical properties for the liquid and solid phase of water-ice, the resulting melt film thickness after 6 iterations is $146.01\,\mu\mathrm{m}$.

i	δ_i [m] (4.10)	$T_i(\delta)$ [°C] (4.20)	C [–] (4.11)
0	0.00100000	-61.06011540	0.24673047
1	0.00024673	-11.25440939	0.63990971
2	0.00015789	-1.42177879	0.93362928
3	0.00014741	-0.16911128	0.99161533
4	0.00014617	-0.01996594	0.99900270
5	0.00014602	-0.00235518	0.99988225
6	0.00014601	-0.00027779	0.99998611

Table 4.1: Iteration steps to obtain the melt film thickness for a 1-dimensional ΔT-driven close-contact melting example.
Parameters: $\lambda = 1$, $U_0 = 1\,\mathrm{m/h}$, $T_S = -20\,°\mathrm{C}$, $T_w = 20\,°\mathrm{C}$, $k_L = 0.57\,\mathrm{W/(m\,K)}$, $k_S = 2.18\,\mathrm{W/(m\,K)}$, $\rho_S = 1000\,\mathrm{kg/m^3}$, $c_{p,S} = 2049.41\,\mathrm{J/(kg\,K)}$

4.3.3 Implementation in Elmer

To solve close-contact melting problems in Elmer, a mesh must be provided, which contains the surrounding PCM with the interface to a not necessarily included heat source, i.e. there must be one body in total. However, during mesh generation, the heat source is needed to produce[8] this interface. In the presented approach, computation time is not increased by the fact, that no equation has to be solved for the heat source body. Therefore, it was not removed from the meshes, which are used in this thesis.

To apply the required boundary conditions, the mesh must provide a set of boundaries. The set is the same for 2- and 3-dimensional geometries, but with the difference that the dimensions of the boundaries must be increased by one for 3-dimensional geometries. A schematic of the required meshes to solve close-contact melting problems in Elmer is shown in figure 4.7.

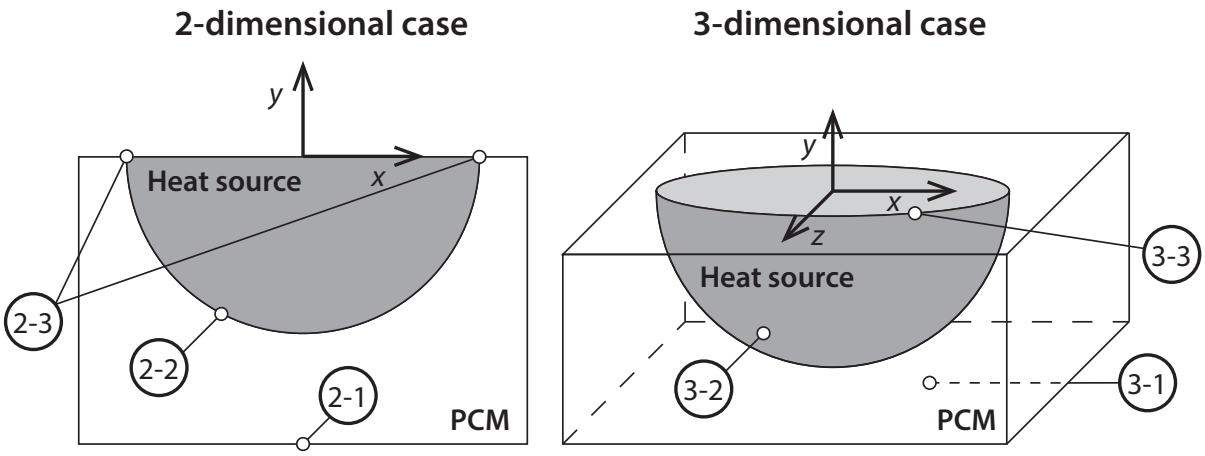

ID	Geometry	Description
2-1	line	ice temperature T_S
2-2	line	heat source to PCM interface
2-3	point	atmospheric pressure p_{atm} at the outer locations of the interface
3-1	surface	ice temperature T_S
3-2	surface	heat source to PCM interface
3-3	line	atmospheric pressure p_{atm}

Figure 4.7: Required boundaries for solving 2 and 3-dimensional close-contact melting problems in Elmer. The IDs were freely chosen here for description and have no relation to the values of the IDs, which are used in the simulation.

To control Elmer, it is necessary to provide a so-called solver input file (SIF). This file contains all information about initial- and boundary conditions, parameters, mesh location and solvers, which are necessary to solve the considered problem. The SIF to solve close-contact melting problems must contain several solvers and subroutines to find the melting velocity for a given temperature on a heat source surface and 2 additional subroutines to save the results. These are (in the order of execution):

[8] The final PCM geometry is created by subtracting (boolean operator) the heat source geometry from the PCM geometry.

1. `NormalSolver:NormalSolver` to compute the normals on the heat source surface (executed only once)
2. `HeatSolve:HeatSolver` to solve the heat equation in the solid domain, which is necessary to determine the melt film thickness
3. `ReynoldsSolver:ReynoldsSolver` to solve Reynolds equation in the liquid domain
4. `ReynoldsSolver:ReynoldsPostprocess` to compute the force and the torque from the solution of Reynolds equation
5. `SaveData:SaveScalars` to save the velocity, minimum and maximum melt film thickness, force and torque after every iteration
6. `SaveData:SaveLine` to save the melt film thickness distribution after every iteration
7. `FindOptimum:FindOptimum` to adjust the melting velocity or curve radius for the next iteration

In order to find both the melting velocity and the curve radius, two different SIFs are needed. One for the melting velocity and one for the curve radius. In the case of rectilinear melting, i.e. when the boundary condition on the heat source is distributed symmetrically, it is not necessary to compute the curve radius, since it is already known ($r_c \to \infty$). In section 3.3.3, it was shown that the curve radius does not depend on the melting velocity. However, other than the theoretical model, in which the ice is included implicitly by using the reduced latent heat of melting, the FEM model explicitly solves the heat equation for the ice. Due to this fundamental difference, the curve radius might not be independent of the melting velocity and the ice temperature in the case of the FEM solution. Therefore, an outside iteration loop is used, in which the curve radius from the last iteration is used in the SIF to calculate the melting velocity iteratively until it converges.

The overall simulation, i.e. in which sequence the solvers are executed and how they interact with each other to find the melting velocity and curve radius is shown in figure 4.8. Starting from the computation of the normals along the heat source surface and an initial guess of the melt film thickness, melting velocity and curve radius, the first step is to solve the heat equation iteratively to obtain the melt film thickness.

To calculate the melt film thickness, it is necessary to provide not only the Stefan boundary condition (4.7), but also the Robin boundary condition (4.19), in which the melt film thickness dependent heat transfer coefficient is changed after every iteration.

For the calculation of the Robin boundary condition, a so-called user defined function (UDF) written in Fortran90 (see appendix D) is used, which is used to calculate first the melt film thickness using equation (4.10) and then the corresponding heat transfer coefficient $\kappa = -k_L/\delta$ for every node at the interface between the heat source and the PCM.

While the heat equation is solved for several times, the temperature at the phase interface converges to the melting temperature. When a predefined convergence tolerance is achieved,

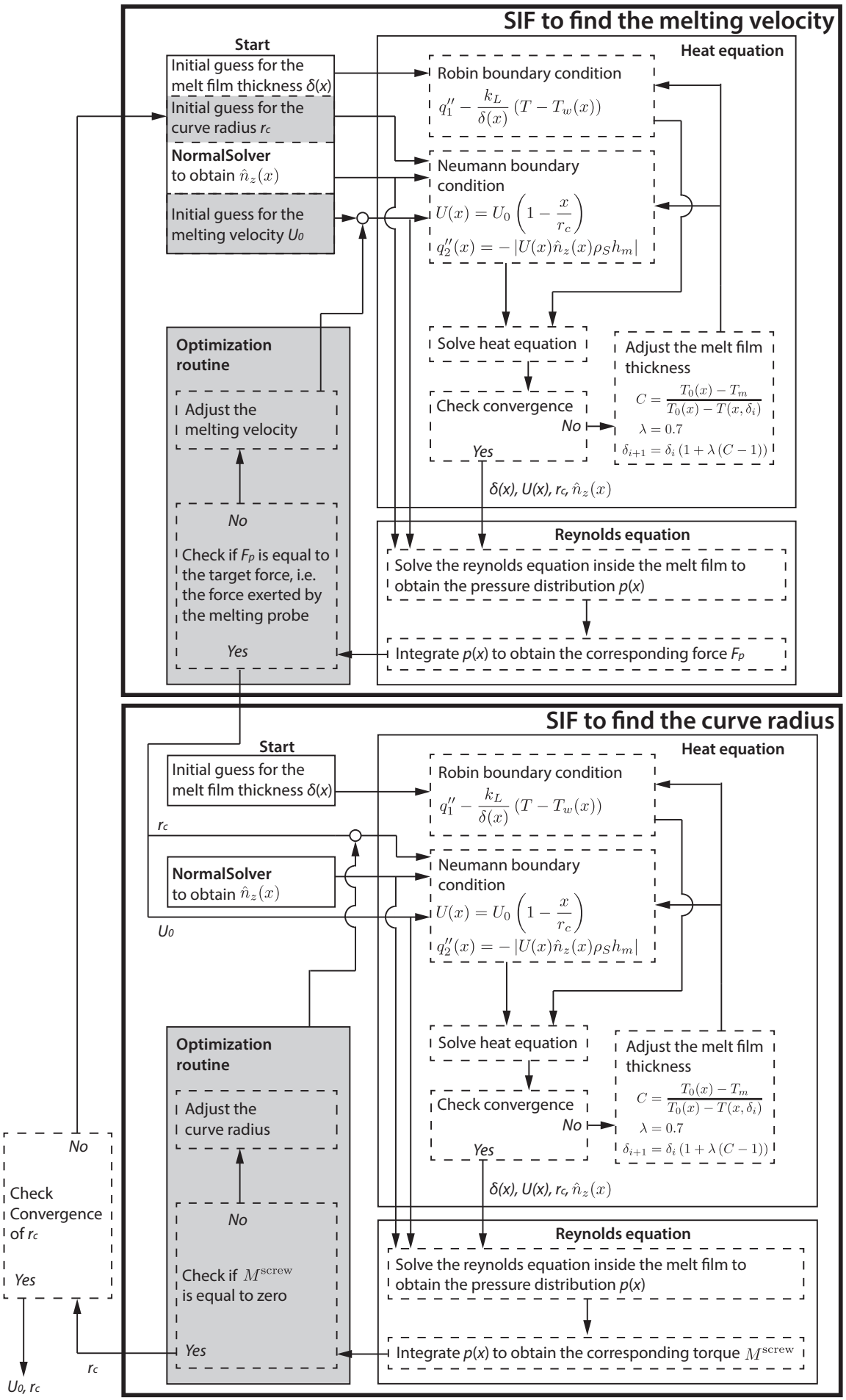

Figure 4.8: Flow sheet of the overall simulation to obtain the melting velocity and curve radius.

the iteration loop will be interrupted and the melt film thickness, which also converges to a certain value, of the last iteration will be used as an input to solve the reynolds equation.

The reynolds equation requires the pressure at the outer regions of the interface between the heat source and the PCM. This is normally the ambient pressure or just zero, if it is small compared to the film pressure. Additionally, the melt mass flow must be considered. Therefore, the normal velocity must be specified, which is the product of the density radio ρ_S/ρ_L, the local melting velocity and the local component of the heat source surface unit normal parallel to the melting direction (4.6).

The solution of the reynolds equation is the pressure distribution in the melt film, from which the resulting force (integration of the pressure distribution over the melt film) and the torque around a predefined location (integration of the pressure distribution multiplied with the tangential coordinate over the melt film) can be calculated by the `ReynoldsPostprocess` subroutine.

An optimization routine then uses the force or torque to adjust either the melting velocity or the curve radius by secant method for the next iteration until the respective value converges. In the case of finding the melting velocity, it is helpful to make use of the linear dependency between the logarithm of the force and the logarithm of the velocity to increase convergence and therefore computation time. The implemented optimization routine uses this dependency and outputs the result into a variable called `logVelo`, which has the value of $\log U_0$. Therefore, it is necessary to use `logVelo` as an exponent to the base 10, if the velocity should be used somewhere in the SIF, i.e. $U_0 = 10^{\texttt{logVelo}}$. The optimization routine to find the curve radius for which the torque around a predefined location vanishes does not make use of any linearized dependency and the output can therefore be used directly in the SIF. It is important to define the minimum curve radius in the optimization routine as the half-length of the heat source to prevent numerical errors.

The output of the SIF to find the melting rate (melting velocity and initial guess of the curve radius) is used as an input for the SIF to find the curve radius. The output of the SIF to find the curve radius (curve radius) is used as an input for the SIF to find the melting velocity. This repeats as long as a predefined convergence tolerance for the curve radius is not achieved. If the convergence tolerance is achieved, the curve radius and the melting velocity were found.

5 Experimental investigation

In order to validate the theoretical and FEM model, experiments must be conducted with a real melting device. Unfortunately, the IceMole is not a good choice for this task, because its length will have a huge influence on the resulting curve radius and the models do not include any effects resulting from the length of the considered heat source. Moreover, its dimensions do not allow laboratory tests, in which the probe is fully surrounded by ice.

Therefore, a melting device has been developed and constructed, which is similar to the IceMole but less complex in geometry and in its thermo-physical properties. Starting with the general design overview of this device in subsection 5.1, the experimental setup will be presented in subsection 5.2. The measurement hardware and the data acquisition is described in subsection 5.3. Since the used sensor setup does not allow for a direct measurement of the curve radius, subsection 5.4 shows the method, which was used for the determination of the curve radius from the available data. In subsection 5.5, the first experimental results are discussed and a final configuration is chosen for the required set of experiments to validate the theoretical and FEM model. This set is presented in subsection 5.6. Finally in subsection 5.7, the measured data and the determination of the curve radius is shown for one example experiment.

5.1 General design overview

The requirements to the curvilinear melting experiment (CME) are mainly dictated by the underlying assumptions of the FEM model. These are

- differential heating
- continuously acting force normal to the heat source surface
- determination of the applied boundary condition and the melting trajectory
- center of mass must be located in the geometric center
- small height to reduce geometric effects on the curvilinear melting characteristics
- high thermal diffusivity

Furthermore, the CME must be waterproof to a depth of $\approx 0.2\,\mathrm{m}$, because inflowing water could destroy the inner electronics.

The final design of the CME is shown in figure 5.1 and the corresponding drawings can be found in appendix G. The measured overall mass of the CME is 3.2 kg. It is a cuboid of copper with a heating front area of $150 \times 80\,\mathrm{mm}$ and a height of 45 mm. The smaller sides (80 mm) are tilted by $5°$ to reduce the geometrical effect of the walls on the curve radius. Four heater inlets are placed inside the CME on the heating front area. Each inlet contains one heating cartridge with the power of 200 W, which are used for differential heating. Below each inlet is a blind hole containing one DS1820 digital temperature sensor to measure the applied boundary condition, which is of the Dirichlet type, i.e. the surface temperature. The distance of the hole grounds

to the outer surface is 2 mm to prevent cold spots on the heating surface. So the temperature sensors do not exactly measure the temperature of the outer surface. On top of the heater inlets is the IMU board bracket located, on which the IMU is mounted. The CME is covered by an aluminum plate to ensure that no water flows in during the melting process. The power cables and data lines are passed through two holes in the plate. To measure the distance by an encoder, a hook-like device is used, which is glued on top of the plate near to the CME's center (not included in figure 5.1). In the middle of the CME is a through hole, which is used for three different configurations, i.e. to leave it as it is or to position either an ice-screw or a bolt.

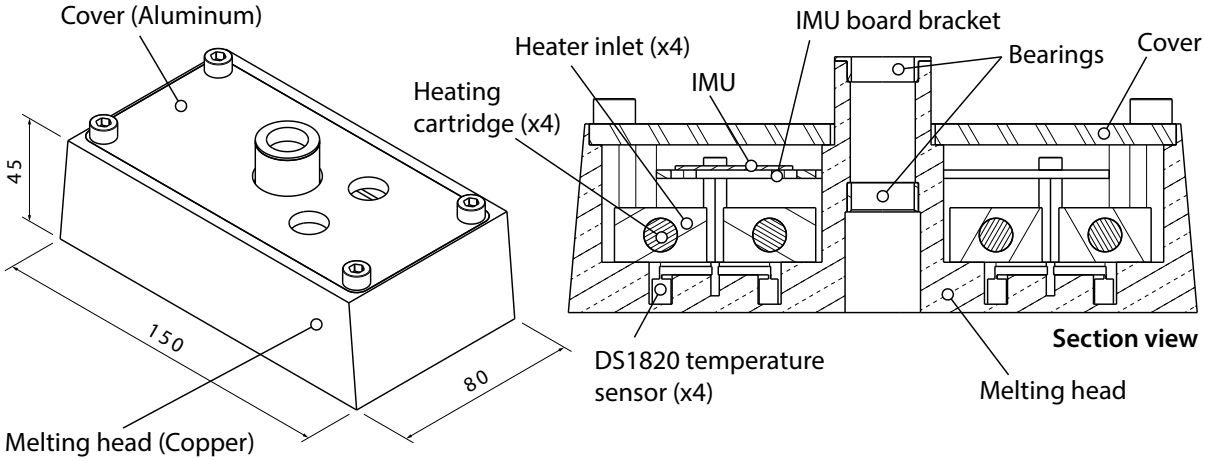

Figure 5.1: Isometric (left) and section view (right) of the assembled CME (dimensions in millimeters).

Figure 5.2 shows a photography of the interior of the assembled CME and the numbering of the heaters, which is used by the software for control. The numbering goes from 1 to 4 and starts left (left is defined as the position where the IMU is placed). There are three connectors in total inside of the CME. One for the IMU data lines and two to power the heating cartridges, where each connector combines either heater 1 and 2 or heater 3 and 4.

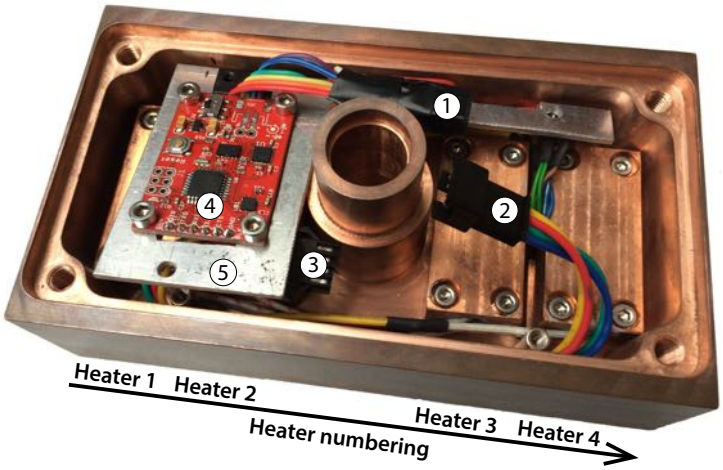

Figure 5.2: Photography of the interior of the assembled CME and the numbering of the heaters. The numbering of the heaters used in the software goes from left (heater 1) to right (heater 4). Heater 1 and 2 are covered by the IMU board bracket (5) and the IMU (4). Three connectors are inside of the CME: IMU connector (1), connector for heater 1 and 2 (2) and connector for heater 3 and 4 (3).

5.2 Experimental setup

The general experimental setup is shown in figure 5.3. The data lines of the CME (IMU and temperature sensors) are connected to an Arduino UNO, which is placed near to a computer outside of the CME. A 4-channel relay module, which is controlled by the Arduino UNO, is used to switch the heating cartridges separately on and off. A certain switching pattern is used to maintain a predefined temperature profile along the heating front of the CME. On top of the CME is a fishing line connected, which is used to rotate the shaft of an encoder as the CME melts into the ice. The rotation of the shaft is then processed by the Arduino UNO. Inside of the ice are three additional temperature sensors to measure the ice temperature, which are also connected to the Arduino UNO.

The Arduino UNO is connected to the computer via USB for serial communication. On the computer runs a Matlab-based graphical user interface (GUI), which was written to set the temperature profile along the CME's heating front. Furthermore, it is used to monitor and log the data, which will be send by the Arduino UNO every two seconds. Since the GUI is able to take, display and save pictures in a predefined time interval, it is also possible to connect a camera to the computer.

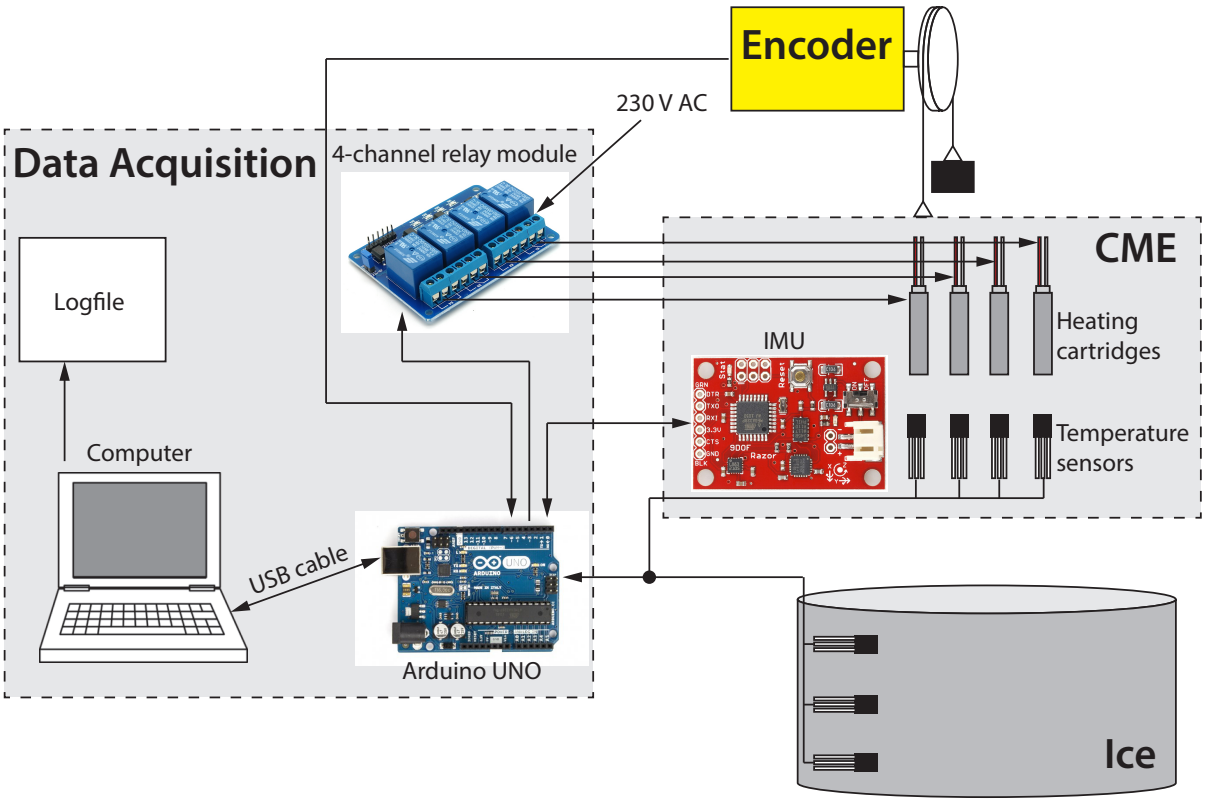

Figure 5.3: Overview of the experimental setup.

5.3 Measurement hardware and data acquisition

For the determination of the melting trajectory and the applied boundary conditions, several types of sensors are used.

The surface temperature is measured by 4 DS1820 one-wire digital temperature sensors. Using this type of temperature sensors has the big advantage, that only three wires are necessary to read all temperatures, because they can be connected in series. Moreover, they provide an accuracy of $\pm 0.5\,°\mathrm{C}$ at a temperature range of $-10\,°\mathrm{C}$ to $+85\,°\mathrm{C}$ and an accuracy of $\pm 2\,°\mathrm{C}$ at a temperature range of $-55\,°\mathrm{C}$ to $+125\,°\mathrm{C}$ without calibration. To read out the temperature sensors with the Arduino UNO, an external library (Arduino Library for Dallas Temperature ICs[9]) has been used.

The melting trajectory is determined by post-processing the inclination of the CME and its vertical distance. How this post-processing works will be described in section 5.4.

The distance is measured by an incremental shaft encoder, which provides 500 counts per revolution. It is placed above the CME and redirects a fishing line. One end of the fishing line is connected to the CME and the other is connected to a mass (a nut is used). The center of the fishing line is placed on the shaft of the encoder. So when the CME melts into ice, the fishing line moves and forces the shaft to rotate due to static friction. As the shaft rotates, it transmits a logical signal at a certain time interval, which is counted by the Arduino UNO. The total amount of counts is then further processed by the GUI into a distance. This is done by multiplying the counts with a conversion factor, which has been experimentally determined by measuring the distance manually and dividing this value by the displayed counts.

To measure the inclination of the CME, the so-called 9DOF-arduIMU (also called Razor IMU) is used. It interfaces a micro-controller with three different sensors (accelerometer, gyro and magnetometer) to directly produce a serial output of the Euler angles. The board comes programmed with the 8 MHz Arduino bootloader and some example firmware that demos the outputs of all the sensors. There exist several firmwares, which include calibration to improve the IMU's performance. However, for the CME, the original firmware is used and the calibration is done externally via the GUI. Therefore, the inclination angle from the IMU was compared to a manually measured inclination angle. This was repeated for several angles. The result is an error curve for the inclination angle, which is used to compensate the error.

5.4 Determination of the curve radius from experimental data

To determine the curve radius, the melting trajectory must be known. One possible way to determine the trajectory would be to measure the deflection angle of the fishing line that is connected to the CME and redirected by the encoder. The sine or cosine of the deflection angle multiplied with the distance gives then the horizontal or vertical position. Unfortunately, the deflection angle will be very small. Therefore, a sensor with a very high resolution would be needed, which would be too expensive.

Another way to determine the melting trajectory is to evaluate the distance and the inclination angle of the CME incrementally at all time steps, as it is shown in figure 5.4. The difference of the distance at a time step i is denoted as ΔL_i. The trajectory begins at position p_0 and follows a vertical line of the length $\Delta L_0 = L_1 - L_0$, which ends at position p_1. At p_1, the trajectory

[9] https://github.com/milesburton/Arduino-Temperature-Control-Library (October 2014)

moves on, but this time in the direction of the current inclination angle ϕ_1. The length of this straight line, which begins at p_1 and ends at p_2, is $\Delta L_1 \cos\phi_1$. This repeats for all time steps until the full melting trajectory is determined.

The curve radius is determined by the intersection points of normals on the melting trajectory. Since there will not be one point, in which all normals intersect, the average of the coordinates of the intersection points is used. The distance of the initial position of the CME to this point is the curve radius.

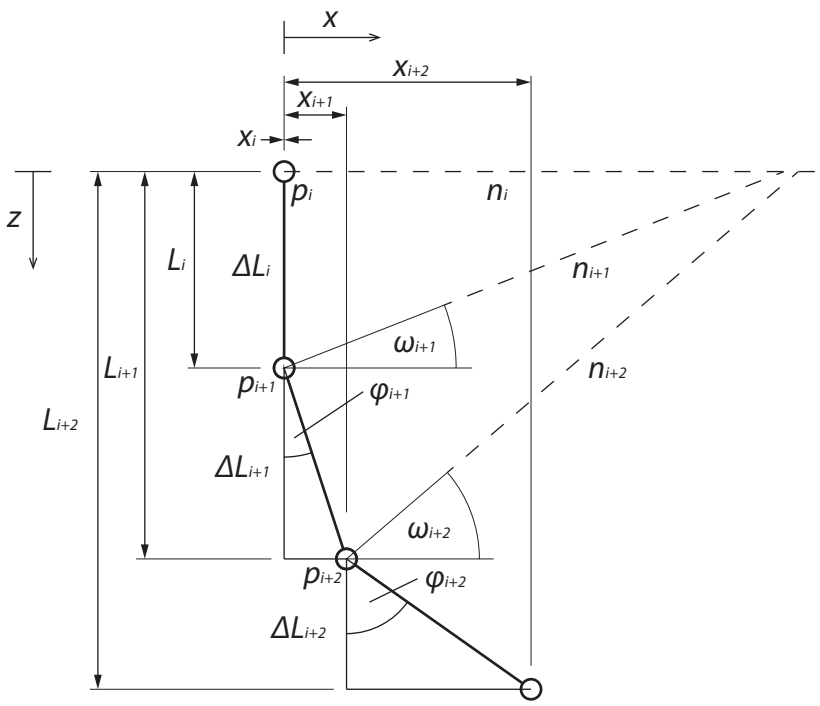

Figure 5.4: Determination of the curve radius from the distance and the inclination angle.

5.5 First experimental results and determination of the final configuration

For the very first experiment, the CME was configured with an ice-screw that had a screw length of 60 mm, as it is shown in figure 5.5. A torque wrench was used to control the exerted torque on the screw. It turned out that a torque of 28 Nm or higher values is necessary to ensure that the CME is continuously in contact with the ice. This is because of the low temperature of the ice ($\approx -20\,°$C). In combination with the low heat transfer from the CME into the long ice-screw, this caused the screw to freeze in. For a temperature gradient of 6 °C (starting at a minimum temperature of 4 °C) along the CME's heating front, the overall inclination angle was only 2 ° at a depth of 170 mm, which is far too small compared to the FEM model. At this point it was clear, that the ice-screw introduces effects on the curve radius, which would cause huge differences compared to the results of the FEM model. Therefore, this configuration was excluded from the planned set of experiments.

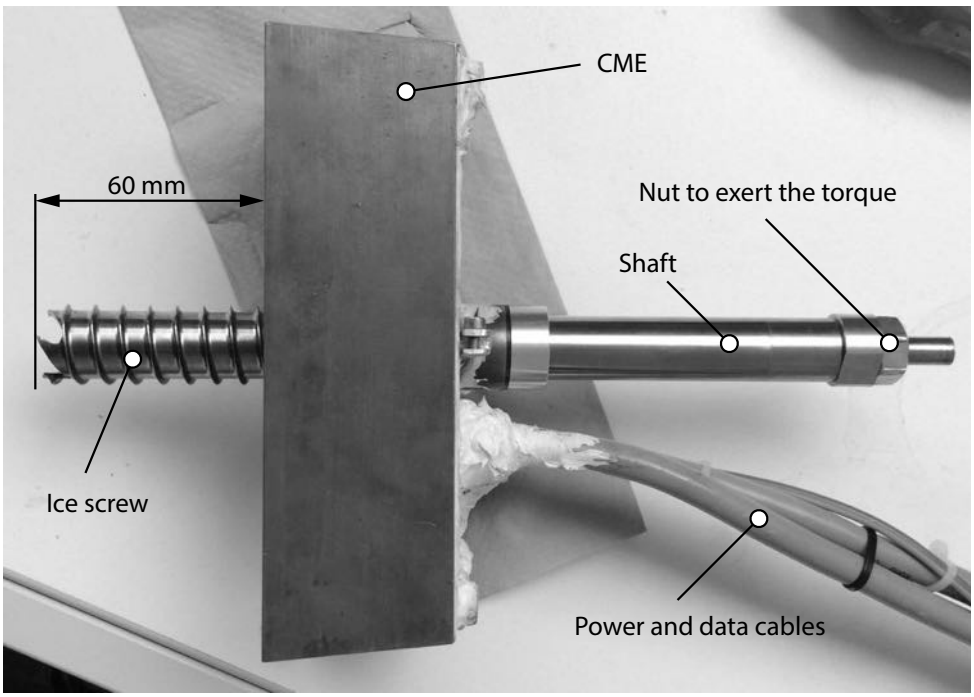

Figure 5.5: Configuration with an ice-screw inserted into the CME.

The second configuration was without an ice-screw. So there is no normal force continuously exerted on the CME, which will result in no[10] horizontal motion during melting. However, at the initial phase of melting, the weight of the CME acts nearly normal to its heating front, because the inclination angle is small. So a real melting trajectory can be reproduced by considering only the initial phase of the CME without an ice-screw.

Compared to the configuration with an ice-screw, the inclination angle was considerably larger (28 ° at a depth of 170 mm) for the same temperature profile along the CME's heating front. But the hole through the CME causes an interesting effect, which is shown in figure 5.7. It turned out, that an ice core builds up in the hole, as the CME melts through the ice. This core forces the CME to move horizontally, which was not expected since the exerted force of the CME (its weight) acts continuously in vertical direction. Unfortunately, the core breaks at a certain interval, which causes an oscillation in the inclination angle. Therefore, this configuration was also excluded from the planned set of experiments.

[10] A small horizontal motion is caused by sliding of the CME due to the slope of the ice below.

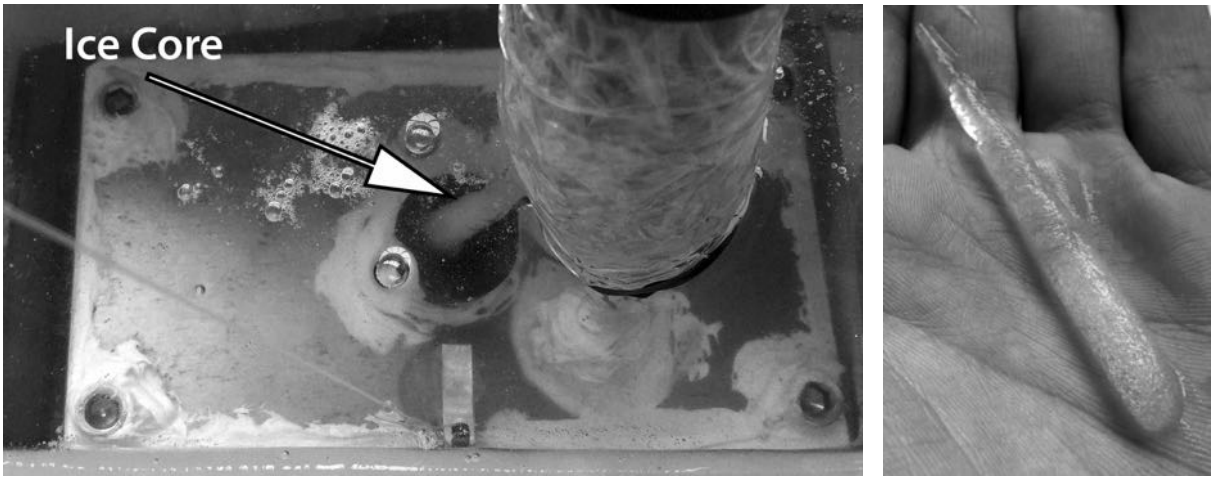

(a) (b)

Figure 5.6: Pictures of the ice core that builds up for the CME configuration without an ice-screw or a bolt in its center hole. (a) shows the core building up during the experiment and (b) shows the broken core.

The third configuration was to use a bolt of copper instead of an ice-screw to reproduce a plane heating surface. After the first tests, it turned out that this configuration works best.

Figure 5.7(b) shows the final configuration, which was used for all following experiments. It is the third configuration with a bolt instead of the ice-screw. The bolt was later equipped with a DS1820 temperature sensor to increase the resolution of the measured temperature profile along the heating surface.

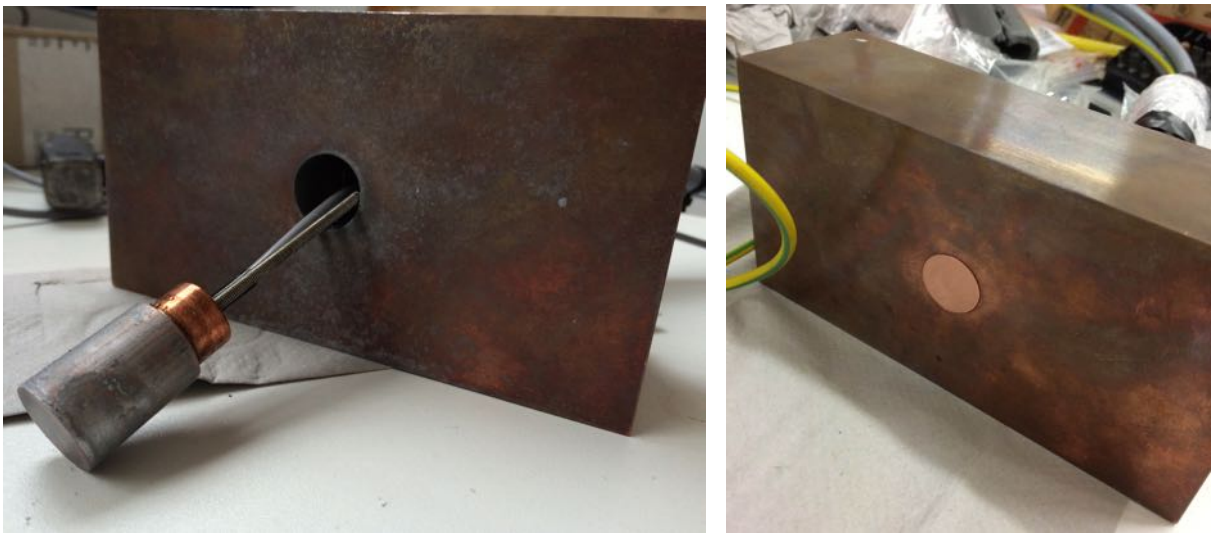

(a) (b)

Figure 5.7: Configuration with a bolt inserted into the CME. (a) shows the bolt covered with heat paste before it is inserted into the CME. (b) shows the heating front with the bolt inserted.

5.6 Overview of all conducted experiments

The validation of the FEM model requires several experiments with different temperature profiles along the CME's heating front. It turned out, that there is a limitation of about 18 °C for the maximum attainable temperature. This limitation is mainly driven by the power of the heating cartridges in combination with the mass of the CME, i.e. the pressure exerted on the melt film below.

Table 5.1 gives an overview of all conducted experiments (a chronological overview in given in appendix B). The columns define the minimum temperature $T_{\min}$ and the rows define the overall temperature difference ΔT along the CME's heating front for a linear temperature profile of the form

$$T(x) = T_{\min} - \frac{\Delta T}{2}\left(\frac{x}{L} + 1\right) \tag{5.1}$$

where x goes from $-L$ to L (L is half the length of the heating front, i.e. $L = 7.5\,\mathrm{cm}$).

$T_{\min}$ \ ΔT	0 °C	4 °C	6 °C	8 °C
0 °C	–	–	1(a)	–
2 °C	1(a)	2(a)	2(a)	2(a)
5 °C	1(a)	–	–	–
4 °C	–	2(a)	3(a) 2(b) 1(c)	2(a)
6 °C	–	5(a)	–	–
10 °C	1(a)	–	–	–
12 °C	1(a)	–	–	–
max	2(a)	–	–	–

Table 5.1: Amount of experiments for different temperature gradients and minimum temperatures (a) with bolt (b) without bolt (c) with ice screw in the central hole of the melting head.

For rectilinear melting ($\Delta T = 0$), 6 experiments were conducted in total. Because there was no considerable variation between the 2 experiments with maximum temperature, all other vertical melting experiments were only conducted once.

The experiments with a non-zero temperature gradient ($\Delta T \neq 0$) were conducted more than once for the same temperature profile. This is because the inclination angle highly depends on the exerted torque on the CME. Even though, the cables of the CME were positioned in a way that this torque is minimized, they introduce one with a value that changes stochastically from experiment to experiment. This results in a total number of 19 experiments using the bolt-configuration with three different non-zero temperature gradients.

5.7 Example results and post-processing

Because a detailed discussion of all conducted experiments would go beyond the scope of this thesis, the aim of this section is to give the idea on how the results look like by presenting the

results of an exemplary experiment.

The predefined linear temperature profile (5.1) for this experiment was given by a temperature gradient of $\Delta T = 6\,°\mathrm{C}$ and a minimum temperature of $T_{\mathrm{min}} = 4\,°\mathrm{C}$. The measurement of the ice temperature over time is shown in figure 5.8. It can be seen that the ice temperature increases continuously with time. At $t = 0$, the temperature in the middle of the ice is is about $4\,°\mathrm{C}$ smaller than the temperatures measured near to the top and near to the bottom of the ice, which are nearly equal. This difference comes from the installation time, which is not included in figure 5.8, in combination with the thermal diffusivity of the ice. Due to the CME, which is placed on top of the ice, the measured temperature near to the top increases faster than the temperature near to the bottom of the ice.

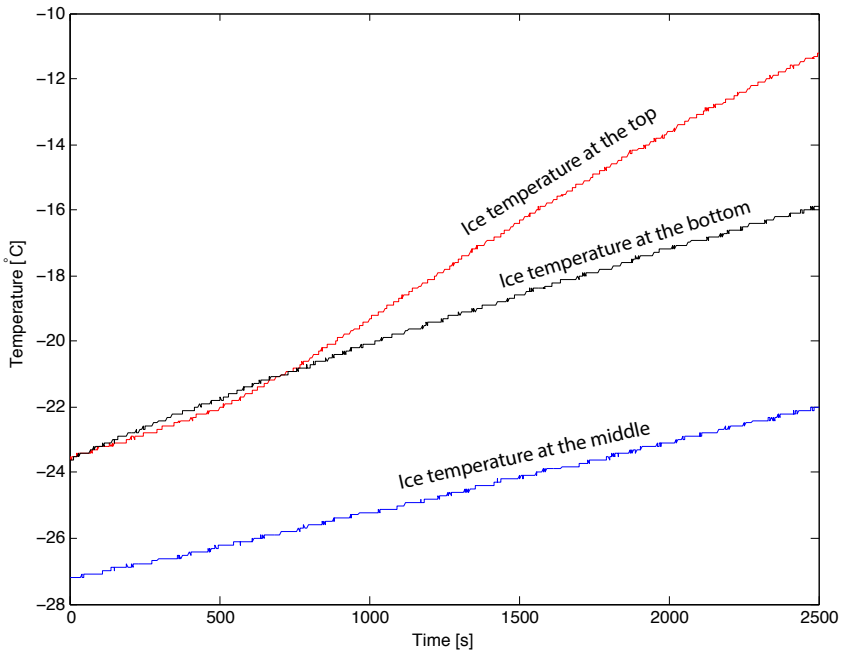

Figure 5.8: Plot of the measured ice temperature distribution over time.

Figure 5.9 shows the measured temperatures at the heating front of the CME for the considered setup. To improve readability, the presented range goes from 0 to 300 seconds. All temperature measurements show oscillations, which come from the switching patterns of the heating cartridges. Even though, the switch-off temperature is defined as the predefined target temperature, the temperature increases further until it reaches a certain value. The same can be observed for the switch-on point. This is because of the thermal diffusivity inside of the CME and the resulting delay of heat transfer. Because the temperature sensors were fixed using epoxy resin, the thermal diffusivity is even smaller in the vicinity of the sensors.

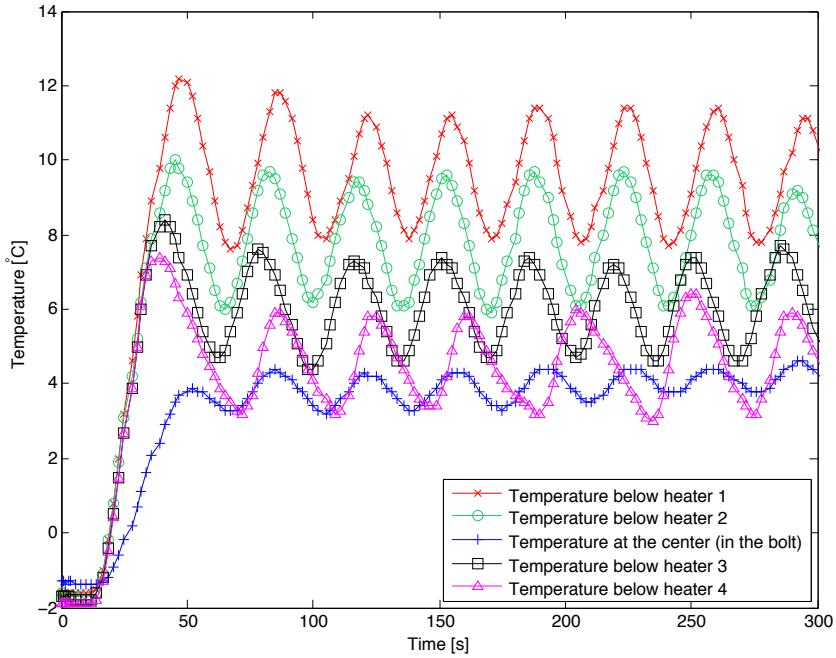

Figure 5.9: Plot of the measured temperatures over time.

However, since the measured temperatures oscillate around a nearly constant value, the overall temperature profile along the heating front can be determined by using the average of the temperature curves. Figure 5.10 illustrates the average of the measured temperature curves compared to the predefined temperature profile. It can be seen that the temperature in the center of the CME is smaller than the temperature using equation 5.1 at this position. There are two possible reasons for this. Since the temperature sensor at this position is located inside the bolt, the low temperature might result from a small heat transfer coefficient between the CME and the bolt, which is defined by the contact conditions. To increase the heat transfer coefficient, heat paste has been used at the interface. But there were no noticeable differences, which implies that the heat transfer coefficient is not the main reason for the too low temperature.

Another possible explanation is that the hole, in which the temperature sensor is located, has been drilled too deep into the bolt. It is expected that there is a high temperature gradient in the vicinity of a CME's heating front. Therefore, small changes in distance can cause remarkable differences in temperature.

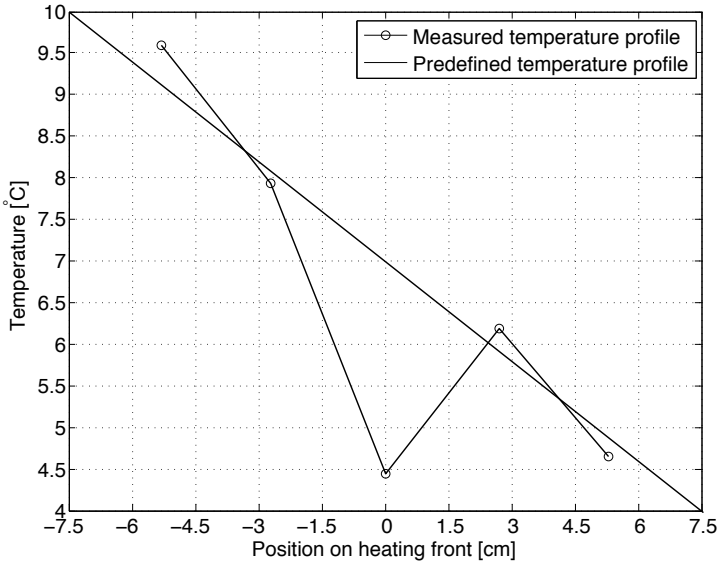

Figure 5.10: Comparison of the measured temperature profile with the target temperature profile.

Figure 5.11 shows the inclination angle and distance over time. It can be seen that the slope of the distance is nearly constant and the slope of the inclination angle shows some variations. Since the force is always acting in vertical direction and not normal to the heating front, the inclination angle will be constant after a certain time, which is denoted as the final phase. Before this angle is reached, the slope continuously decreases. It turned out that this range begins at an inclination angle of about 10 °. This range is also not considered for the determination of the curve radius. During the initial phase, the slope of the inclination angle continuously decreases until a stable slope is reached after about 4 minutes. At this point begins the range, which is used to calculate the curve radius until the range of decreasing slope is reached.

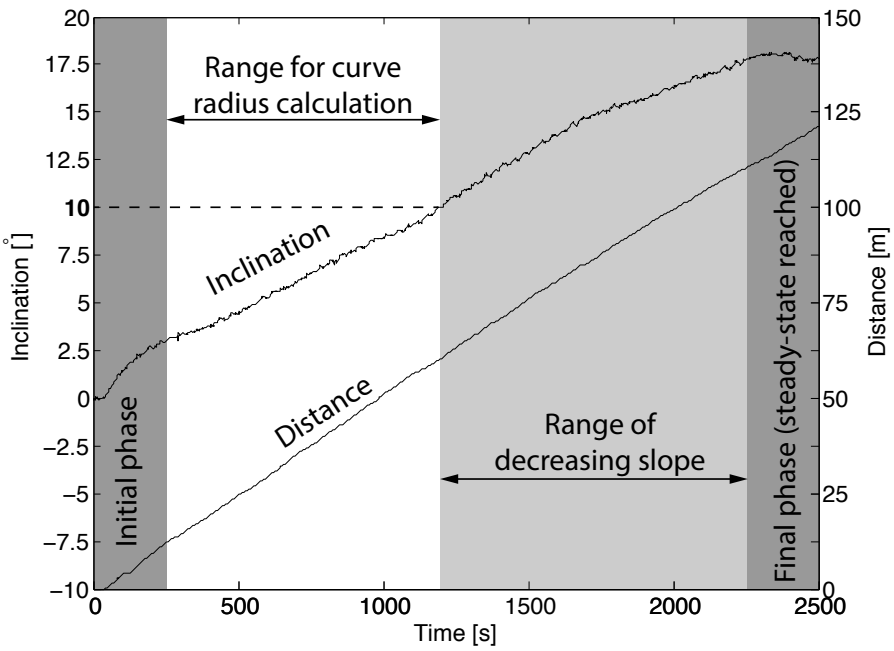

Figure 5.11: Measured inclination angle and distance over time.

The calculated melting trajectory and its normals using the method from section 5.4 are shown in figure 5.12. Note that the normals do not look like normals in the figure, because the axes are not aligned equally. It can be clearly seen that the normals along the melting trajectory intersect not in a point but in a certain region. The curve radius can be determined by averaging over all x-values of the intersections.

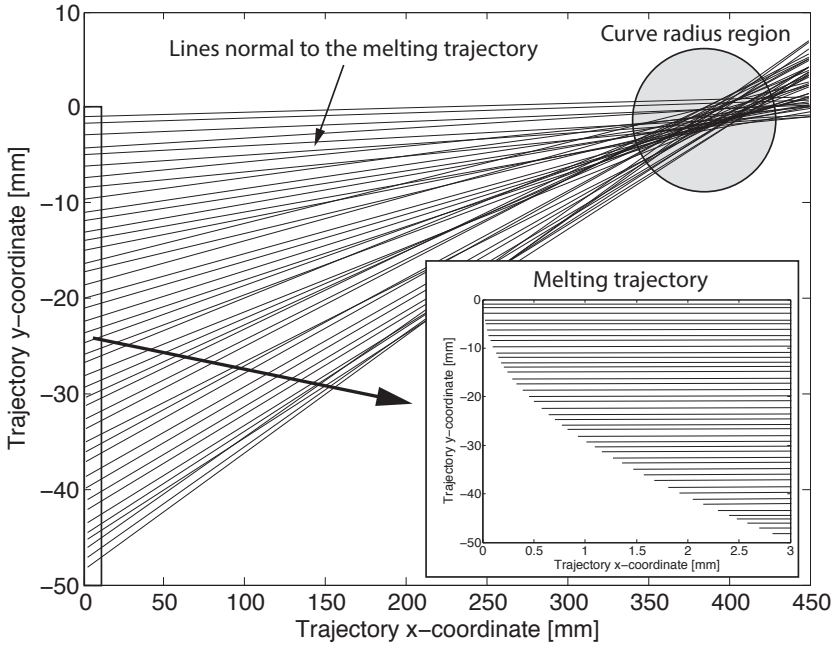

Figure 5.12: Calculated melting trajectory and determination of the curve radius from the measured inclunation angle and distance using the method presented in section 5.4.

6 Results and discussion

In this section, several results of the FEM model and the theoretical solution are presented and discussed. The results are compared with analytical and experimental solutions to validate the FEM model.

In subsection 6.1, the FEM model is compared with analytical solutions for simple geometries and also with experimental data, in terms of rectilinear melting. In subsection 6.2.1, the curvilinear melting results of the FEM model and the theoretical solution are compared to study the difference between them. Finally in subsection 6.2.2, the curve radii from the experiments are compared with the theoretical solution using Matlab.

6.1 Rectilinear melting

6.1.1 Comparison with analytical solutions

In section 2.3, in was shown that there exist analytical solutions to calculate the melting velocity for a given exerted force for simple geometries. The corresponding equations were

rectangular heat source

$$U_0 = \left(\frac{\alpha_L^3 f^3(\mathrm{Ste})}{8L^3 \mu_L} \hat{F} \right)^{1/4} \tag{6.1}$$

cylindrical heat source

$$U_0 = \left(\frac{5\alpha_L^3 f^3(\mathrm{Ste})}{16R^3 \mu_L} \hat{F} \right)^{1/4} \tag{6.2}$$

spherical heat source

$$U_0 = \left(\frac{2\alpha_L^3 \, f^3(\mathrm{Ste})}{\pi \, \mu_L \, R^4} F \right)^{1/4} \tag{6.3}$$

where $f^3(\mathrm{Ste}) \approx \mathrm{Ste}^3 = (c_{p,L}(T_w - T_m)/(h_m + c_{p,S}(T_m - T_S)))^3$ for small Ste, which is the case for water-ice.

The analytical solutions (6.1), (6.2) and (6.3) will now be used to validate the developed FEM model in terms of its ability to simulate the characteristics of rectilinear melting. Therefore, the corresponding geometries have been created and meshed using Salome, an open-source software to create FEM meshes. The thermo-physical properties which were used are summarized in table 6.1. Two different sets of parameters were then used for solving the problem in Elmer. The first set was with phase-independent thermo-physical properties as it is also assumed in the analytical solutions (equations (6.1) to (6.3)), i.e. the parameters for the liquid phase were also used for the corresponding parameters of the solid phase. The second set was with phase-dependent thermo-physical properties to show the differences of the more realistic calculation compared to the simplified assumptions of the analytical solutions.

The results are shown in figure 6.1. It can be seen that for the same exerted force, the melting velocity of the spherical heat source is much larger than the melting velocity of the cylindrical and rectangular heat source. But it must be noticed that in the case of 2-dimensional geometries, a force per length $\hat{F}$ must be used instead of just a force.

When comparing the results for the cylindrical and rectangular heat source, it can be seen that the melting velocity of the cylindrical heat source is larger. This is in accordance to the findings of Shreve [1962], that the melting velocity of the rectangular heat source is lower than any other geometry for the same surface temperature.

In the case of using phase-independent parameters, the simulation reproduces the analytical solutions. There is only a small error, which comes from predefined numerical tolerances used in the simulation. In the case of phase-independent parameters, the simulation gives higher velocities for the same exerted force. The main reason for this is that the difference in density was not considered in the derivation of the analytical solutions, i.e. it was assumed, that the rate at which ice melts is equal to the rate at which new melt is produced. But this is only valid for equal densities, because mass conservation requires that the mass flow is constant along the phase interface. When a PCM has phase-dependent densities, the rate at which ice melts and the rate at which new melt is produced must be different.

Parameter	Symbol	Value	Unit
ice temperature	T_S	-10	°C
heat source wall temperature	T_w	20	°C
heat source radius, half length	R,L	0.075	m
latent heat of melting	h_m	334000	J/kg
density of ice	ρ_S	920	kg/m^3
density of water	ρ_L	1000	kg/m^3
thermal conductivity of ice	k_S	2.18	W/(m K)
thermal conductivity of water	k_L	0.57	W/(m K)
heat capacity of ice	$c_{p,S}$	2049.41	J/(kg K)
heat capacity of water	$c_{p,L}$	4222.22	J/(kg K)
dynamic viscosity of water	μ_L	0.001	N s/m^2

Table 6.1: Parameters which were used for comparison of the results of the simulation with analytical solutions.

Transfered to a real melting probe, one may think that the melting velocity can be easily increased by increasing the exerted force, as it is shown in figure 6.1. But since the temperature on a heat source surface is limited by the available constant heating power, the surface temperature will decrease when the exerted force is increased, because the melt film thickness will be smaller.

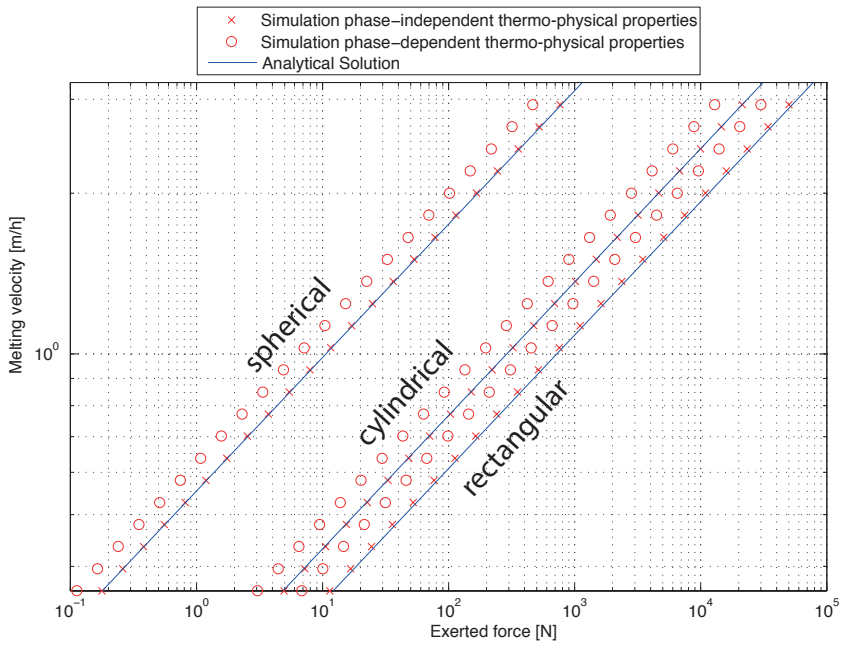

Figure 6.1: Comparison of the simulation results with analytical solutions for rectilinear melting. The plot shows the results of simulations using two different sets of parameters. The crosses are the results for phase-independent thermo-physical properties, i.e. the properties of water are also used for ice. The circles are the results for phase-dependent thermo-physical properties.

6.1.2 Comparison with experimental results

There were not only experimental configurations using a temperature gradient along the heating front of the CME but also some configurations in which no temperature gradient has been used, as it is shown in table 5.1. The reason for this set of conducted experiments was to have experimental data to study the ability of the FEM model to predict the melting velocity for a given surface temperature. Therefore, a FEM mesh has been created from a simplified geometry of the CME, which consists of a cuboid that has the same cross-sectional area of the heating front, i.e. a length of 150 mm and a width of 75 mm. All other dimensions (height of the CME and ice) were freely chosen. The thermo-physical properties from table 6.1 were used together with a set of different heating front temperatures and an exerted force of 32 N (CME's mass is 3.2 kg). To take care of the temperature increase of the ice during the melting, two different ice temperatures were used in the simulations, −15 °C and −20 °C.

The results are shown in figure 6.2. In addition to the experimental and simulation results, the solution using the measured heat rate (≈ 725 W) in equation (2.4) from [Aamot, 1967] is included in the figure to compare both methods. The lines correspond to simulation results using an ice temperature of −20 °C and the dashed lines to simulation results using an ice temperature of −15 °C. It can be seen that with increasing heating front temperature, the difference between those two lines increases. This is because of the difference in the Stefan number. But since the difference of the sensible heats[11] in the ice is small compared to the latent heat of melting

[11] $c_{p,S}\Delta T_S = 2049.41\,\mathrm{J/(kg\,K)} \cdot (20\,^\circ\mathrm{C} - 15\,^\circ\mathrm{C}) = 10247.05\,\mathrm{J/kg}$

($\approx 3\,\%$), there is no big difference, even for higher temperatures of the heating front.

The maximum possible melting velocity is limited by the heat rate (horizontal lines in figure 6.2). This is accordance with the experimental results, since they are all below this value. The highest melting velocity obtained with the CME was $\approx 0.56\,\mathrm{m/h}$, when no temperature control was used, i.e. the heating cartridges were continuously on. The average measured temperature for this configuration was $\approx 16\,°\mathrm{C}$. For the same value of the melting velocity, the simulation predicts a temperature of $\approx 5\,°\mathrm{C}$. There are two possible reasons for this discrepancy. The first is that the temperature is not uniformly distributed over the heating front, so that there exist hot points below each heating cartridge but also cold regions somewhere else. This does also mean that the heat flux is not uniformly distributed, which causes a decrease in the value of the melting velocity. Since these cold regions dominate the melting characteristics, a measurement below the heating cartridges gives a too high temperature. The second possible reason is that the temperature gradient in the vicinity of the melting front is so large that even a small distance of 2 mm, at which the sensors below the heating cartridges were positioned, is not sufficient to measure the temperature at the surface. This is in accordance to the measurements of the sensor inside the bolt, because it was always smaller than all other measurement values due to a manufacturing defect (the bore-hole was drilled too deep).

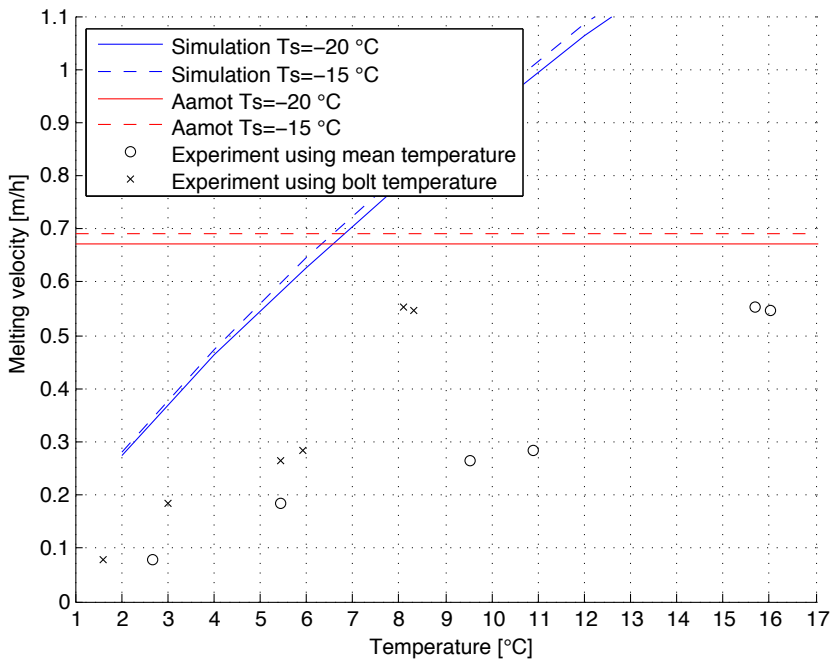

Figure 6.2: Comparison of the simulation with the experimental data in terms of the melting velocity for rectilinear melting. Additional to the data from the experiments and simulations, the solution of equation (2.4) from [Aamot, 1967] is included. The lines correspond to results using an ice temperature of $-20\,°\mathrm{C}$ and the dashed lines to an ice temperature of $-15\,°\mathrm{C}$. The crosses are the measured melting velocitys plotted over the bolt temperature and the circles are the measured melting velocitys plotted over the averaged temperature measurements.

When using the bolt temperatures (crosses) instead of the averaged temperatures (circles) for plotting, the slope of the resulting curve fits better to the slope of the simulation results. This

confirms the assumption that not the real temperature of the surface was measured by the sensors. Unfortunately, there are no measurements which were taken directly at the surface. However, it can be observed from the existing measurements that there is a tendency that if the real surface temperature would have been measured, it would agree better with the simulation results.

6.2 Curvilinear melting

6.2.1 Comparison of the FEM model with the theoretical results

Although the FEM model is based on the same method as the theoretical solution to determine the curve radius, it is a good idea to compare the results of both to check if there are any differences regarding the solutions. The main difference between them is that within the simulation, the heat equation is solved for the ice. Since the movement of the ice in the direction of the heat source is considered in the heat equation, it is obvious, that the melting velocity and the ice temperature are the two parameters, which drive the difference between those solutions.

Figure 6.3 shows the comparison between the results of the FEM model and the theoretical solution using Matlab for different ice temperatures and melting velocities. The parameters from table 6.1 were used for both solutions. In terms of the FEM model, a 2-dimensional mesh was used with a length of 150 mm (length of the CME, which was described in section 5).

It can be seen, that the curve radii are nearly the same, if the melting velocity is higher than 1 m/h. For lower velocities, the curve radii differ from each other. If the ice temperature is near to the melting temperature, there is only a small dependency on the velocity, whereas for lower ice temperatures the curve radius strongly depends on the melting velocity.

The velocity range, which was used in the plots reaches from very low to very high values. In real configurations, melting velocities higher than 2 m/h are unusual, due to power requirements. Nevertheless, it demonstrates the robustness of the FEM model, because there are no numerical difficulties for melting velocities lower than 20 m/h.

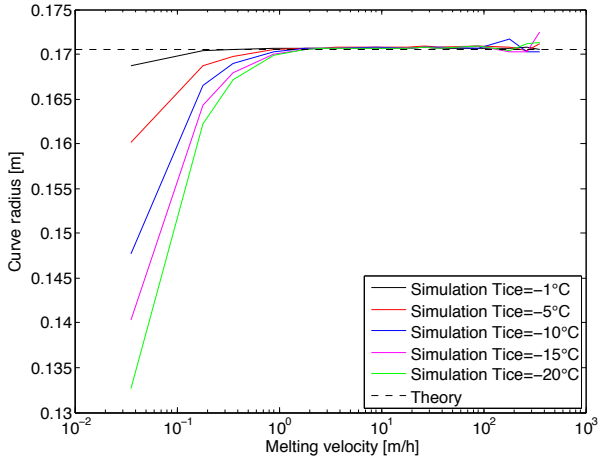

(a) $T(0) = 4\,°\mathrm{C}$, $\Delta T = 4\,°\mathrm{C}$

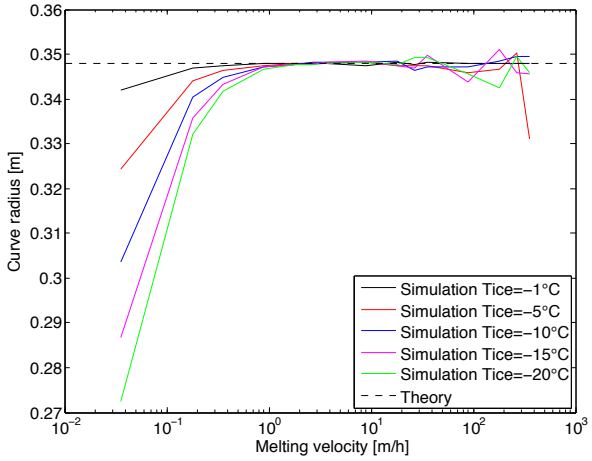

(b) $T(0) = 8\,°\mathrm{C}$, $\Delta T = 4\,°\mathrm{C}$

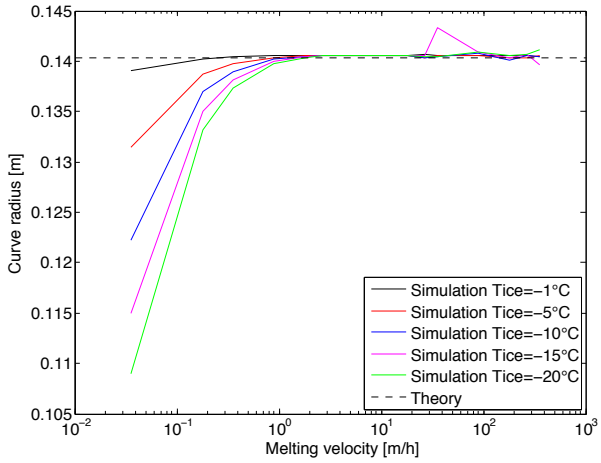

(c) $T(0) = 5\,°\mathrm{C}$, $\Delta T = 6\,°\mathrm{C}$

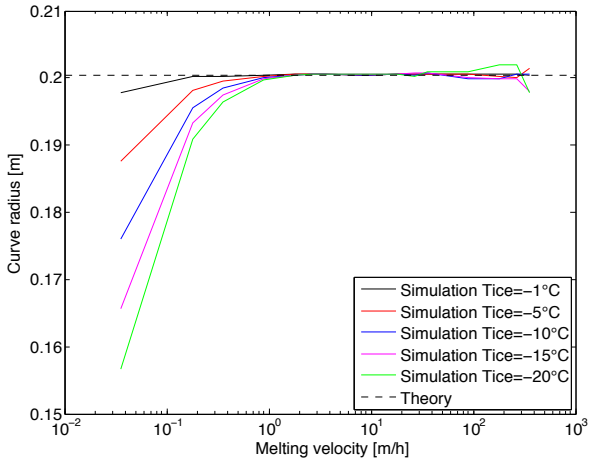

(d) $T(0) = 7\,°\mathrm{C}$, $\Delta T = 6\,°\mathrm{C}$

Figure 6.3: Simulation results compared to the theoretical solution for different ice temperatures and temperature profiles.

To study the difference, which has to be expected for real configurations, table 6.2 shows the results for the obtained melting velocities of the CME. The measured temperatures and velocities were used as input values for the FEM model and the theoretical solution. The resulting curve radii were then used to obtain the absolute and relative errors between both numerical methods. The average relative error is 5.9 %.

$T(0)$ [°C]	ΔT [°C]	U_0 [m/h]	r_c [m]	$r_{c,\text{theory}}$ [m]	$r_{c,\text{sim}}$ [m]	ϵ_{abs} [m]	ϵ_{rel} [%]
7.120	4.820	0.196	0.268	0.256	0.245	0.011	4.4
7.120	4.820	0.184	0.281	0.256	0.244	0.012	4.8
7.070	5.060	0.177	0.341	0.241	0.230	0.011	5.0
5.200	5.360	0.143	0.203	0.165	0.155	0.011	6.9
5.240	5.320	0.058	0.166	0.168	0.142	0.026	18.3
3.555	5.310	0.107	0.111	0.110	0.099	0.011	10.8
4.530	3.660	0.119	0.197	0.213	0.197	0.016	8.1
4.425	3.650	0.158	0.231	0.209	0.197	0.011	5.8
6.230	3.320	0.173	0.327	0.326	0.310	0.016	5.1
6.345	3.470	0.197	0.386	0.318	0.303	0.014	4.8
7.965	3.170	0.198	0.591	0.438	0.421	0.017	4.1
7.855	3.390	0.213	0.631	0.404	0.389	0.015	3.8
8.000	3.080	0.193	0.651	0.453	0.433	0.020	4.5
7.950	2.740	0.218	0.494	0.506	0.488	0.019	3.8
7.950	2.920	0.247	0.583	0.475	0.460	0.015	3.3
5.990	6.820	0.171	0.155	0.149	0.141	0.008	5.7
5.940	6.960	0.194	0.170	0.144	0.137	0.007	4.9
8.025	6.610	0.179	0.228	0.209	0.199	0.010	5.0
7.825	6.470	0.259	0.254	0.208	0.202	0.006	3.1

Table 6.2: Error between the theoretical results and the simulation for the experimental data points in terms of the curve radius. $T(0)$ is the temperature at the center of the heating front, ΔT is the measured temperature difference, U_0 is the measured melting velocity, r_c is the post-processed curve radius from experimental data, $r_{c,\text{theory}}$ is the predicted curve radius by the theory using Matlab, $r_{c,\text{sim}}$ is the predicted curve radius using the FEM-model, ϵ_{abs} is the absolute error of the curve radius of the theory and the FEM model and ϵ_{rel} is the relative error.

6.2.2 Comparison with experimental results

Now the experimental results, using a temperature gradient along the heating front, will be used to validate the FEM model. Since there is no big difference in the results of the FEM solution and the solution using Matlab ($\epsilon_{\text{rel}} \approx 5.9\,\%$), the latter is used for comparison, because it required less computation time to create the necessary set of solutions.

To visualize possible errors due to the temperature sensor accuracy $\pm 0.5\,°\text{C}$, an error region has been included in all following figures. The upper and lower bounds of this regions were calculated by solving the curve radius for an extended ($\Delta T_{\text{max}} = \Delta T + 2 \cdot 0.5\,°\text{C}$) or a reduced ($\Delta T_{\text{min}} = \Delta T - 2 \cdot 0.5\,°\text{C}$) total temperature difference.

Figures 6.4(a) and 6.4(b) show the experimental results for the two predefined temperature gradients (4 °C and 6 °C) compared to the theoretical solutions for the curve radius over the temperature at the center, i.e. the temperature in the center $T(0)$ using a linear temperature profile of the form $T(x) = T(0) - \Delta T x/(2 \cdot 0.075\,\text{m})$. Since the predefined target temperatures were used for plotting, the experimental results are vertically distributed for every temperature at the center.

The variation between the experimental results increases with increasing temperature at the center. This is because external forces become more dominant to the curvilinear melting characteristics, when the temperature at the center increases. To study the influence of the not-centered CME's cable positions, some experiments were conducted with an interchanged temperature profile, i.e. the half on which the cables are positioned is hotter. The corresponding data points are marked as crosses in figure 6.4(a). The results show that the cables exert a force on the CME that decreases or increases the curve radius, depending on the sign of the temperature gradient, i.e. the curve radius will be decreased if a force is acting on the hotter half and increased if a force is acting on the colder half.

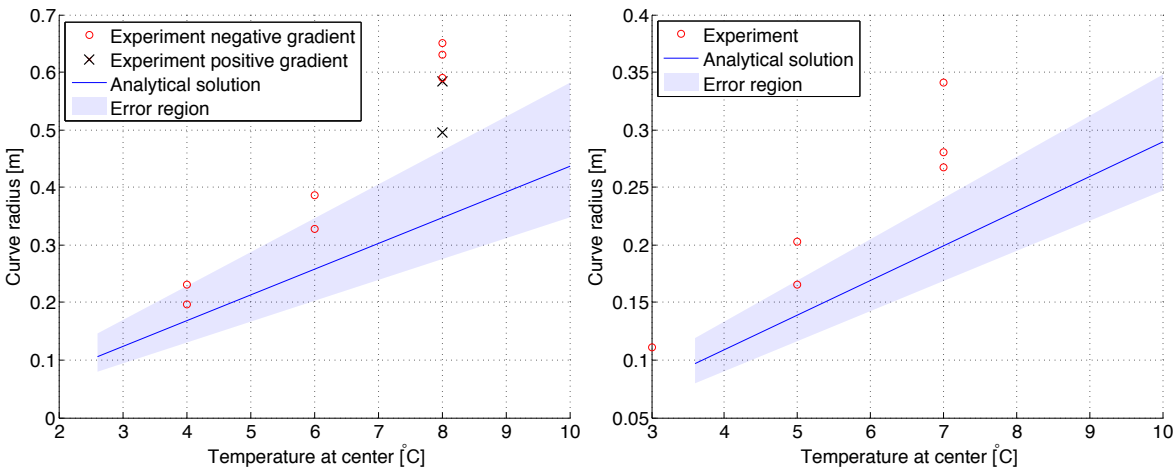

(a) $\Delta T = 4\,°\mathrm{C}$ (b) $\Delta T = 6\,°\mathrm{C}$

Figure 6.4: Comparison of theoretical results with the experimental data in terms of the curve radius over the temperature at the center using the predefined temperature values. (a) shows the results for a temperature gradient of $\Delta T = 4\,°\mathrm{C}$ and (b) shows the results for a temperature gradient of $\Delta T = 6\,°\mathrm{C}$. The upper and lower bounds of the error regions are caused by the accuracy of the temperature sensors, which is $\pm 0.5\,°\mathrm{C}$ for the considered temperature range.

It can be seen that the values and the slopes of the curve radii from the experimental data are higher than those predicted by the theory. In figure 5.10 it was shown that the predefined and the measured temperature profiles differ from each other in a way that the total temperature difference is smaller in reality. Observation of the measured temperatures does also show that the temperature at the center differs slightly. Therefore, it would be a better approach to use the measured temperature values for plotting and computation of the theoretical curve radii, instead of the predefined values. This have been done in figures 6.5(a) and 6.5(b). The theoretical curve radii were computed using an averaged total temperature difference. The figures show a very good agreement between the theoretical and experimental results, even if there is a small discrepancy for higher temperatures at the center, which is expected to result from external forces introduced by the position of the cables.

Figures 6.6(a) and 6.6(b) show the effect of variations in the total temperature difference ΔT on the curve radius for a predefined constant minimum temperature ($T_{\min} = T(0) - \Delta T/2$). The

theoretical curve radii were computed using an averaged minimum temperature. It can be seen that there is a good agreement for both minimum temperatures.

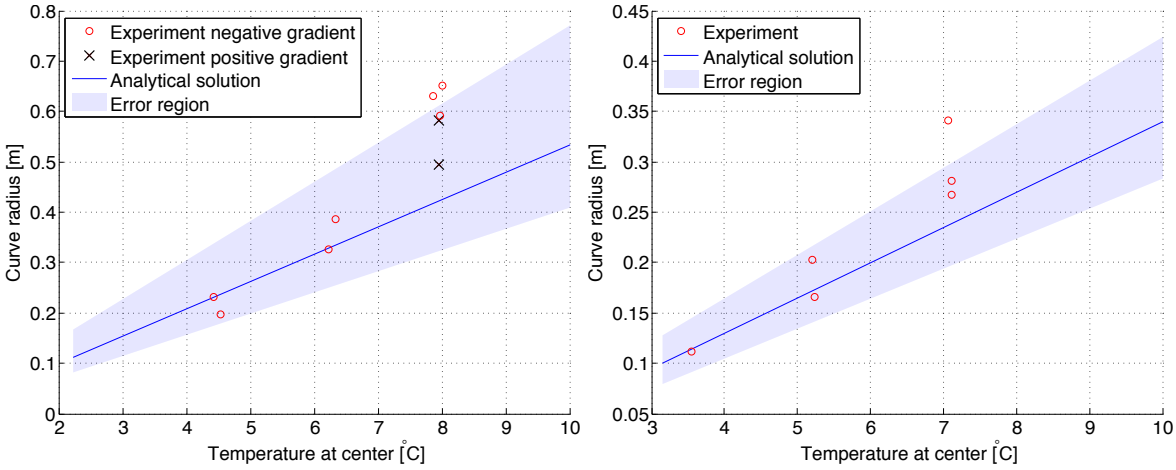

(a) $\Delta T = 3.27\,°\mathrm{C}$ (b) $\Delta T = 5.12\,°\mathrm{C}$

Figure 6.5: Comparison of theoretical results with the experimental data in terms of the curve radius over the temperature at the center using the measured temperature values. (a) shows the results for an averaged measured temperature gradient of $\Delta T = 3.27\,°\mathrm{C}$ and (b) shows the results for an averaged measured temperature gradient of $\Delta T = 5.12\,°\mathrm{C}$.

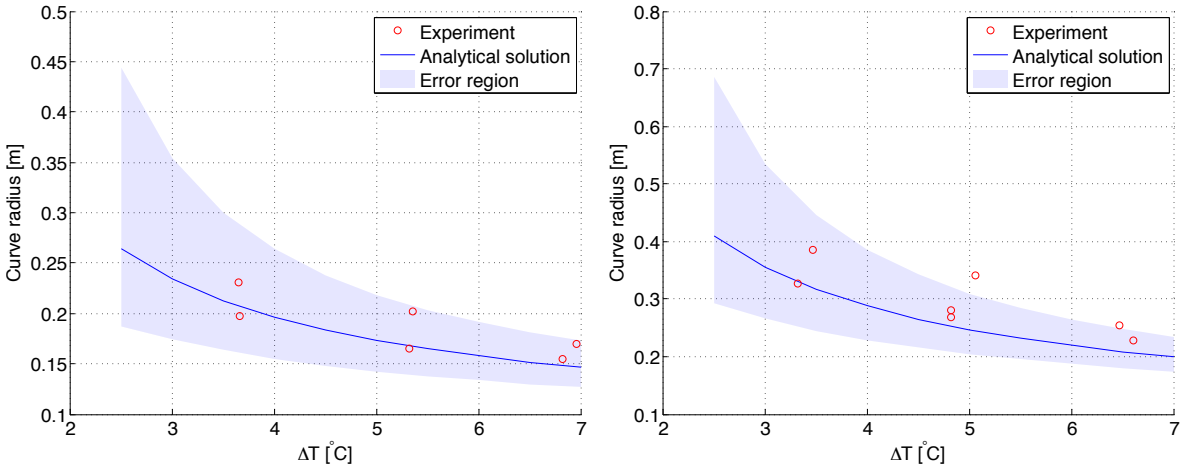

(a) $T_{\mathrm{min}} = 2.57\,°\mathrm{C}$ (b) $T_{\mathrm{min}} = 4.64\,°\mathrm{C}$

Figure 6.6: Comparison of theoretical results with the experimental data in terms of the curve radius over the total temperature difference using the measured temperature values. (a) shows the results for an averaged measured minimum temperature of $2.57\,°\mathrm{C}$ and (b) shows the results for an averaged measured minimum temperature of $4.64\,°\mathrm{C}$.

In subsection 6.1.2, it was shown that the measured temperatures are too high, because of the distance of the temperature sensors to the surface (2 mm). So it is expected, that the experimentally obtained curve radii might be shifted horizontally to the left in figure 6.5 and vertically downward in figure 6.6, if the real surface temperatures would have been used. Unfortunately,

these temperatures are unknown. But since there is a very good agreement for all considered configurations, it is assumed that the amount of this shifting is small.

7 Summary and conclusions

The IceMole is a maneuverable ice exploration probe. One of its main features is the ability to melt curved trajectories. This is possible due to its unique configuration, in which an ice screw is used in addition to a melting head that allows for differential control of the heaters and therefore a variable temperature profile along its surface. So it is possible to follow a certain path or to reach a certain position in the ice. Beside an accurate determination of the IceMole's current position, a successful navigation requires the prediction of its melting dynamics over a certain distance.

The objective of this thesis was to develop a FEM model, which can be used to describe those melting dynamics, i.e. the melting velocity and the curve radius, with a focus on the main physical reasons. Therefore, a simplified version of the IceMole was considered, in which the effect of its length on the curve radius was neglected and the internal heat transfer was replaced by a Dirichlet boundary condition (temperature) at the surface. Moreover, its ice screw was simplified by a normal force in the center of the melting head in the direction of the ice.

The existing theories for describing melting probes are limited in a way, that they cannot predict the melting velocity for a real configuration with a certain complexity of the geometry and the heat transfer characteristics. Therefore, the theory of close-contact melting, which is more general, has been chosen for the fundamental framework of the developed FEM model. Since the considered curvilinear melting problem has never been studied the past, this was one of the main tasks during this thesis. Therefore a linear velocity profile, which contains the curve radius, has been introduced and used in governing equations of close-contact melting theory. The result was an equation for the pressure distribution in the melt film. A solution procedure was proposed, which makes use of the resulting force and torque to obtain the melting velocity and curve radius, respectively. It was found out, that for an arbitrary temperature profile along the heating front of the form $T(x) = T_0 + f(x)$, the curve radius increases linearly with T_0. Since this feature was observed for both, the rectangular and the cylindrical heat source, it is expected for all geometries. Moreover, it was shown that in the theoretical model, the curve radius does only depend on 3 variables, namely the geometry of the heat source, the melting temperature of the PCM and the temperature profile along the heat source surface.

Then, a FEM model was developed and implemented in the open source software Elmer. The model extends the theoretical model, because it solves the heat equation for the ice explicitly, whereas in the theoretical model, the ice was only considered implicitly by using a reduced latent heat of melting. Therefore, the curve radius depends also on the melting velocity and the ice temperature, if the FEM model is used. But for velocities in the vicinity of 1 m/h and if the ice temperature is near to the melting temperature (temperate ice), the curve radii predicted by the theoretical and the FEM model are nearly the same.

To validate the theoretical and the FEM model, a melting device was constructed and then used for several rectilinear and curvilinear melting experiments. The usage of an ice screw was excluded from the considered set of experiments, because the geometrical effect of the screw on the curve radius was too high and not considered in the models. Instead, a bolt was used for

the final configuration. The translation of the measured data (distance and inclination angle) into the curve radius was done by an incremental post-processing method.

The velocities for rectilinear melting using the FEM model accord to the analytical solutions for simple geometries when phase-independent thermo-physical properties are used. For phase-dependent properties, the FEM model predicts slightly higher velocities. The main reason for this is that the volume flow through the melt film is higher for the analytical solutions, which results in a higher pressure. This means that for the same melting velocity, the resulting force is smaller for the FEM model. Since an inverse technique is used to adjust the melting velocity until it is equal to a predefined target force, the melting velocity is always higher if phase-dependent thermo-physical properties are used.

Compared to the experimentally obtained velocities for rectilinear melting, the FEM model predicts higher velocities for the same surface temperatures. It is assumed that this comes from the position of the temperature sensors. Since their distance to the surface is about 2 mm and the temperature gradient in the vicinity of the surface is large, the measured temperatures are always higher than the corresponding surface temperatures.

For the data points, which where considered for the set of curve radius experiments, the average relative error between the theoretical and FEM model was 5.9 %. Therefore, the theoretical model was used for comparison with the experimental results, because it needed less computation time. The comparison of the predicted with the experimentally obtained curve radii shows a very good agreement, when the measured temperatures are used for the model. Unfortunately, the real surface temperatures are unknown due to the distance of the temperature sensors. But since the agreement is good for all tested configurations, it is expected that there will be no big difference.

It was shown that the developed FEM model is capable to predict the melting velocity and the curve radius for problems, in which an arbitrary temperature profile along a heat source surface is given. Even though, only a simplified version of the IceMole is modeled, the developed curvilinear melting theory will be the fundamental framework for future models, which might be able to predict the melting dynamics of a more realistic version of the IceMole. Some of the next steps to obtain this objective are:

- Extension to use boundary conditions of the Neumann type, i.e. a heat flux distribution of the melting head surface.
- Extension to consider the heat transfer inside the melting head. If this works, there is no more need for a boundary condition on the melting head surface.
- Implementation to compute the curve radius for 3-dimensional geometries.
- Experimental investigation of the ice screw and the IceMole length, in terms of the geometrical effect on the curve radius.
- Implementation of the ice screw and IceMole length effects on the curve radius.

References

[Aamot 1967] Aamot, Haldor W.: *HEAT TRANSFER AND PERFORMANCE ANALYSIS OF A THERMAL PROBE FOR GLACIERS.* 1967

[Alboudwarej 1998] Alboudwarej, Hussein: *Analysis of close contact melting.* University of Calgary, 1998

[Alexiades & Solomon 1993] Alexiades, Vasilios ; Solomon, Alan D.: *Mathematical Modeling of Melting and Freezing Processes.* Taylor & Francis Group, 1993

[Bejan 1992] Bejan, Adrian: Single correlation for theoretical contact melting results in various geometries. In: *International communications in heat and mass transfer* 19 (1992), no. 4, p. 473–483

[Chen et al. 2008a] Chen, Wenzhen ; Zhao, Yuansong ; Sun, Fengrui ; Chen, Zhiyun ; Gong, Miao: Analysis of ΔT-driven contact melting of phase change material around a horizontal cylinder. In: *Energy Conversion and Management* 49 (2008), no. 5, p. 1002–1007

[Chen et al. 2008b] Chen, Wenzhen ; Zhu, Bo ; Chen, Zhiyun ; Li, Haofeng ; Sun, Fengrui: New analysis of contact melting of phase change material around a hot sphere. In: *Heat and Mass Transfer* 44 (2008), no. 3, p. 281–286

[Emerman & Turcotte 1983] Emerman, Steven H. ; Turcotte, DL: Stokes's problem with melting. In: *International journal of heat and mass transfer* 26 (1983), no. 11, p. 1625–1630

[Fisher 1976] Fisher, HN: Thermal analysis of some subterrene penetrators. In: *Journal of Heat Transfer* 98 (1976), no. 3, p. 485–490

[Fomin et al. 1995] Fomin, SA ; Wei, PS ; Chugunov, VA: Contact melting by a non-isothermal heating surface of arbitrary shape. In: *International journal of heat and mass transfer* 38 (1995), no. 17, p. 3275–3284

[Fomin & Cheng 1991] Fomin, Sergei A. ; Cheng, Shangmo: Optimization of the heating surface shape in the contact melting problem. In: *Third International Conference on Inverse Design Concepts and Optimization in Engineering Sciences (ICIDES-3)* vol. 1, 1991, p. 253–262

[Hamrock et al. 2004] Hamrock, Bernard J. ; Schmid, Steven R. ; Jacobson, Bo O.: *Fundamentals of fluid film lubrication.* vol. 169. CRC press, 2004

[Hu & Shi 1997] Hu, Yaojiang ; Shi, Mingheng: Close-contact melting around a hot sphere. In: *Journal of Thermal Science* 6 (1997), no. 1, p. 51–57

[Jackson 1965] Jackson, F: Moving heat sources with change of phase. In: *Journal of Heat Transfer* 87 (1965), no. 3, p. 329–332

[Jansen & Stepnewski 1973] Jansen, G ; Stepnewski, DD: Fast reactor fuel interactions with floor material after a hypothetical core meltdown. In: *Nuclear Technology* 17 (1973), p. 85–96

[Kumano et al. 2005] Kumano, Hiroyuki ; Saito, Akio ; Okawa, Seiji ; Yamada, Yuichi: Direct contact melting with asymmetric load. In: *International journal of heat and mass transfer* 48 (2005), no. 15, p. 3221–3230

[Lide 2010] Lide, David R.: *CRC Handbook of Chemistry and Physics.* 90th Edition (Internet Version 2010). Boca Raton, FL. : CRC Press/Taylor and Francis, 2010

[Marsh 1978] Marsh, BD: On the cooling of ascending andesitic magma. In: *Philosophical Transactions of the Royal Society of London. Series A, Mathematical and Physical Sciences* 288 (1978), no. 1355, p. 611–625

[Mayer & Moaveni 2008] Mayer, Paul ; Moaveni, Saeed: Close-contact melting as a subtractive machining process. In: *The International Journal of Advanced Manufacturing Technology* 37 (2008), no. 9-10, p. 980–995

[Moallemi & Viskanta 1985] Moallemi, MK ; Viskanta, R: Melting around a migrating heat source. In: *Journal of heat transfer* 107 (1985), no. 2, p. 451–458

[Moallemi & Viskanta 1986] Moallemi, MK ; Viskanta, R: Analysis of melting around a moving heat source. In: *International journal of heat and mass transfer* 29 (1986), no. 8, p. 1271–1282

[Moallemi et al. 1986] Moallemi, MK ; Webb, BW ; Viskanta, R: An experimental and analytical study of close-contact melting. In: *Journal of heat transfer* 108 (1986), no. 4, p. 894–899

[Myers et al. 2008] Myers, TG ; Mitchell, SL ; Muchatibaya, G: Unsteady contact melting of a rectangular cross-section material on a flat plate. In: *Physics of Fluids (1994-present)* 20 (2008), no. 10

[Raback 2013a] Raback, Peter: *Personal communication.* June 2013

[Raback 2013b] Raback, Peter: *Personal communication.* August 2013

[Raback et al. 2013] Raback, Peter et al.: *ElmerSolver Manual.* Februar 2013

[Raback et al. 2014] Raback, Peter et al.: *Elmer Models Manual.* CSC – IT Center for Science, November 2014

[Schlichting 1979] Schlichting, H: Boundary-layer theory. In: *Boundary-layer theory.* McGraw-Hill, 1979

[Schüller 2013] Schüller, Kai: *Thermalsimulation des IceMole-Kopfes in Elmer.* February 2013. – in german

[Shreve 1962] Shreve, RL: Theory of performance of isothermal solid-nose hot-points boring in temperate ice. In: *J. Glaciol* 4 (1962), no. 32, p. 151–160

[Stefan 1889] Stefan, J: Über die Theorie der Eisbildung, insbesondere ueber die Eisbildung im Polarmeere. In: *Sitzungsberichte der Kaiserlichen Akademie der Wissenschaften, Mathematisch-naturwissenschaftliche Classe* 98 (1889), p. 965–983

[Ulamec et al. 2007] Ulamec, Stephan ; Biele, Jens ; Funke, Oliver ; Engelhardt, Marc: Access to glacial and subglacial environments in the Solar System by melting probe technology. In: *Reviews in Environmental Science and Bio/Technology* 6 (2007), no. 1-3, p. 71–94

[Yaojiang et al. 1999] Yaojiang, Hu ; Suyi, Huang ; Mingheng, Shi: A generalized analysis of close-contact melting processes in two-dimensional axisymmetric geometries. In: *International communications in heat and mass transfer* 26 (1999), no. 3, p. 339–347

[Zhao et al. 2008] Zhao, YS ; Chen, WZ ; Sun, FR ; Chen, ZY: Analysis of contact melting driven by surface heat flux around a cylinder. In: *Journal of Thermal Science* 17 (2008), no. 1, p. 64–68

Appendix

A Thermophysical properties of water-ice

Phase	T °C	ρ $kg\,m^{-3}$	k $\mathrm{W\,m^{-1}\,K^{-1}}$	c_p $\mathrm{kJ\,kg^{-1}\,K^{-1}}$	h $\mathrm{kJ\,kg^{-1}}$
	90,00	965,3100	0,6753	4,2052	710,8467
	80,00	971,7900	0,6700	4,1968	668,9471
	70,00	977,7600	0,6631	4,1901	627,0434
	60,00	983,2000	0,6544	4,1850	585,1355
	50,00	988,0300	0,6436	4,1813	543,2234
liquid	40,00	992,2200	0,6306	4,1794	501,3071
	30,00	995,6500	0,6155	4,1798	459,3866
	20,00	998,2100	0,5985	4,1841	417,4619
	10,00	999,7000	0,5800	4,1952	375,5330
	4,00	999,9700			350,3737
	0,01	999,8400	0,5611	4,2194	333,6419
	0,00	916,7000	2,1400	2,1100	0,0000
	-10,00	918,7000	2,3000	2,0300	-20,6802
	-20,00	920,3000	2,4000	1,9600	-40,6062
	-30,00	921,6000	2,5000	1,8800	-59,7779
solid	-40,00	922,8000	2,6000	1,8000	-78,1953
	-50,00	924,0000	2,8000	1,7200	-95,8585
	-60,00	925,2000	3,0000	1,6500	-112,7674
	-80,00	927,4000	3,3000	1,5000	-144,3225
	-100,00	929,2000	3,7000	1,3600	-172,8605

Table A.1: Thermophysical properties of water-ice.
Data from: [Lide, 2010]

B Conducted experiments

ID	Date	Configuration	$T_{\min}$	ΔT	Comments
1	31.10.2014	screw			Problem: The minimum temperature was never reached, because it was higher than attainable by the heating cartridges. So there was no temperature gradient along the melting head.
2		screw			
3	04.11.2014	screw	4 °C	6 °C	
4		hole	4 °C	6 °C	
5	07.11.2014	hole	4 °C	6 °C	
6	12.11.2014	bolt v1	4 °C	6 °C	
7	24.11.2014	bolt v2	4 °C	6 °C	
8	27.11.2014	bolt v2	4 °C	6 °C	
9	01.12.2014	bolt v2	4 °C	6 °C	
10	04.12.2014	bolt v2	6 °C	4 °C	Problem: The GUI crashed shortly after starting the experiment and therefore a logfile does not exist.
11	05.12.2014	bolt v2	≈ 0 °C	≈ 10 °C	Problem: the temperature ranges for the heater control were not properly transmitted to the Arduino, which resulted in a non-reproducible control behavior.
12	08.12.2014	bolt v2	6 °C	4 °C	
13	10.12.2014	bolt v2	6 °C	4 °C	
14	12.12.2014	bolt v2	6 °C	4 °C	
15	15.12.2014	bolt v2	2 °C	6 °C	
16	17.12.2014	bolt v2	2 °C	6 °C	
17		bolt v2	≈ 18 °C	0 °C	
18	19.12.2014	bolt v2	0 °C	6 °C	
19		bolt v2	≈ 18 °C	0 °C	
20	05.01.2015	bolt v2	2 °C	4 °C	
21		bolt v2	2 °C	4 °C	
22	07.01.2015	bolt v2	4 °C	4 °C	
23		bolt v2	4 °C	4 °C	
24	09.01.2015	bolt v2	6 °C	4 °C	negative gradient
25		bolt v2	6 °C	4 °C	negative gradient
26	12.01.2015	bolt v2	10 °C	0 °C	
27		bolt v2	5 °C	0 °C	
28	14.01.2015	bolt v2	4 °C	8 °C	
29		bolt v2	4 °C	8 °C	
30	19.01.2015	bolt v2	12 °C	0 °C	
31		bolt v2	2 °C	0 °C	
32	19.01.2015	bolt v2	2 °C	8 °C	
33		bolt v2	2 °C	8 °C	

Table B.1: Chronological overview of all conducted experiments.

C Curvilinear melting of a cylindrical heat source

In this appendix, the close-contact curvilinear melting of a cylindrical heat source will be derived. Because most of the steps are similar to the derivation of the rectangular heat source, which was presented in section 3.3.

The physical problem is shown in figure C.1. A cylindrical heat source with the radius R and a constant force F, which is acting at the center of the melting front, migrates through a block of a PCM, due to an imposed temperature $T(\phi)$ on the heat source surface. The thickness of the melt film is given by $\delta(\phi)$.

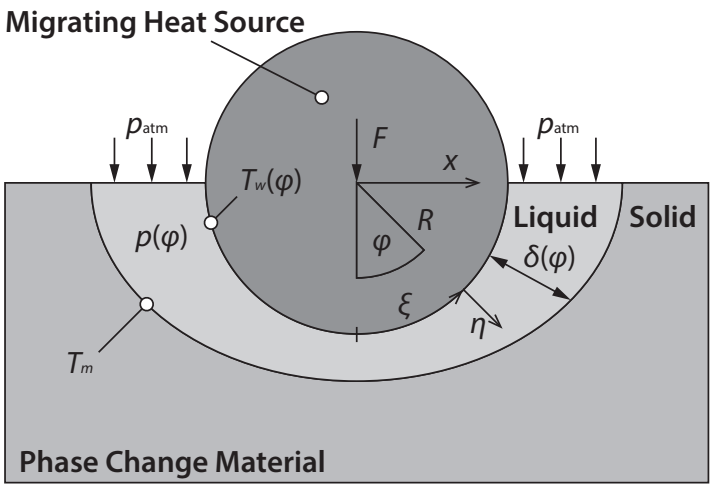

Figure C.1: Physical model and coordinates for a migrating heat source with a cylindrical shape.

The connections of the underlying coordinate systems are

$$x = R \sin \phi \tag{C.1}$$

$$\xi = \phi R \tag{C.2}$$

The velocity of the melt in the tangential direction (along ξ) is denoted as u and in normal direction (along η) as w. The continuity, momentum and energy equations for the considered geometry then are

$$\frac{\partial u}{\partial \xi} + \frac{\partial w}{\partial \eta} = 0 \tag{C.3}$$

$$\mu_L \frac{\partial^2 u}{\partial \eta^2} = \frac{dp}{d\xi} \tag{C.4}$$

$$u \frac{\partial T}{\partial \xi} + w \frac{\partial T}{\partial \eta} = \alpha_L \frac{\partial^2 T}{\partial z^2} \tag{C.5}$$

The boundary conditions at the heat source are

$$u(\xi, 0) = w(\xi, 0) = 0, \qquad T(\xi, 0) = T_w(\xi), \qquad q''(\xi, 0) = q''_w(\xi) \tag{C.6}$$

And at the phase interface the boundary conditions are

$$u(\xi, \delta(\phi)) = 0, \qquad w(\xi, \delta(\phi)) = -\frac{\rho_S}{\rho_L} U(\phi) \cos\phi, \qquad T(\xi, \delta(\phi)) = T_m \tag{C.7}$$

The Stefan condition is

$$\left.\frac{\partial T}{\partial \eta}\right|_{\eta=\delta(\phi)} = -\frac{\rho_S U(\phi) \cos\phi}{k_L} \left[h_m + c_{p,S} \left(T_m - T_S\right)\right] \tag{C.8}$$

The pressure at the right- and left-hand side if the melt film is

$$p(-\pi/2) = p(\pi/2) = p_{\text{atm}} \tag{C.9}$$

The velocity in the tangential direction can be found by integrating (C.4) and substituting the boundary conditions (C.6) and (C.7)

$$u(\xi, \eta) = \frac{1}{2\mu_L} \frac{dp}{d\xi} \eta \left(\eta - \delta(\phi)\right) \tag{C.10}$$

Substituting (C.10) into continuity equation (C.3) and integrating over the melt film thickness yields

$$\frac{dp}{d\xi} = -\frac{12\mu_L \left(\frac{\rho_S}{\rho_L} \int_0^{\xi} U(\phi) \cos\phi d\xi + C_4\right)}{\delta^3(\phi)} = -\frac{12\mu_L \left(\frac{\rho_S}{\rho_L} \int_0^{\phi} U(\tilde{\phi}) \cos\tilde{\phi} R d\phi + C_4\right)}{\delta^3(\phi)} \tag{C.11}$$

Or using (C.2) in combination with (C.11)

$$\begin{aligned} \frac{dp}{d\xi}\frac{d\phi}{d\phi} = \frac{dp}{d\phi}\frac{d\phi}{d\xi} = \frac{1}{R}\frac{dp}{d\phi} &= -\frac{12\mu_L \left(\frac{\rho_S}{\rho_L} \int_0^{\phi} U(\tilde{\phi}) \cos\tilde{\phi} R d\phi + C_4\right)}{\delta^3(\phi)} \\ \Rightarrow \frac{dp}{d\phi} &= -\frac{12R\mu_L \left(\frac{\rho_S}{\rho_L} \int_0^{\phi} U(\tilde{\phi}) \cos\tilde{\phi} R d\phi + C_4\right)}{\delta^3(\phi)} \end{aligned} \tag{C.12}$$

The melting velocity as a function of ϕ can be found by substituting (C.1) in (3.22)

$$\begin{aligned} U(x) &= U_0 \left(1 - \frac{x}{r_c}\right) \\ U(\phi) &= U_0 \left(1 - \frac{R \sin\phi}{r_c}\right) \end{aligned} \tag{C.13}$$

Inserting (C.13) into (C.12) and integrating yields

$$\begin{aligned} \frac{dp}{d\phi} &= -\frac{12R\mu_L \left(\frac{\rho_S}{\rho_L} \int_0^{\phi} U_0 \left(1 - \frac{R\sin\tilde{\phi}}{r_c}\right) \cos\tilde{\phi} R d\phi + C_4\right)}{\delta^3(\phi)} \\ \frac{dp}{d\phi} &= -\frac{12R\mu_L \left(\frac{\rho_S}{\rho_L} U_0 R \left(\frac{R\cos^2\phi}{2r_c} + \sin\phi\right) + C_4\right)}{\delta^3(\phi)} \end{aligned} \tag{C.14}$$

The pressure is found by integrating (C.14)

$$p(\phi) - p(0) = -12R\mu_L \int_0^{\phi} \frac{1}{\delta^3(\tilde{\phi})} \left(\frac{\rho_S}{\rho_L} U_0 R \left(\frac{R\cos^2\tilde{\phi}}{2r_c} + \sin\tilde{\phi} \right) + C_4 \right) d\tilde{\phi} \tag{C.15}$$

The integration constant C_4 and the pressure at $\phi = 0$ are found by substituting the boundary conditions (C.9) into (C.15)

$$p(\pi/2) - p(-\pi/2) = 0 = \int_{-\pi/2}^{\pi/2} \frac{1}{\delta^3(\phi)} \frac{\rho_S}{\rho_L} U_0 R \left(\frac{R\cos^2\phi}{2r_c} + \sin\phi \right) d\phi + C_4 \int_{-\pi/2}^{\pi/2} \frac{1}{\delta^3(\phi)} d\phi$$

$$C_4 = -\frac{\frac{\rho_S}{\rho_L} U_0 R \int_{-\pi/2}^{\pi/2} \frac{1}{\delta^3(\phi)} \left(\frac{R\cos^2\phi}{2r_c} + \sin\phi \right) d\phi}{\int_{-\pi/2}^{\pi/2} \frac{1}{\delta^3(\phi)} d\phi} \tag{C.16}$$

$$p(0) = -12\frac{\rho_S}{\rho_L} U_0 R^2 \mu_L \int_0^{\pi/2} \frac{1}{\delta^3(\tilde{\phi})} \left(\frac{R\cos^2\tilde{\phi}}{2r_c} + \sin\tilde{\phi} - \frac{\int_{-\pi/2}^{\pi/2} \frac{1}{\delta^3(\phi)} \left(\frac{R\cos^2\phi}{2r_c} + \sin\phi \right) d\phi}{\int_{-\pi/2}^{\pi/2} \frac{1}{\delta^3(\phi)} d\phi} \right) d\tilde{\phi} + p_{\text{atm}} \tag{C.17}$$

Substituting (C.16) and (C.17) into (C.15) yields

$$p(\phi) = -12\frac{\rho_S}{\rho_L} U_0 R^2 \mu_L \int_{\phi}^{\pi/2} \frac{1}{\delta^3(\tilde{\phi})} \left(\frac{R\cos^2\tilde{\phi}}{2r_c} + \sin\tilde{\phi} - \frac{\int_{-\pi/2}^{\pi/2} \frac{1}{\delta^3(\phi)} \left(\frac{R\cos^2\phi}{2r_c} + \sin\phi \right) d\phi}{\int_{-\pi/2}^{\pi/2} \frac{1}{\delta^3(\phi)} d\phi} \right) d\tilde{\phi} + p_{\text{atm}} \tag{C.18}$$

The melt film thickness is found by a linear polynomial approximation of the temperature through the melt film in combination with the Stefan condition (C.8)

$$\delta(\phi) = \frac{k_L \left(T_w(\phi) - T_m \right)}{\rho_L h_m^* U_0 \left(1 - \frac{R\sin\phi}{r_c} \right) \cos\phi} \tag{C.19}$$

The force and torque due to the pressure inside the melt film are

$$F = R \int_{-\pi/2}^{\pi/2} p(\phi) \cos\phi d\phi \tag{C.20}$$

$$M = R^2 \int_{-\pi/2}^{\pi/2} p(\phi) \sin\phi d\phi \tag{C.21}$$

Please note that for an alternative solution procedure, as it was given in section 3.3.3 for the rectangular heat source, the full nominator of equation C.14 must be taken into account and not only the integration constant (C.16), because of the cosine.

D User defined function to calculate the melt film thickness and heat transfer coefficient

```
FUNCTION HTCoeff( Model, n, x ) RESULT(f)

  USE Types
  USE Lists
  USE DefUtils

  IMPLICIT NONE
  TYPE(Model_t) :: Model
  INTEGER :: n
  REAL(KIND=dp) :: x,f

  INTEGER :: i,j,k,k2,Iter, PrevIter = 1
  TYPE(Variable_t), POINTER  :: PVar, AllVars
  REAL(KIND=dp), POINTER :: Gap(:)=>NULL(), Temp(:)=>NULL(), &
      Nonlin(:)=>NULL(), MoleTemp(:) => NULL()
  INTEGER, POINTER :: GapPerm(:)=>NULL(), TempPerm(:)=>NULL(), &
      MoleTempPerm(:)=>NULL()
  REAL(KIND=dp) :: cond, coeff, coeffmax, coeffmin, thot, g, &
      GapRelax, MeltingTemp, Tcold
  TYPE(ValueList_t), POINTER :: Material
  LOGICAL :: Found

  SAVE Gap, GapPerm, Temp, TempPerm, PrevIter, &
      Nonlin, GapRelax, MoleTemp, MoleTempPerm, MeltingTemp

  AllVars => Model % Variables
  IF( .NOT. ASSOCIATED( AllVars ) ) CALL Fatal('MeltBC','Err0')

  ! Do the following inside the if-condition only one time
  ! for the whole simulation
  IF( .NOT. ASSOCIATED( Temp ) ) THEN

    PVar => VariableGet( Model % Variables, 'nonlin iter',ThisOnly=.TRUE.)
    IF( .NOT. ASSOCIATED( PVar ) ) CALL Fatal('MeltBC','Err1')
    Nonlin => PVar % Values

    PVar => VariableGet( AllVars,'Temp',ThisOnly=.TRUE.)
    IF( .NOT. ASSOCIATED( PVar ) ) CALL Fatal('MeltBC','Err2')
    Temp => PVar % Values
    IF( .NOT. ASSOCIATED( PVar % Perm ) ) CALL Fatal('MeltBC','Err21')
    TempPerm => PVar % Perm

    PVar => VariableGet( AllVars,'MoleTemp',ThisOnly=.TRUE.)
    IF( .NOT. ASSOCIATED( PVar ) ) CALL Fatal('MeltBC','Err22')
    MoleTemp => PVar % Values
    IF( .NOT. ASSOCIATED( PVar % Perm ) ) CALL Fatal('MeltBC','Err23')
    MoleTempPerm => PVar % Perm

```

```
    PVar => VariableGet( AllVars,'Gap',ThisOnly=.TRUE.)
    IF( .NOT. ASSOCIATED( PVar ) ) CALL Fatal('MeltBC','Err3')
    ! Because Gap is a pointer, the Gap will be changed inside this
    ! user-defined-function
    Gap => PVar % Values
    GapPerm => PVar % Perm

    GapRelax = ListGetConstReal( Model % Solver % Values, &
        'Gap Relaxation Factor',Found)
    IF(.NOT. Found ) GapRelax = 1.0_dp

    ! if melting temperature will be variable in the future, it must be
    ! outside this if-condition
    MeltingTemp = ListGetConstReal( Model % Solver % Values, &
        'Melting Temperature',Found)
    IF(.NOT. Found ) MeltingTemp = 0.0_dp

  END IF

  Material => GetMaterial()
  IF( .NOT. ASSOCIATED( Material ) ) THEN
    CALL Fatal('MeltBC','No material found!')
  END IF

  Iter = NINT( Nonlin(1) )

  IF( Iter /= PrevIter ) THEN
    PrevIter =  Iter

    coeffmin = 0.2_dp ! Relaxation parameters to limit overshooting
    coeffmax = 5.0_dp

    DO i=1,SIZE( GapPerm )

      j = GapPerm(i)
      ! GapPerm(i) is 0 if GapPerm(i) is not a node on the gap
      ! so just cycle if the current index is not a node on the gap
      IF( j == 0 ) CYCLE

      k = TempPerm(i)
      IF( k == 0 ) CALL Fatal('MeltBC','Err4')

      k2 = MoleTempPerm(i)
      IF( k2 == 0 ) CALL Fatal('MeltBC','Err41')

      ! Thot is the temperature of the node on the side the
      ! heat source, which is defined in the *.sif
      Thot = MoleTemp(k2)

      ! Tcold is the temperature of the node on the side the
      ! solid phase change material, which is calculated by the heat solver
      ! with growing number of iteration it will converge to the melting
      ! temperature (for example 0C for ice)
```

```
      Tcold = Temp(k)

      ! with growing number of iteration, i.e. the better the value
      ! of the gap is, coeff will converge to one
      coeff = (Thot-MeltingTemp) / ( Thot - Tcold )

      ! This is just to ensure that no overshooting occurs
      coeff = MAX( MIN( coeff, coeffmax ), coeffmin )

      ! This expression defines the new gap heights for all nodes
      ! for the next iteration
      ! Gap decreases if coeff<1
      ! Gap increases if coeff>1
      Gap(j) = ( 1- GapRelax + GapRelax * coeff ) * Gap(j)

    END DO

  END IF

  cond = GetConstReal( Material,'Heat Conductivity' )

  ! n is the current node index. Let i be the amount of nodes on the
  ! heat source boundary, then MeltBC will be executed i times
  IF( n > SIZE( GapPerm ) )  CALL Fatal('MeltBC','Err5')
  i = GapPerm(n)

  IF( i > SIZE( Gap ) ) CALL Fatal('MeltBC','Err6')

  g = Gap( i ) ! g is the gap height for the current node

  ! EPSILON(X) gives the accuracy of the type of the variable X
  ! For example, if using double precision float, then the accuracy
  ! is 2.220446049250313 1E-016
  ! if the gap height is below this accuracy, the simulation will stop
  IF( g < EPSILON( g ) ) THEN
    CALL Fatal('MeltBC','Err7')
  ELSE
    ! else calculate the heat transfer coefficient (1D assumption)
    f = cond / g
  END IF


END FUNCTION HTCoeff
```

E Solver input files

E.1 Description

Comments

Comments are in the case definition files by the exclamation mark „!“defined.

Structure

The case definition file consists of multiple entries that contain commands to ElmerSolver for solving. In table E.1, these entries are listed. A detailed description can be found in [Raback et al., 2013]

Entry	Description
Header	- Inclusion of the FE mesh - Path definition of the result file
Constants	- Declaration of the constants
Simulation	- Definition of the type of simulation (steady-state or transient) - Definition of the method of time-discretization (BDF or Crank-Nicholson) - time-step size - output interval ...
Solver	- Definition and setup of the solver
Body	- Assignment of the initial conditions, material properties, equations
Equation	- Summary of solvers
Body Force	- Specification of body forces, e.g. heat source
Material	- Definition of material properties
Initial Condition	- Definition of initial conditions
Boundary Condition	- Definition of boundary conditions

Table E.1: Description of the entries in the Elmer solver input file.

E.2 Solver input file to find the melting velocity

```
Header
  Mesh DB "." "Mesh_1"
End

$lat = 3.34e5              ! latent heat                       [J/kg]
$visc = 0.001              ! dynamic viscosity of melt         [Ns/m^2]
$tice = -20.0              ! temperature of solid PCM          [degC]
$tmelt = 0.0               ! phase change temperature          [degC]
$tmole = 20.0              ! temperature of heat source        [degC]
$watercap = 4222.22        ! heat capacity of melt             [J/(kgK)]
$icecap = 2049.41          ! heat capacity of solid PCM        [J/(kgK)]
$watercond = 0.57          ! thermal conductivity of melt      [W/(mK)]
$icecond = 2.18            ! thermal conductivity of solid PCM [W/(mK)]
```

```
$gap = 0.01                 ! initial melt thickness            [m]
$waterdens = 1000.0         ! density of melt                   [kg/m^3]
$icedens = 920              ! density of solid PCM              [kg/m^3]

$function moletemp_func(tx) {\
deltaT=4;\
varTemp=10;\
_moletemp_func=varTemp-(deltaT/2)/(0.075)*tx; }

$curveRadius=0.5;

Constants
End

Simulation
  Max Output Level = 5
  Coordinate System = Cartesian
  Simulation Type = Scanning
  Timestep Intervals = 500
  Output Intervals = 0
  Coordinate Scaling = Real 0.0015
  Post File = "mole_fine.vtu"
End

Body 1
  Name = "Ice"
  Target Bodies(1) = 1
  Equation = 1
  Material = 1
  Initial Condition = 1
End

Body 2
  Name = "HeatSource"
  Target Bodies(1) = 2
  Equation = 2
  Material = 2
  Initial Condition = 1
End

Body 3
  Name = "Gap"
  Equation = 3
  Material = 3
  Initial Condition = 1
End

Equation 1
  Name = "Heat"
  Active Solvers(1) = 1
  Convection = constant
End

```

```
Equation 2
  Name = "Nothing"
End

Equation 3
  Name = "Reynolds"
  Active Solvers(3) = 2 3 4
End

Solver 1
  Equation = "Heat"
  Variable = Temp
  Procedure = "HeatSolve" "HeatSolver"
  Linear System Solver = Iterative
  Linear System Iterative Method = BiCGStabL
  Linear System Max Iterations = 500
  Linear System Convergence Tolerance = 1.0e-10
  Linear System Preconditioning = ILU0
  Linear System Residual Output = 0
  Steady State Convergence Tolerance = 1.0e-5
  Nonlinear System Convergence Tolerance = 1.0e-6
  Nonlinear System Max Iterations = 400
  Nonlinear System Relaxation Factor = 1.0
  Nonlinear System Newton After Iterations = 0
  Nonlinear System Newton After Tolerance  = 1.0e-2
  Stabilize = Logical True
  Gap Relaxation Factor = Real 0.7
  Melting Temperature = Real $ tmelt
End

Solver 2 ! Compute consistant normals with Galerkin
  Exec Solver = Before All
  Equation = ComputeNormals
  Procedure = "NormalSolver" "NormalSolver"
  Variable = -nooutput nrm_temp
  Exported Variable 1 = F[normal:2]
  Normals Result Variable = String "F"
  Linear System Solver = "Iterative"
  Linear System Iterative Method = "BiCGStab"
  Linear System Preconditioning = None
  Linear System Residual Output = 0
  Linear System Max Iterations = 500
  Linear System Convergence Tolerance = 1.0e-10
End

Solver 3 ! Compute pressure caused by the given gap and velocity
  Equation = "Reynolds"
  Procedure = File "ReynoldsSolver" "ReynoldsSolver"
  Variable = FilmPressure
  Variable DOFS = 1
  Linear System Solver = Iterative
  Linear System Iterative Method = BiCGStab
  Linear System Max Iterations = 500
```

```
  Linear System Convergence Tolerance = 1.0e-8
  Linear System Preconditioning = ILU0
  Linear System Residual Output = 0
  Steady State Convergence Tolerance = 1.0e-5
  Nonlinear System Convergence Tolerance = 1.0e-5
  Nonlinear System Max Iterations = 1
  Nonlinear System Newton After Iterations = 3
  Nonlinear System Newton After Tolerance = 1.0e-2
  Nonlinear System Relaxation Factor = 1.0
  Exported Variable 1 = Gap ! initialize the gap
  Exported Variable 2 = MoleTemp
End

Solver 4 ! Deduce the forces resulting from the Reynolds equation
  Exec Solver = After Timestep
  Equation = "ReynoldsPost"
  Procedure = File "ReynoldsSolver" "ReynoldsPostprocess"
  Linear System Solver = Direct
  Linear System Direct Method = umfpack
  Linear System Iterative Method = BiCGStab
  Linear System Max Iterations = 500
  Linear System Convergence Tolerance = 1.0e-8
  Linear System Preconditioning = ILU0
  Linear System Residual Output = 0
  Steady State Convergence Tolerance = 1.0e-5
  Calculate Force = Logical True
  Moment About(2) = Real 0.0 0.0
End

Solver 5
  Exec solver = after timestep
  Equation = SaveScalars
  Procedure = "SaveData" "SaveScalars"
  Filename = "g_fine.dat"
  Variable 1 = time
  Variable 2 = Temp
  Operator 2 = max
  Variable 3 = Gap
  Operator 3 = max
  Operator 4 = min
  Variable 5 = FilmPressure
  Operator 5 = max abs
  Expression 1 = Variable lnv
    Real MATC "exp(tx)"
  Target Variable 12 = String Fy ! Create a variable to be used in the optimization
End

Solver 6 ! save the data along the whole line
  Exec Solver = after timestep!never
  Equation = String SaveLine
  Procedure = File "SaveData" "SaveLine"
  Filename = File "ss.dat"
End
```

```
Solver 7 ! Optimization
  Exec Solver = "before timestep"
  Equation = String "Optim"
  Procedure = File "FindOptimum" "FindOptimum"
  Variable = -global lnv ! the name of the design variable
  Variable Dofs = 1
  $ftarget=32.0
  Cost Function = Variable "Fy"
    Real MATC "ln(tx)"
  Cost Function Target = Real $ln(ftarget)
  History File = File "cost.dat"
  Optimization Method = String "secant"
  Step Size = Real 1.0
  Max Step Size = Real 10.0
  Relaxation Factor = Real 0.7
  Optimization Tolerance = Real 1.0e-6
  Initial Parameter 1 = Real $ln(1.0e-6)
End

Initial Condition 1
  Temp = Real $ tmelt
  FilmPressure = Real 0.0
  Gap = Real $ gap
  MoleTemp = Variable "Coordinate 1"
    Real MATC "moletemp_func(tx)"
End

Material 1
  Name = "Ice"
  Latent Heat = $ lat
  Melting Point = Real $ tmelt
  Heat Capacity  = $ icecap
  Heat Conductivity = $ icecond
  Convection Velocity 1 = 0.0
  Convection Velocity 2 = Variable "lnv", "Coordinate 1"
    Real MATC "exp(tx(0))*(1-tx(1)/curveRadius)"
  Density = $icedens
End

Material 2
  Name = "Mole"
End

Material 3
  Name = "Water"
  Gap Height = Equals Gap
  Normal Velocity = Variable lnv, Normal 2, Coordinate 1
   Real MATC "icedens/waterdens*exp(tx(0))*(1-tx(2)/curveRadius)*tx(1)"
  Viscosity = $visc
  Density = $waterdens
  Heat Conductivity = $watercond
End
```

```
Boundary Condition 1
  Name = "Mole_vertical"
  Target Boundaries(2) = 4 5
  Body Id = 3
  Save Line = Logical True
  FilmPressure = Real 0.0
  Heat Transfer Coefficient = Variable time
    Real Procedure "./MeltBC" "HTCoeff"
  External Temperature = Equals MoleTemp
  Heat Flux = Variable lnv, normal 2, Coordinate 1
   Real MATC "exp(tx(0))*(1-tx(2)/curveRadius)*icedens*lat*tx(1)"
End

Boundary Condition 2
  Name = "Mole_bottom"
  Target Boundaries(1) = 3
  Body Id = 3
  Save Line = Logical True
  Heat Transfer Coefficient = Variable time
    Real Procedure "./MeltBC" "HTCoeff"
  External Temperature = Equals MoleTemp
  Heat Flux = Variable lnv, normal 2, Coordinate 1
   Real MATC "exp(tx(0))*(1-tx(2)/curveRadius)*icedens*lat*tx(1)"
End

Boundary Condition 3
  Name = "Ice_sides"
  Target Boundaries(2) = 7 8
  Infinity BC Temp = Logical True
  Infinity BC Temp Offset = Real $tice
End

Boundary Condition 4
  Name = "Ice_bottom"
  Target Boundaries(1) = 6
  Infinity BC Temp = Logical True
  Infinity BC Temp Offset = Real $tice
End
```

E.3 Solver input file to find the curve radius

```
Header
  Mesh DB "." "Mesh_1"
End

$lat = 3.34e5              ! latent heat                      [J/kg]
$visc = 0.001              ! dynamic viscosity of melt        [Ns/m^2]
$tice=-1.0                 ! temperature of solid PCM         [degC]
$tmelt = 0.0               ! phase change temperature         [degC]
$tmole = 20.0              ! temperature of heat source       [degC]
$watercap = 4222.22        ! heat capacity of melt            [J/(kgK)]
```

```
$icecap = 2049.41           ! heat capacity of solid PCM        [J/(kgK)]
$watercond = 0.57           ! thermal conductivity of melt      [W/(mK)]
$icecond = 2.18             ! thermal conductivity of solid PCM [W/(mK)]
$gap = 0.01                 ! initial melt thickness            [m]
$waterdens = 1000.0         ! density of melt                   [kg/m^3]
$icedens = 920              ! density of solid PCM              [kg/m^3]

$function molevelo(tx1,tx2,tx3) {\
varVelo=0.005;\
_molevelo=varVelo*(1-tx2/tx3); }

$function moletemp_func(tx) {\
deltaT=4;\
varTemp=10;\
_moletemp_func=varTemp-(deltaT/2)/(0.075)*tx; }

Constants
End

Simulation
  Max Output Level = 5
  Coordinate System = Cartesian
  Simulation Type = Scanning
  Timestep Intervals = 500
  Output Intervals = 0
  Coordinate Scaling = Real 0.0015
  Post File = "mole_fine.vtu"
End

Body 1
  Name = "Ice"
  Target Bodies(1) = 1
  Equation = 1
  Material = 1
  Initial Condition = 1
End

Body 2
  Name = "HeatSource"
  Target Bodies(1) = 2
  Equation = 2
  Material = 2
  Initial Condition = 1
End

Body 3
  Name = "Gap"
  Equation = 3
  Material = 3
  Initial Condition = 1
End

Equation 1
```

```
  Name = "Heat"
  Active Solvers(1) = 1
  Convection = constant
End

Equation 2
  Name = "Nothing"
End

Equation 3
  Name = "Reynolds"
  Active Solvers(3) = 2 3 4
End

Solver 1
  Equation = "Heat"
  Variable = Temp
  Procedure = "HeatSolve" "HeatSolver"
  Linear System Solver = Iterative
  Linear System Iterative Method = BiCGStabL
  Linear System Max Iterations = 500
  Linear System Convergence Tolerance = 1.0e-10
  Linear System Preconditioning = ILU0
  Linear System Residual Output = 0
  Steady State Convergence Tolerance = 1.0e-5
  Nonlinear System Convergence Tolerance = 1.0e-6
  Nonlinear System Max Iterations = 400
  Nonlinear System Relaxation Factor = 1.0
  Nonlinear System Newton After Iterations = 0
  Nonlinear System Newton After Tolerance  = 1.0e-2
  Stabilize = Logical True
  Gap Relaxation Factor = Real 0.7
  Melting Temperature = Real $ tmelt
End

Solver 2 ! Compute consistant normals with Galerkin
  Exec Solver = Before All
  Equation = ComputeNormals
  Procedure = "NormalSolver" "NormalSolver"
  Variable = -nooutput nrm_temp
  Exported Variable 1 = F[normal:2]
  Normals Result Variable = String "F"
  Linear System Solver = "Iterative"
  Linear System Iterative Method = "BiCGStab"
  Linear System Preconditioning = None
  Linear System Residual Output = 0
  Linear System Max Iterations = 500
  Linear System Convergence Tolerance = 1.0e-10
End

Solver 3 ! Compute pressure caused by the given gap and velocity
  Equation = "Reynolds"
  Procedure = File "ReynoldsSolver" "ReynoldsSolver"
```

```
  Variable = FilmPressure
  Variable DOFS = 1
  Linear System Solver = Iterative
  Linear System Iterative Method = BiCGStab
  Linear System Max Iterations = 500
  Linear System Convergence Tolerance = 1.0e-8
  Linear System Preconditioning = ILU0
  Linear System Residual Output = 0
  Steady State Convergence Tolerance = 1.0e-5
  Nonlinear System Convergence Tolerance = 1.0e-5
  Nonlinear System Max Iterations = 1
  Nonlinear System Newton After Iterations = 3
  Nonlinear System Newton After Tolerance = 1.0e-2
  Nonlinear System Relaxation Factor = 1.0
  Exported Variable 1 = Gap ! initialize the gap
  Exported Variable 2 = MoleTemp
End

Solver 4 ! Deduce the forces resulting from the Reynolds equation
  Exec Solver = After Timestep
  Equation = "ReynoldsPost"
  Procedure = File "ReynoldsSolver" "ReynoldsPostprocess"
  Linear System Solver = Direct
  Linear System Direct Method = umfpack
  Linear System Iterative Method = BiCGStab
  Linear System Max Iterations = 500
  Linear System Convergence Tolerance = 1.0e-8
  Linear System Preconditioning = ILU0
  Linear System Residual Output = 0
  Steady State Convergence Tolerance = 1.0e-5
  Calculate Force = Logical True
  Moment About(2) = Real 0.0 0.0
End

Solver 5
  Exec solver = after timestep
  Equation = SaveScalars
  Procedure = "SaveData" "SaveScalars"
  Filename = "g_fine.dat"
  Variable 1 = time
  Variable 2 = Temp
  Operator 2 = max
  Variable 3 = Gap
  Operator 3 = max
  Operator 4 = min
  Variable 5 = FilmPressure
  Operator 5 = max abs
  Expression 1 = Variable time, "Coordinate 1", curveRadius
    Real MATC "molevelo(tx(0),tx(1),tx(2))"
  Variable 6 = curveRadius
  Target Variable 16 = String reynolds moment 3
End
```

```
Solver 6 ! save the data along the whole line
  Exec Solver = after timestep!never
  Equation = String SaveLine
  Procedure = File "SaveData" "SaveLine"
  Filename = File "ss.dat"
End

Solver 7 ! Optimization
  Exec Solver = "before timestep"
  Equation = String "Optim"
  Procedure = File "MyFindOptimum" "FindOptimum"
  Variable = -global curveRadius ! the name of the design variable
  Variable Dofs = 1
  $ftarget=0.0
  Cost Function = Variable "reynolds moment 3"
    Real MATC "tx"
  Cost Function Target = Real $ftarget
  History File = File "cost.dat"
  Optimization Method = String "secant"
  Step Size = Real 0.1
  Max Step Size = Real 1.0
  Relaxation Factor = Real 0.7
  Optimization Tolerance = Real 1.0e-6
  Initial Parameter 1 = Real 0.075
  Min Parameter 1 = Real 0.075
End

Initial Condition 1
  Temp = Real $ tmelt
  FilmPressure = Real 0.0
  Gap = Real $ gap
  MoleTemp = Variable "Coordinate 1"
    Real MATC "moletemp_func(tx)"
End

Material 1
  Name = "Ice"
  Latent Heat = $ lat
  Melting Point = Real $ tmelt
  Heat Capacity  = $ icecap
  Heat Conductivity = $ icecond
  Convection Velocity 1 = 0.0
  Convection Velocity 2 = Variable Time, "Coordinate 1", curveRadius
    Real MATC "molevelo(tx(0),tx(1), tx(2))"
  Density = $icedens
End

Material 2
  Name = "Mole"
End

Material 3
  Name = "Water"
```

```
  Gap Height = Equals Gap
  Normal Velocity = Variable Time, Normal 2, "Coordinate 1", curveRadius
   Real MATC "icedens/waterdens*molevelo(tx(0),tx(2), tx(3))*tx(1)"
  Viscosity = $visc
  Density = $waterdens
  Heat Conductivity = $watercond
End

Boundary Condition 1
  Name = "Mole_vertical"
  Target Boundaries(2) = 4 5
  Body Id = 3
  Save Line = Logical True
  FilmPressure = Real 0.0
  Heat Transfer Coefficient = Variable time
    Real Procedure "./MeltBC" "HTCoeff"
  External Temperature = Equals MoleTemp
  Heat Flux = Variable time, normal 2, "Coordinate 1", curveRadius
   Real MATC "molevelo(tx(0),tx(2), tx(3))*lat*icedens*tx(1)"
End

Boundary Condition 2
  Name = "Mole_bottom"
  Target Boundaries(1) = 3
  Body Id = 3
  Save Line = Logical True
  Heat Transfer Coefficient = Variable time
    Real Procedure "./MeltBC" "HTCoeff"
  External Temperature = Equals MoleTemp
  Heat Flux = Variable time, normal 2, "Coordinate 1", curveRadius
    Real MATC "molevelo(tx(0),tx(2), tx(3))*lat*icedens*tx(1)"
End

Boundary Condition 3
  Name = "Ice_sides"
  Target Boundaries(2) = 7 8
  Infinity BC Temp = Logical True
  Infinity BC Temp Offset = Real $tice
End

Boundary Condition 4
  Name = "Ice_bottom"
  Target Boundaries(1) = 6
  Infinity BC Temp = Logical True
  Infinity BC Temp Offset = Real $tice
End
```

F Matlab files

F.1 Shreve

```
function [E,N,tau,T,varargout] = Shreve( varargin )
%SHREVE Numerical Solution of the equations presented in
%Shreve, RL: Theory of performance of isothermal solid-nose
%hot-points boring in temperate ice.
%In: J. Glaciol 4 (1962), Nr. 32, S. 151?160
%
%   Usage:
%
%   [E,N,tau,T] = Shreve('B',1.0)
%       This returns the efficiency E, the performance number N,
%       the dimensionless temperature tau and the temperature T in deg C
%   [E,N,tau,T,V] = Shreve('Q',800,'F',200,'S',0.372,'a',0.25)
%       This returns the efficiency E, the performance number N,
%       the dimensionless temperature tau, the temperature T in deg C and
%       the velocity V for a given power input Q, exerted force F,
%       shape factor S and radius a
%   Optional Parameters:
%       mu_0:   dynamic viscosity [kg/(s*m)]
%       c:      heat capacity [J/(kg*K)]
%       K:      thermal conductivity [J/(s*m*K)]
%       lambda: latent heat of fusion [J/kg]
%       rho_w:  density [kg/(m^3)]

%% Variables
cal2J_factor=4.184;         % factor to convert cal to joule

%% Parse function inputs

% Create an InputParser object
p = inputParser;

% Add inputs
default.iterTol = 1e-8;                     % tolerance for iterations
default.B = 0.1;                            % must be given

% Parameters used by the author and conversion to SI units

default.mu_0=1.8*10^(-2)/10;                % dynamic viscosity [kg/(s*m)]
default.c=1*cal2J_factor*1000;              % heat capacity [J/(kg*K)]
default.K=1.4*10^(-3)*cal2J_factor*100;     % thermal conductivity [J/(s*m*K)]
default.lambda=80*cal2J_factor*1000;        % latent heat of fusion [J/kg]
default.rho_w=0.91/1000*1e6;                % density [kg/(m^3)]

addParameter(p,'iterTol',default.iterTol,@isnumeric);
addParameter(p,'B',default.B,@isnumeric);
addParameter(p,'mu_0',default.mu_0,@isnumeric);
addParameter(p,'c',default.c,@isnumeric);
```

```
addParameter(p,'K',default.K,@isnumeric);
addParameter(p,'lambda',default.lambda,@isnumeric);
addParameter(p,'rho_w',default.rho_w,@isnumeric);

addParameter(p,'F',0,@isnumeric);
addParameter(p,'Q',0,@isnumeric);
addParameter(p,'S',0,@isnumeric);
addParameter(p,'a',0,@isnumeric);

% Parse the inputs
parse(p,varargin{:});

B=p.Results.B;

%% Definition of alpha
% alpha=xi/h
% where xi is the distance measured radially outward along the frontal
% surface and h is the local thickness of the layer of melt water.
alpha=0:0.1:1; % alpha goes from 0 to 1 in 0.1-steps

%% Specific viscosity of water (eta) as a function of the normalized temperature
% using Fig. 2 and cftool the following parameters are used to describe the
% specific viscosity of water:
%     eta(x) = (p1*x^3 + p2*x^2 + p3*x + p4) / (x + q1)
p1 =    -0.03185;
p2 =      0.1621;
p3 =     -0.3145;
p4 =      0.4783;
q1 =      0.4784;

%% Initialization of function handles

% specific viscosity of water (eta)
eta_func = @(tau) (p1.*tau.^3 + p2.*tau.^2 + p3.*tau + p4) ./ (tau + q1);

% definition of a trial normalized temperature profile (tau(alpha))
% note: tau=T*c/lambda, where T is the temperature in degrees celsius
tau_func = @(alpha) 1-alpha;

% integrants (see equation 7)
I_0 = @(x) (eta_func(tau_func(x))).^(-1);
I_1 = @(x) ((eta_func(tau_func(x))).^(-1)).*x;
I_2 = @(x) ((eta_func(tau_func(x))).^(-1)).*x.^2;

% declaration of the size of the necessary variables which are used to
% store the resulty of the integrations for all alpha
int_I_0=zeros(1,length(alpha));
int_I_1=zeros(1,length(alpha));
int_I_2=zeros(1,length(alpha));

Phi=zeros(1,length(alpha)); % (see equation 9)

tau_new=zeros(1,length(alpha));
```

```
iterations=-1;

N_vec=[];
B_vec=[];

%% Iteration loop
while(1)    % this loop is necessary when V should be calculated
    while(1)    % this is the loop for the iterations of tau

        % integration for all alpha (see equation 7)
        for i=1:length(alpha)
           int_I_0(i)=integral(I_0,0,alpha(i));
           int_I_1(i)=integral(I_1,0,alpha(i));
           int_I_2(i)=integral(I_2,0,alpha(i));
        end

        % calculation of Phi for all alpha (see equation 9)
        for i=1:length(alpha)
           Phi(i)=(1/int_I_0(length(alpha)))*(int_I_1(length(alpha))*...
               (alpha(i)*int_I_0(i)-int_I_1(i))-...
               int_I_0(length(alpha))*(alpha(i)*int_I_1(i)-int_I_2(i)));
        end

        % calculation of A (see equation 9)
        A=1/Phi(length(alpha));

        % Define Phi as a function handle
        % This is necessary, because Phi is only an array and we need a
        % function that gives the Phi for a given alpha
        % Interp1 is used to interpolate between the elements in the Phi array
        Phi_func = @(x) interp1(alpha,Phi,x);

        int_tau = @(x) exp(A*B*integral(Phi_func,x,1));

        for i=1:length(alpha)
            tau_new(i) = B*integral(int_tau,alpha(i),1,'ArrayValued',true);
        end

        iterations=iterations+1;
        if iterations>=1
            if abs(tau_old(1)-tau_new(1))<p.Results.iterTol
                break;
            end
        end

        tau_old=tau_new;

        tau_func = @(x) interp1(alpha,tau_new,x);
        eta_func = @(tau) (p1.*tau.^3 + p2.*tau.^2 + p3.*tau + p4) ./ (tau + q1);

        I_0 = @(x) (eta_func(tau_func(x))).^(-1);
        I_1 = @(x) ((eta_func(tau_func(x))).^(-1)).*x;
```

```
        I_2 = @(x) ((eta_func(tau_func(x))).^(-1)).*x.^2;
    end

    % use the last calculated values for tau
    tau=tau_new;

    %  calculation of the efficiency E (see equation 23a)
    E=exp(-A*B*integral(Phi_func,0,1));

    % calculation of the temperature T from the dimensionless temperature tau
    T=(p.Results.lambda/p.Results.c).*tau;

    % calculation of the performance number N (see equation 19b)
    N=(2*pi*B/(8*pi*A*B)^(1/4))*exp(A*B*integral(Phi_func,0,1));

    if p.Results.F > 0 % if force is a parameter -> velocity must be calculated

        % calculation of the velocity V in [m/s] (see equation 23b)
        V=3600*(p.Results.Q*E/(p.Results.a^2))*...
            (pi*p.Results.rho_w*p.Results.lambda)^(-1);
        varargout{1} = V; % return V

        % calculation of Lambda (see equation 19a)
        Lambda=((p.Results.mu_0*p.Results.c^3)/...
            (4*p.Results.K^3*p.Results.lambda^4*p.Results.rho_w))^(1/4);

        % calculation of the performance number N (see equation 22)
        N2=Lambda*p.Results.Q*p.Results.S/(p.Results.a*p.Results.F^(1/4));

        %% Change B iteratively until abs(N-N2) is smaller than 1e-8
        N_vec(length(N_vec)+1)=N;
        B_vec(length(B_vec)+1)=B;
        if length(N_vec)<6
            if N2<N
                B=B*0.6;
            else
                B=B*1.1;
            end
        else
            B_old=B;

            % new value for B is found by extrapolation
            B=interp1(N_vec,B_vec,N2,'spline','extrap');
            B=B(1);

            if B<0 % B must be positive
                B=B_old*0.2;
            end

            err=abs(N-N2); % calculation of the error

            if err<1e-8
                % if the error is smaller than 1e-8 than the corresponding
```

```
                % V was found
                break;
            end
        end

    else
        % if force is not a parameter -> velocity must not be calculated
        break;
    end
end

end % function Shreve
```

F.2 Zhao

```
function out=ZhaoHeatfluxCylinderMelting(heatflux,force,R,...
                                         rho_l,k_l,cp_l,...
                                         latentheat,dynViscosity,p0)
%ZHAOHEATFLUXCYLINDERMELTING solves the close-contact melting problem of
%                            a cylindrical heat source with a constant
%                            heat flux on its wall melting through a
%                            phase change material (PCM)
%   Inputs:
%      heatflux              the heat flux on the wall of the cylinder
%      force                 the exerted force
%      R                     radius of the cylinder
%      rho_l                 density of the liquid phase of the PCM
%      k_l                   thermal conductivity of the liquid phase
%                            of the PCM
%      cp_l                  specific heat capacity of the liquid phase of
%                            the PCM
%      latentheat            latent heat of fusion of the PCM
%      dynViscosity          dynamic viscosity of the liquid phase of the
%                            PCM
%      p0                    pressure at the outer edges of the cylinder
%                            e.g. ambient pressure
%   Outputs:
%      out.heatflux          the heatfux from input
%      out.U_0               the melting rate
%      out.F                 the force (normally a little bit different
%                            from the input force) which suits to out.U_0
%      out.Gap.angle         vector of the angular positions in radian for
%                            the melt film thickness given in out.Gap.y
%      out.Gap.value         vector of the melt film thickness
%      out.Pressure.angle    vector of the angular positions in radian for
%                            the pressure distribution in the melt film
%      out.Pressure.value    vector of the pressure distribution in the
%                            melt film
%
%   Example:
%      out = ZhaoHeatfluxCylinderMelting ( 20000, 100, 0.0254/2,...
%                                          774, 0.152, 2.18*1000,...
```

```
%                                          244000, 3.9*10^(-3), 0 )

% calculate the thermal diffusivity of the liquid phase of the PCM
alpha_l=k_l/(rho_l*cp_l);

% calculate the highest possible velocity (from Stefan Condition)
U_0max=heatflux/(rho_l*latentheat);

% define a function which changes the melting rate slightly
% at each iteration
U_0=@(tx) U_0max-1.0*1.0e-8*1.1^(tx-1);

i=0;
while 1
    i=i+1;
    data=calcForce_heatfluxdriven(U_0(i));
    F(i)=data.F;
    V(i)=data.U_0;
    if F(i)<force
        break;
    end
end

out.heatflux=heatflux;
out.U_0=interp1(F,V,force);

if(isnan(out.U_0))
    out.U_0=interp1(F,V,force,'spline','extrap');
end

data=calcForce_heatfluxdriven(out.U_0);

out.F=data.F;
out.Gap=data.Gap;
out.Pressure=data.Pressure;

    function out=calcForce_heatfluxdriven(U_0)
        Gap0=20*alpha_l*(heatflux-rho_l*U_0*latentheat)/...
             (3*U_0*heatflux+7*rho_l*U_0^2*latentheat);

        options=odeset('MaxStep',pi/150);
        Gap=ode45(@dGap,[0.00000001 pi/2],Gap0,options);

        out.Gap.angle=Gap.x;
        out.Gap.value=Gap.y;

        Pressure=ode45(@dPressure,[pi/2 0.0001],p0,options);

        out.Pressure.angle=Pressure.x;
        out.Pressure.value=Pressure.y;

        x_order = Pressure.x(end:-1:1); %fliplr
        y_order = Pressure.y(end:-1:1); %fliplr
```

```

        out.F=2*R*trapz(x_order,(y_order-p0).*cos(x_order));
        out.U_0=U_0;

        function dy=dGap(t,y)

            dy=((3*heatflux*sin(t)+3.5*rho_l*U_0*latentheat*sin(2*t))^(-1))*(...
                20*alpha_l*(heatflux/U_0-rho_l*latentheat*cos(t))-...
                3*heatflux*y(1)*cos(t)-...
                3.5*rho_l*U_0*latentheat*y(1)*2*cos(2*t));

        end

        function dy=dPressure(t,~)

            dy=-12*dynViscosity*U_0*R^2*sin(t)/(interp1(Gap.x,Gap.y,t))^3;

        end

    end

end
```

F.3 Curvilinear melting

```
function [ U_0,x_r,delta,p ] = curve( varargin )
%CURVE Summary of this function goes here
%   Detailed explanation goes here

%% Parse function inputs

% Create an InputParser object
p = inputParser;

% Set the default values, which are used, when the user do not define them
default.mu=0.001;
default.k_L=0.57;
default.T_m=0;
default.T_inf=-20;
default.h_m=2.435e5;
default.c_p_L=4222.22;
default.c_p_S=2049.41;
default.rho_L=1000;
default.rho_S=920;
default.L=0.075;
default.F_screw=30/0.08;
default.T_w = @(x) 30-10.0*x/default.L;
default.usefsolve = false;
default.DisplayIterSteps=false;
default.shape='rectangular';
default.externalTorque=0;

```

```
addParameter(p,'mu',default.mu,@isnumeric);
addParameter(p,'k_L',default.k_L,@isnumeric);
addParameter(p,'T_m',default.T_m,@isnumeric);
addParameter(p,'T_inf',default.T_inf,@isnumeric);
addParameter(p,'h_m',default.h_m,@isnumeric);
addParameter(p,'c_p_L',default.c_p_L,@isnumeric);
addParameter(p,'c_p_S',default.c_p_S,@isnumeric);
addParameter(p,'rho_L',default.rho_L,@isnumeric);
addParameter(p,'rho_S',default.rho_S,@isnumeric);
addParameter(p,'L',default.L,@isnumeric);
addParameter(p,'F_screw',default.F_screw,@isnumeric);
addParameter(p,'T_w',default.T_w,@(x)isa(x,'function_handle'));
addParameter(p,'DisplayIterSteps',default.DisplayIterSteps,@islogical);
addParameter(p,'shape',default.shape);
addParameter(p,'externalTorque',default.externalTorque,@isnumeric);

% Parse the inputs
parse(p,varargin{:});

mu=p.Results.mu;
k_L=p.Results.k_L;
T_m=p.Results.T_m;
T_inf=p.Results.T_inf;
h_m=p.Results.h_m;
c_p_L=p.Results.c_p_L;
c_p_S=p.Results.c_p_S;
rho_L=p.Results.rho_L;
rho_S=p.Results.rho_S;
L=p.Results.L;
F_screw=p.Results.F_screw;
T_w=p.Results.T_w;
DisplayIterSteps=p.Results.DisplayIterSteps;
shape=p.Results.shape;
externalTorque=p.Results.externalTorque;

%% Calculation of some variables
h_m_star=h_m+c_p_S*(T_m-T_inf);

%% Initialization
U_0=1.9e-4;     % Initital velocity at the center of the heat source
x_r=1000;       % Initial curve radius
M_tol=1e-6;     % Absolute error tolerance for the torque
F_tol=1e-6;     % Absolute error tolerance for the force

%% Solve the nonlinear system

% initialize the counter variable for loops of the main while-loop
i_main=0;

% Main loop
while(1)

    i_main=i_main+1;    % increment counter variable of the main while-loop
```

```

    i_cr=0;             % initialization of the counter variable of the
                        % while-loop to calculate the curve radius
    i_v=0;              % initialization of the counter variable of the
                        % while-loop to calculate the velocity at the
                        % center of the heat source

    % Inititalize or remove old values from previous calculations
    M_vec=[];   % to store the calculated torques (vector)
    x_r_vec=[]; % to store the curve radii, which were used for the
                % calculations of the torques (vector)
    U_vec=[];   % to store the velocities at the center of the heat source,
                % which were used for the calculations of the forces (vector)
    F_vec=[];   % to store the calculated forces (vector)

    updateFuncHandles;  % update the function handles

    % Loop to calculate the curve radius
    % (torque around ice screw must be zero)
    while(1)

        i_cr=i_cr+1; % increment counter variable of this while-loop

        updateFuncHandles;  % update the function handles

        % Calculate the torque around the ice screw
        switch shape
            case 'rectangular'
                M_int=integral(M,-L,L,'ArrayValued',true)-externalTorque;
            case 'cylindrical'
                M_int=integral(M,-pi/2,pi/2,'ArrayValued',true)-externalTorque;
        end

        % if the user wishes to see information about the calculation steps
        if(DisplayIterSteps)
            if i_cr==1
                display(sprintf('Iteration %i: Calculation of x_r',i_main));
            end
            display(sprintf('%i\tM = %e\t x_r = %f', i_cr,M_int,x_r));
        end

        % store the new values (used curve radius and calculated torque)
        x_r_vec=vertcat(x_r_vec,x_r);
        M_vec=vertcat(M_vec,M_int);

        if abs(M_int)<M_tol
            % if the value of M_int is smaller than the absolute tolerance
            % exit this while loop
            break
        else
            if i_cr==1 % if it is the first round in this loop
                % set the curve radius for the next round to -L or L
                % (depends on the sign of the previously calculated torque)
```

```
                x_r=M_int/abs(M_int)*L;
            else
                % linear extrapolation by using the last two curce radii
                % and torques - due to the slope of M_vec it is better
                % to use the reciprocal of x_r_vec
                help=interp1(M_vec(end-1:end),(x_r_vec(end-1:end)).^(-1)...
                    ,0,'linear','extrap');
                x_r=1/help;
            end
        end
    end

    % Loop to calculate the velocity at the center of the heat source
    % (force due to melt film pressure must be zero)
    while(1)

        i_v=i_v+1; % increment counter variable of this while-loop

        updateFuncHandles;  % update the function handles

        % Calculate the force
        switch shape
            case 'rectangular'
                F=integral(p,-L,L,'ArrayValued',true);
            case 'cylindrical'
                F_cyl=@(phi) L*p(phi)*cos(phi);
                F=integral(F_cyl,-pi/2,pi/2,'ArrayValued',true);
        end

        % if the user wishes to see information about the calculation steps
        if(DisplayIterSteps)
            if i_v==1
                display(sprintf('Iteration %i: Calculation of U_0',i_main));
            end
            display(sprintf('%i\tF = %f\t U_0 = %e', i_v,F,U_0));
        end

        if F<0  % If for any reasons, the force is negative, exit this loop
            break
        end

        % store the new values (used velocity and calculated force)
        U_vec=vertcat(U_vec,U_0);
        F_vec=vertcat(F_vec,F);

        if abs(F-F_screw)<F_tol
            % if the difference of F and the given force of the ice screw
            % is smaller than the absolute tolerance exit this while loop
            break;
        else

            if i_v==1 % if it is the first round in this loop
                % use a lower or higher value for the velocity in the next
```

```
                % round of this loop
                if F>F_screw
                    U_0=U_0*0.5;
                else
                    U_0=U_0*1.5;
                end
            else
                U_0new=10^(interp1(10*log10(F_vec),10*log10(U_vec),...
                    10*log10(F_screw),'linear','extrap')/10);

                if U_0new>0
                    U_0=U_0new;
                else
                    % in the case that the velocity would be negative or zero
                    % do not use the value from the extrapolation
                    U_0=U_0/2;
                end
            end
        end

    end

    % Check again if the torque around the ice screw is still smaller than
    % the tolerance - if this is the case then end the main loop
    switch shape
        case 'rectangular'
            M_int=integral(M,-L,L,'ArrayValued',true);
        case 'cylindrical'
            M_int=integral(M,-pi/2,pi/2,'ArrayValued',true);
    end
    if abs(M_int)<M_tol
        break;
    end

end

function updateFuncHandles(varargin)
    % update the function handles

    switch shape
        case 'rectangular'
            delta = @(x) k_L*(T_w(x)-T_m)./(rho_S*h_m_star*U_0*(1-(x./x_r)));

            h_1=@(x) rho_S/rho_L*U_0*x.*(1-x./(2*x_r))./(delta(x).^3);
            h_2=@(x) delta(x)^(-3);
            C_1=-integral(h_1,-L,L,'ArrayValued',true)/integral(h_2,-L,L,...
                'ArrayValued',true);

            dpdx= @(x) -(12*mu*(rho_S/rho_L*U_0*x.*(1-x./(2*x_r))+C_1)./...
                (delta(x).^3));

            warning('OFF');
            try
```

```
                p0=-integral(dpdx,0,L,'ArrayValued',true);
                error(lastwarn);
            catch err
                lastwarn('');
                warning('ON');
                p0=-integral(dpdx,0,-L,'ArrayValued',true);
            end

            p = @(x) integral(dpdx,0,x,'ArrayValued',true)+p0;

            M = @(x) p(x).*x;
        case 'cylindrical'
            R=L;
            delta = @(phi) k_L*(T_w(phi)-T_m)./(rho_S*h_m_star*U_0*...
                cos(phi)*(1-R*sin(phi)./x_r));

            h_1=@(phi) rho_S/rho_L*U_0*R*(R*(cos(phi))^2/(2*x_r)+...
                sin(phi))./(delta(phi).^3);
            h_2=@(phi) delta(phi)^(-3);
            C_1=-integral(h_1,-pi/2,pi/2,'ArrayValued',true)/...
                integral(h_2,-pi/2,pi/2,'ArrayValued',true);

            dpdx= @(phi) -(12*mu*R*(rho_S/rho_L*U_0*R*(R*(cos(phi))^2/...
                (2*x_r)+sin(phi))+C_1)./(delta(phi).^3));
            p0=-integral(dpdx,0,pi/2,'ArrayValued',true);

            p = @(phi) integral(dpdx,0,phi,'ArrayValued',true)+p0;

            M = @(phi) p(phi).*sin(phi)*R^2;
    end

end

end
```

G Drawings

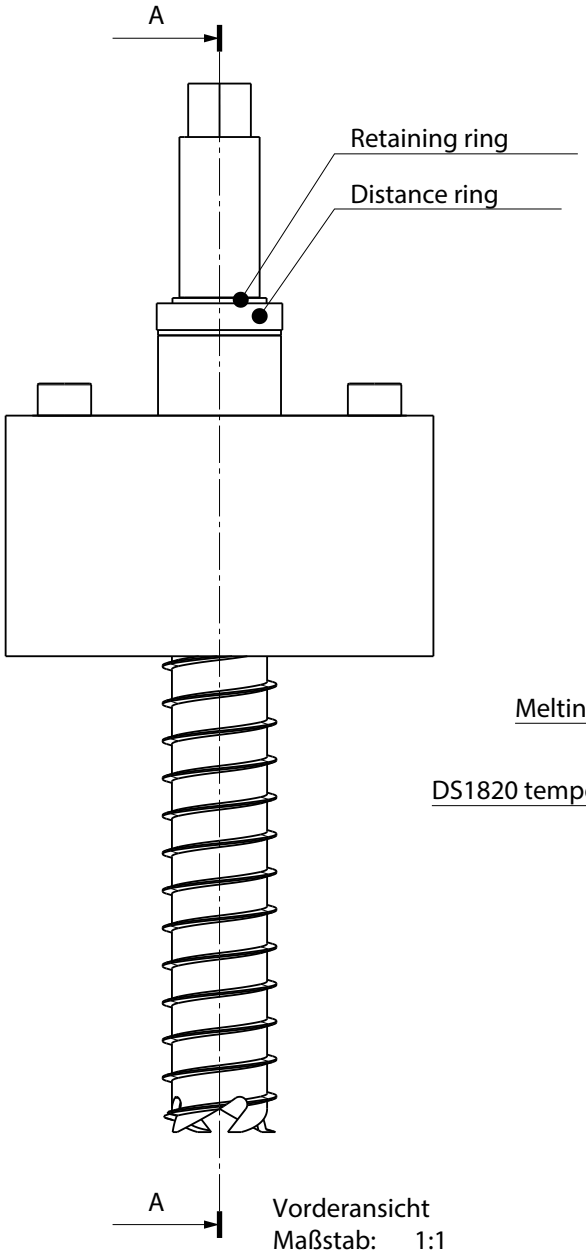

Vorderansicht
Maßstab: 1:1

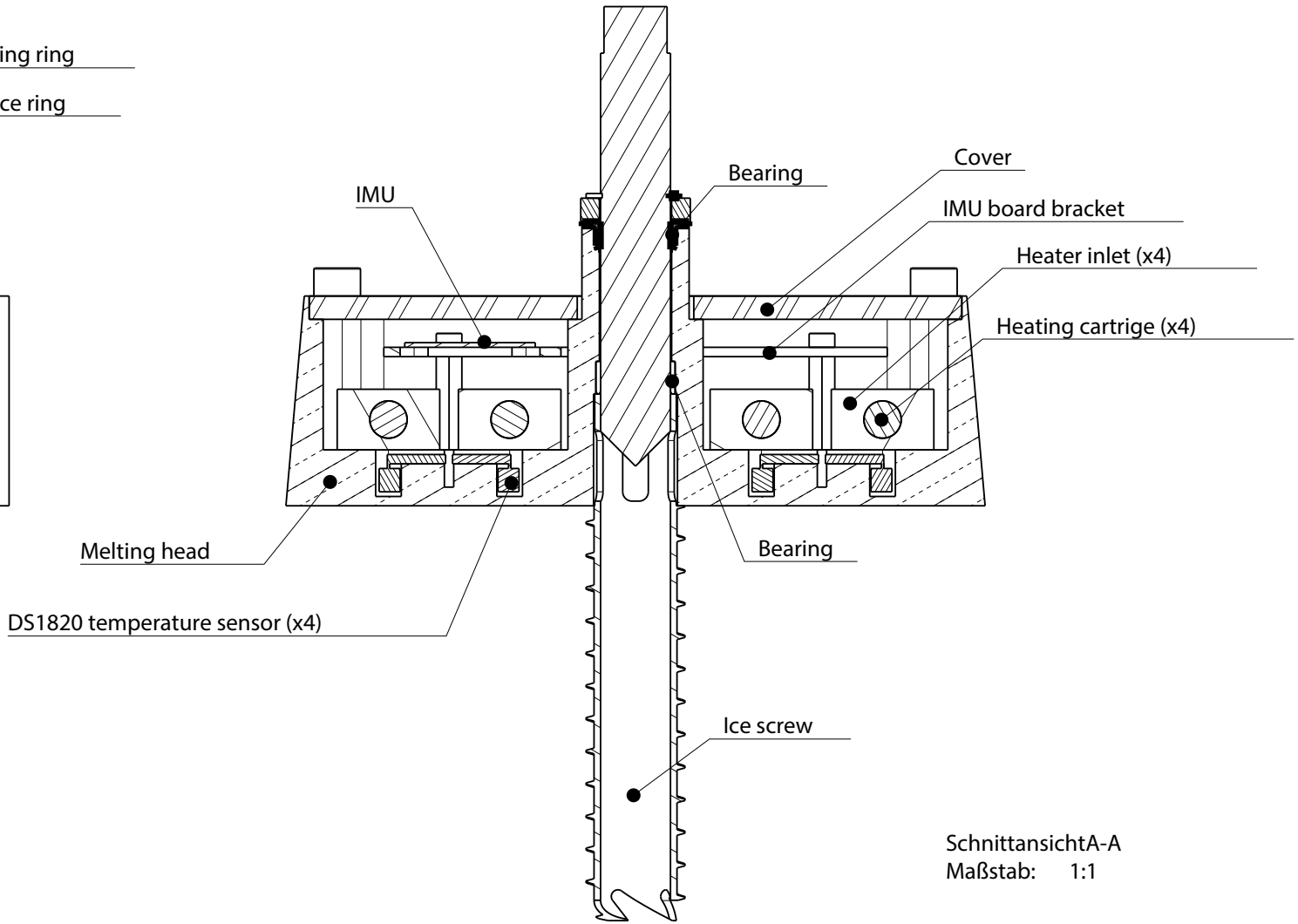

SchnittansichtA-A
Maßstab: 1:1

FH AACHEN UNIVERSITY OF APPLIED SCIENCES	Allgemein toleranzen	Oberflächen-toleranz	Maßstab: 1:1	Anzahl: 1
			Material:	
	Datum	Name	Teilname:	
	Erstellt 05.09.14	Kai Schüller	Assembly	
	Geprüft		Zeichnungsnr.:	Blatt: 1/1
			Kommentar:	Format: A3

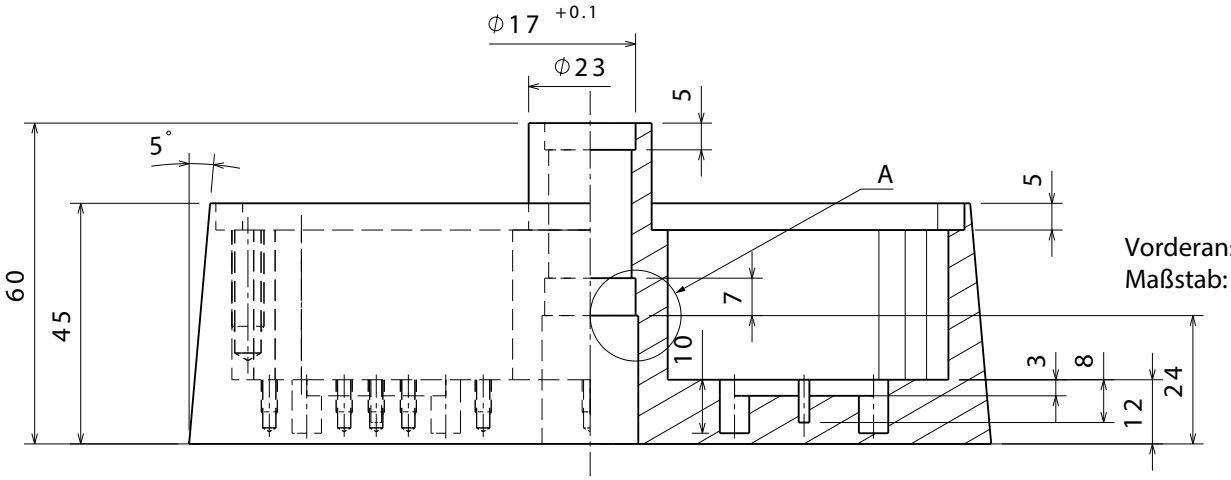

Vorderansicht
Maßstab: 1:1

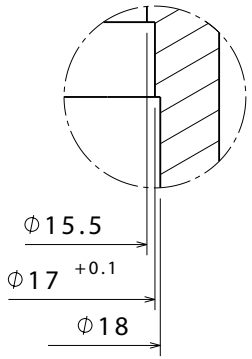

Detail A
Maßstab: 2:1

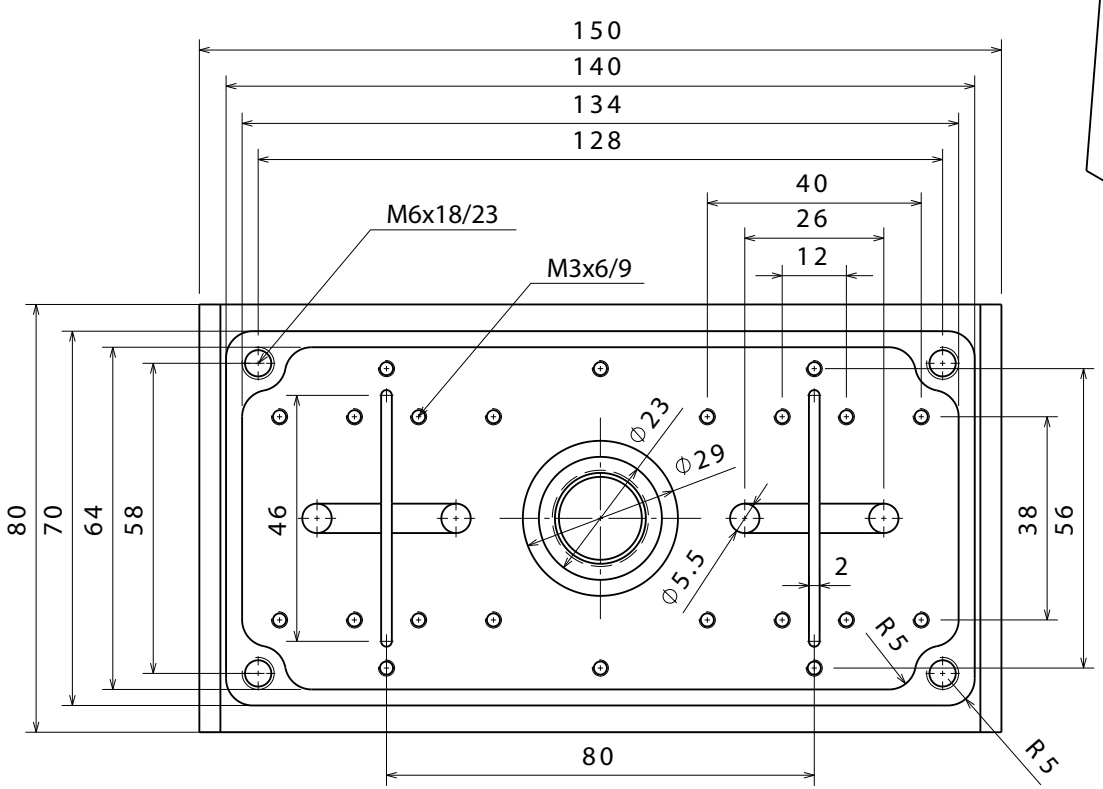

Draufsicht
Maßstab: 1:1

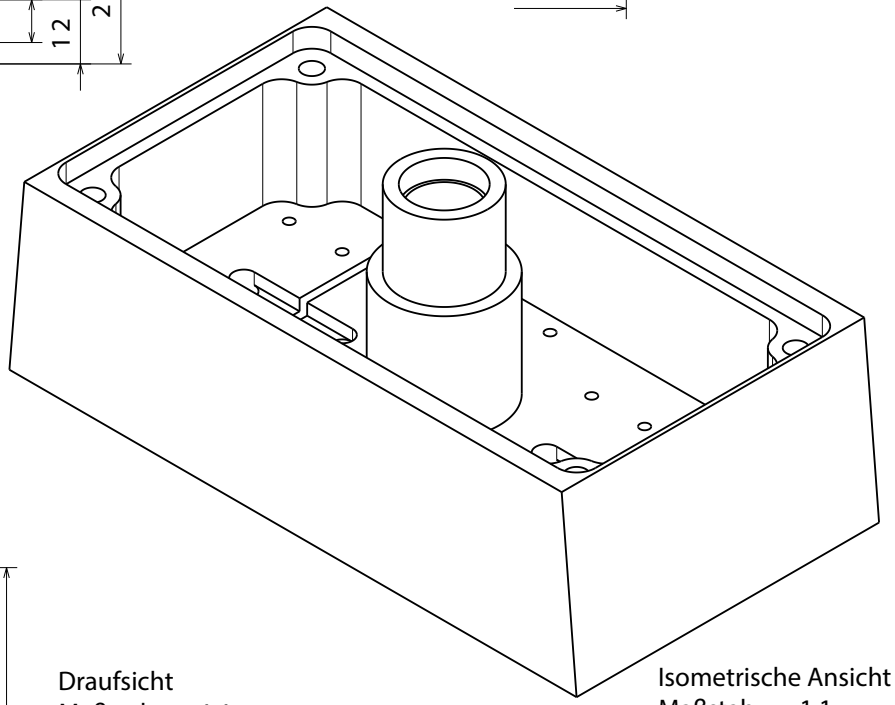

Isometrische Ansicht
Maßstab: 1:1

FH AACHEN UNIVERSITY OF APPLIED SCIENCES

Allgemein toleranzen		Oberflächen-toleranz	Maßstab: 1:1	Anzahl: 1
ISO 2768-mk		DIN ISO 1302	Material: Cu	
	Datum	Name	Teilname:	
Erstellt	05.09.14	Kai Schüller	Melting head	
Geprüft				
			Zeichnungsnr.:	Blatt: 1/1
			Kommentar:	Format: A3

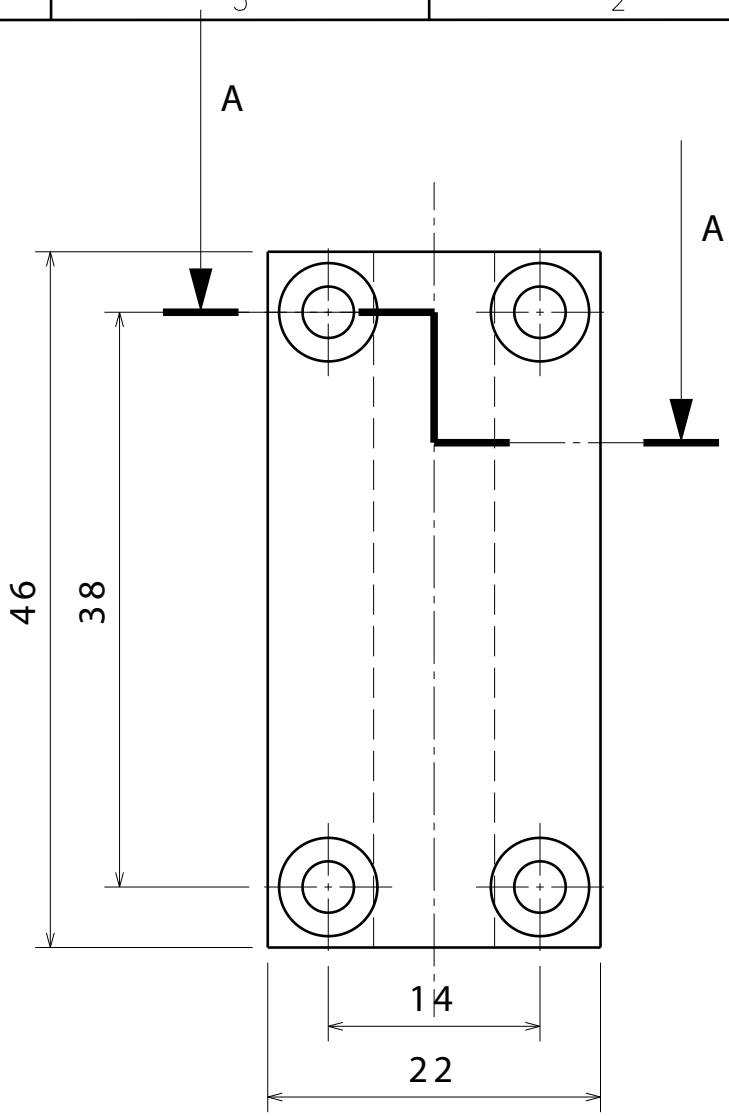

Vorderansicht

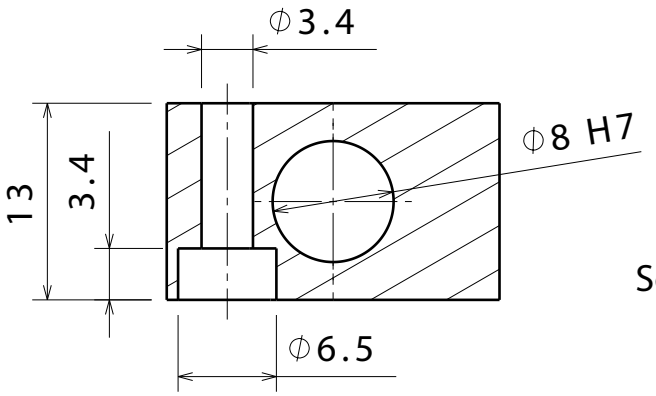

SchnittansichtA-A

FH AACHEN UNIVERSITY OF APPLIED SCIENCES	Allgemein toleranzen: ISO 2768-mk	Oberflächen-toleranz: DIN ISO 1302	Maßstab: 2:1	Anzahl: 4
			Material: Cu	
	Datum	Name	Teilname: Heater inlet	
	Erstellt: 15.08.14	Kai Schüller		
	Geprüft:			
			Zeichnungsnr.:	Format: A4
			Kommentar:	Blatt: 1/1

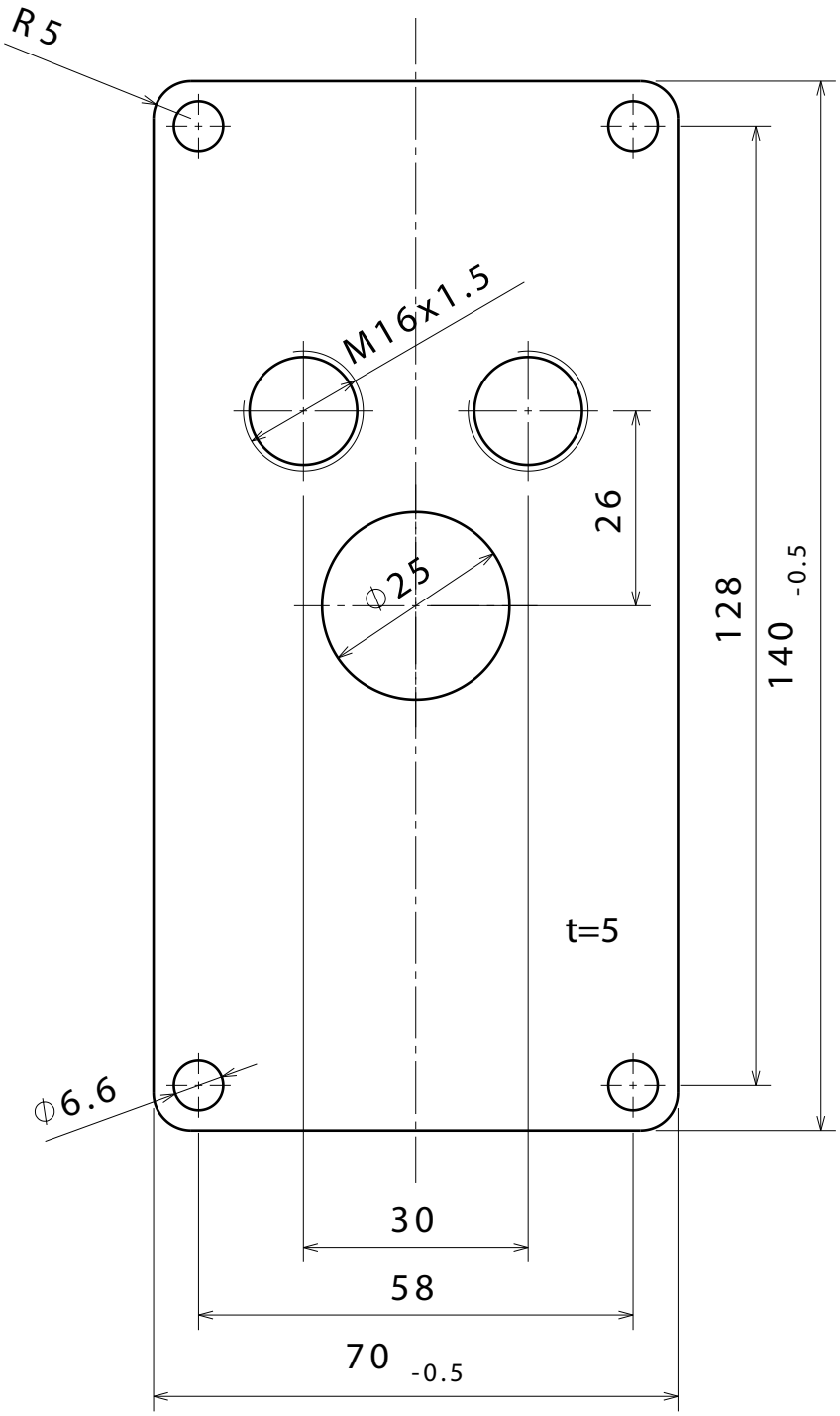

FH AACHEN UNIVERSITY OF APPLIED SCIENCES	Allgemein toleranzen: ISO 2768-mk	Oberflächen-toleranz: DIN ISO 1302	Maßstab: 1:1	Anzahl: 4
			Material: Cu	
	Datum	Name	Teilname: Cover	
	Erstellt: 02.10.14	Kai Schüller		
	Geprüft:			
			Zeichnungsnr.:	Format: A4
			Kommentar:	Blatt: 1/1

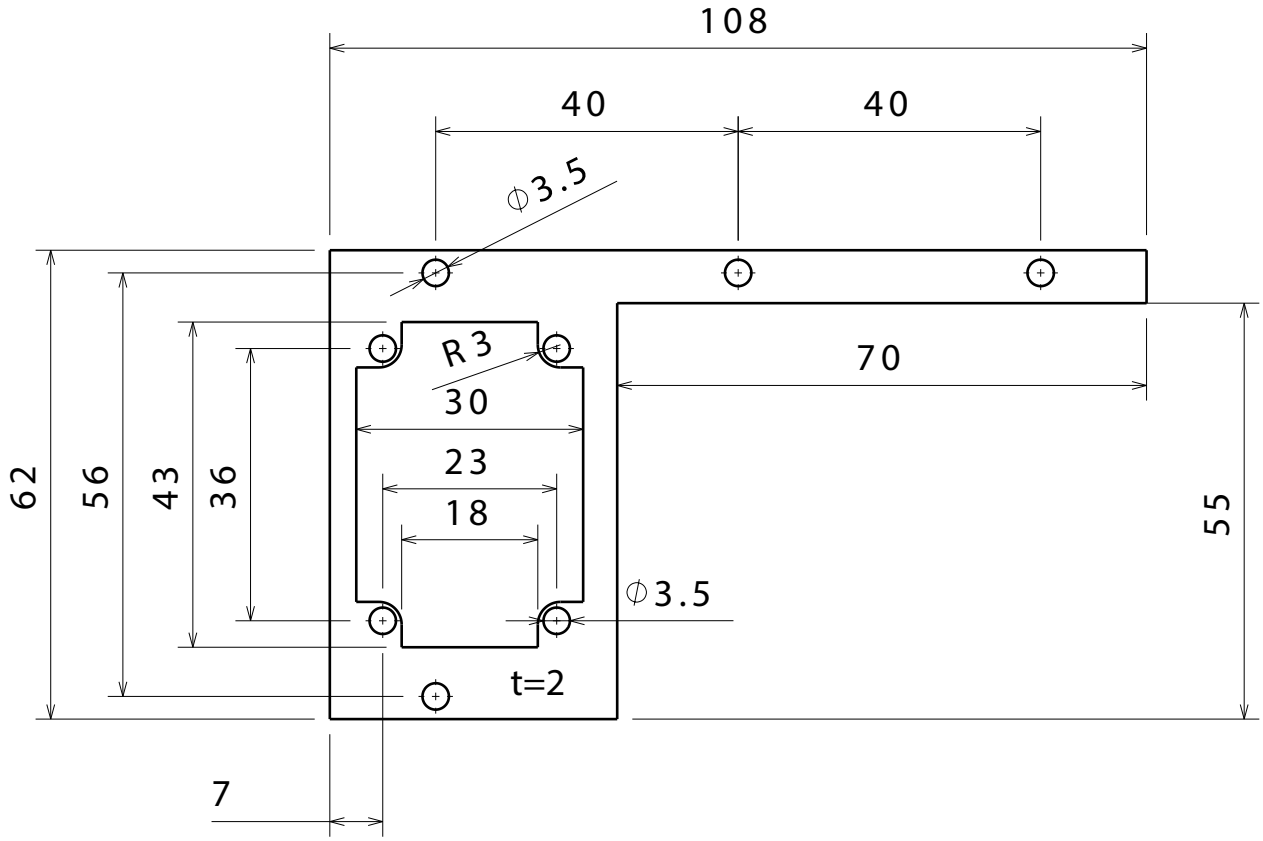

FH AACHEN UNIVERSITY OF APPLIED SCIENCES	Allgemein toleranzen: ISO 2768-mk	Oberflächen-toleranz: DIN ISO 1302	Maßstab: 1:1	Anzahl: 1
			Material: Al	
	Datum	Name	Teilname: IMU board bracket	
	Erstellt: 18.08.14	Kai Schüller		
	Geprüft:			
			Zeichnungsnr.:	Format: A4
			Kommentar:	Blatt: 1/1